Geochemistry Geophysics Geosystems G3
AN ELECTRONIC JOURNAL OF THE EARTH SCIENCES
Published by AGU and the Geochemical Society

Article
Volume 5, Number 4
27 April 2004
Q04008, doi:10.1029/2003GC000623
ISSN: 1525-2027

Recycled metasomatized lithosphere as the origin of the Enriched Mantle II (EM2) end-member: Evidence from the Samoan Volcanic Chain

R. K. Workman, S. R. Hart, and M. Jackson
Woods Hole Oceanographic Institution, 266 Woods Hole Road, Woods Hole, Massachusetts 02543, USA (rworkman@whoi.edu; shart@whoi.edu; mjackson@whoi.edu)

M. Regelous
Max-Planck Institut für Chemie, Postfach 3060, 55020 Mainz, Germany
Now at Department of Earth Sciences, Bristol University, Bristol BS8 17H, UK (m.regelous@bristol.ac.uk)

K. A. Farley
Geological and Planetary Sciences Division, California Institute of Technology, Pasadena, California 91125, USA (farley@gps.caltech.edu)

J. Blusztajn and M. Kurz
Woods Hole Oceanographic Institution, 266 Woods Hole Road, Woods Hole, Massachusetts 02543, USA (jblusztajn@whoi.edu; mkurz@whoi.edu)

H. Staudigel
Scripps Institution of Oceanography, University of California, San Diego, La Jolla, California 92093, USA (hstaudig@ucsd.edu)

[1] An in-depth Sr-Nd-Pb-He-Os isotope and trace element study of the EMII-defining Samoan hot spot lavas leads to a new working hypothesis for the origin of this high $^{87}Sr/^{86}Sr$ mantle end-member. Systematics of the Samoan fingerprint include (1) increasing $^{206}Pb/^{204}Pb$ with time - from 18.6 at the older, western volcanoes to 19.4 at the present-day hot spot center, Vailulu'u Seamount, (2) en-echelon arrays in $^{206}Pb/^{204}Pb$ – $^{208}Pb/^{204}Pb$ space which correspond to the two topographic lineaments of the 375 km long volcanic chain – this is much like the Kea and Loa Trends in Hawai'i, (3) the highest $^{87}Sr/^{86}Sr$ (0.7089) of all oceanic basalts, (4) an asymptotic decrease in $^{3}He/^{4}He$ from 24 R_A [*Farley et al.*, 1992] to the MORB value of 8 R_A with increasing $^{87}Sr/^{86}Sr$, and (5) mixing among four components which are best described as the "enriched mantle", the depleted FOZO mantle, the (even more depleted) MORB Mantle, and a mild HIMU (high $^{238}U/^{204}Pb$) mantle component. A theoretical, "pure" EMII lava composition has been calculated and indicates an extremely smooth trace element pattern of this end-member mantle reservoir. The standard recycling model (of ocean crust/sediment) fails as an explanation for producing Samoan EM2, due to these smooth spidergrams for EM2 lavas, low $^{187}Os/^{188}Os$ ratios and high $^{3}He/^{4}He$ (>8 R_A). Instead, the origin of EM2 has been modeled with the ancient formation of metasomatised oceanic lithosphere, followed by storage in the deep mantle and return to the surface in the Samoan plume.

Components: 21,958 words, 20 figures, 8 tables.

Keywords: EM2; Samoa; metasomatized lithosphere; Sr-Nd-Pb-He-Os isotopes; hot spot chain; Vailulu'u Volcano.

Index Terms: 1040 Geochemistry: Isotopic composition/chemistry; 8121 Tectonophysics: Dynamics, convection currents and mantle plumes; 5480 Planetology: Solid Surface Planets: Volcanism.

Received 21 August 2003; **Revised** 7 January 2004; **Accepted** 22 January 2004; **Published** 27 April 2004.

Workman, R. K., S. R. Hart, M. Jackson, M. Regelous, K. A. Farley, J. Blusztajn, M. Kurz, and H. Staudigel (2004), Recycled metasomatized lithosphere as the origin of the Enriched Mantle II (EM2) end-member: Evidence from the Samoan Volcanic Chain, *Geochem. Geophys. Geosyst.*, *5*, Q04008, doi:10.1029/2003GC000623.

1. Introduction

[2] Although intraplate ocean island volcanism accounts for only a few percent of the total volcanism on Earth, these volcanic piles may be the surface manifestations of the deepest known samplings of the interior of the planet. The relative stationarity of mantle plumes with respect to upper mantle plate flow [*Molnar and Stock*, 1987; *Steinberger and O'Connell*, 1998; *Wang and Wang*, 2001; *Koppers et al.*, 2001], and a growing catalogue of seismic evidence and tomographic images showing velocity anomalies beneath hot spots extending well into the mid-mantle and sometimes to the core-mantle boundary [*Russell et al.*, 1998; *Shen et al.*, 1998; *Zhao*, 2001; *Montelli et al.*, 2004], all support the idea that mantle plumes sample the inner Earth at a much deeper level than do mid-ocean ridge spreading centers. Ocean island chains may thus provide some of the best clues to the chemical character of the lower mantle and the nature of convective interactions between the deep and shallow mantle.

[3] Unlike mid-ocean ridge basalts (MORBs), which derive from a fairly uniform melt-depleted upper mantle, ocean island basalts (OIBs) are isotopically heterogeneous in terms of most radiogenic isotope systems [e.g., *Zindler and Hart*, 1986; *Hart*, 1988; *Hofmann*, 1997]. Isotopic arrays from ocean island chains often extend from a "common" mantle, termed FOZO (i.e., Focus Zone [*Hart et al.*, 1992]), and tend toward one of three "end-member" mantle components: HIMU, the high time-integrated U/Pb mantle, EM1 or EM2, the Enriched Mantles 1 and 2 [*Zindler and Hart*, 1986]. From parent isotope half-lives and parent-daughter ratios, it is inferred that mantle sources for OIBs and MORBs must have been chemically isolated for billions of years in order to develop the observed differences in the abundance of daughter isotopes. Because isotopes of heavy elements are so little fractionated in the melting process, isotopic compositions of oceanic basalt are not only "clocks" for ancient reservoir development, but also "fingerprints" of a melt's solid source. We are left, through geochemical interrogation and theoretical ingenuity, to reverse the processes by which mantle melts were generated and brought to Earth's surface. Ultimately, with some indication for source compositions, the origins and ages of chemically distinct, isolated mantle reservoirs can be deduced.

[4] Although there have been many ideas regarding the origins of the classic mantle end-members, one model has been relied upon most commonly and received the most attention from a modeling point of view. We are in effect "outside looking in", so major differentiation processes occurring at the solid Earth's uppermost layers, namely the formation of continental and oceanic crust, are the most obvious explanations for the creation of volumetrically significant heterogeneities in composition. Many workers have applied this perspective and contributed to what is here referred to as the Standard Model for the origin of mantle components [*Armstrong*, 1968; *Chase*, 1981; *Hofmann and White*, 1982; *Cohen and O'Nions*, 1982; *White*, 1985; *Zindler and Hart*, 1986; *Weaver*, 1991; *Hart et al.*, 1992]. In summary, oceanic crust is subducted at convergent margins, dehydrated (increasing U/Pb, Th/Pb, and Sr/Rb ratios) and put into long term storage in the deep mantle to evolve to HIMU. EM1 and EM2 are generated when trace element-enriched pelagic (i.e., deep-sea) and terrigenous (i.e., continental) sediment, respectively, accompany the subducted and stored oceanic crust (Figure 1). Geochemical models attempting to accurately quantify the compositions of these deeply subducted materials [*Hart and Staudigel*, 1989; *Weaver*, 1991; *Stracke et al.*,

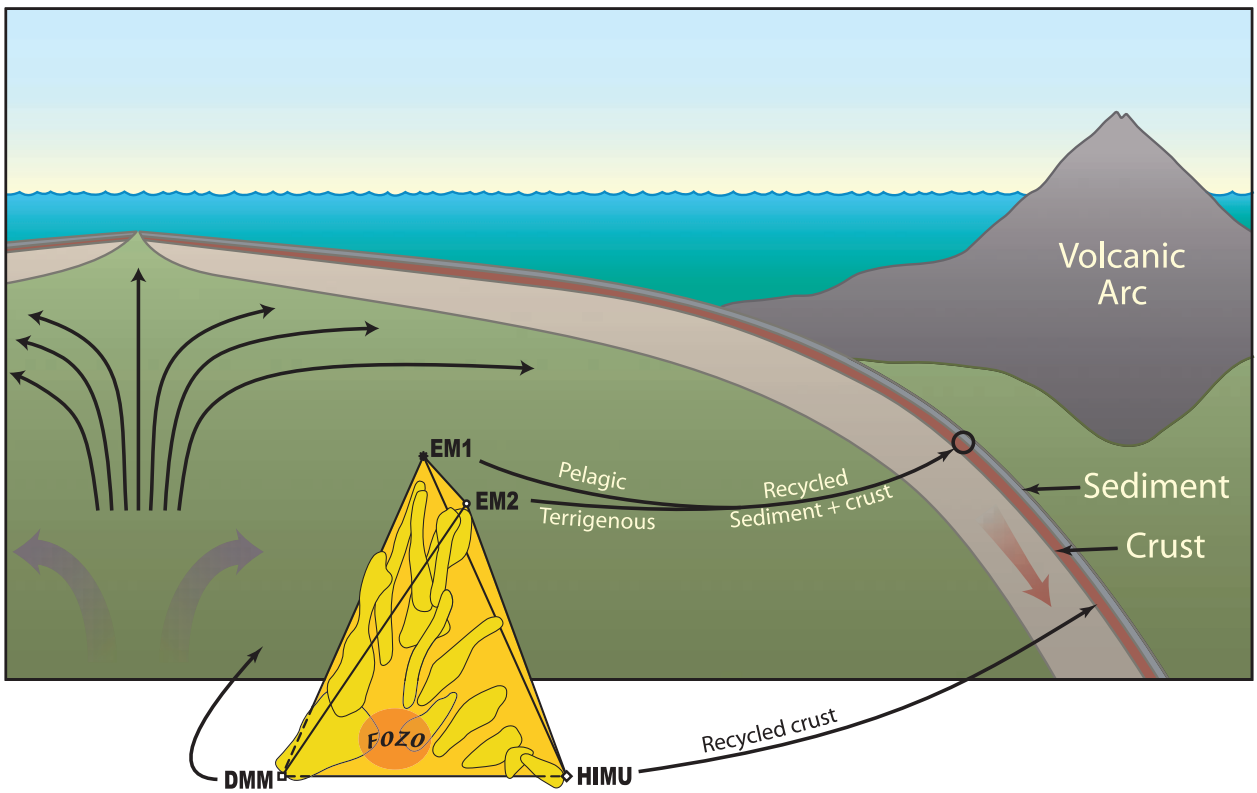

Figure 1. Schematic diagram of the Standard Model for the origin of isotopically defined mantle components. DMM (the Depleted MORB Mantle) is the melt-depleted upper mantle that supplies melts to mid-ocean ridges; HIMU (high U/Pb mantle) is a reservoir derived from recycling and long-term storage (billions of years) of oceanic crust; EM1 and EM2 are derived from recycling and long-term storage of oceanic crust along with pelagic or terrigenous sediment, respectively. Major contributions to the model have been from *Armstrong* [1968], *Chase* [1981], *Hofmann and White* [1982], *Cohen and O'Nions* [1982], *White* [1985], *Zindler and Hart* [1986], *Weaver* [1991], and *Hart et al.* [1992].

2003] are greatly hindered by a lack of knowledge regarding (1) hydrothermal alteration of the oceanic crust, (2) partition coefficients for both the dehydration of crust and sediments and the melting of sediments, (3) the thermal structure of mantle wedges, (4) the variable compositions of sediments in space and time, and (5) the lifespan of a subducted slab in the deep mantle. Although much progress has been made in each of these topics, the constraints are not strong enough to provide the needed resolution in parent/daughter ratios. Ironically, it may be exactly the lack of constraints that ultimately makes the Standard Model nonviable. By all indications from today's geodynamical systems, sediments and the subduction zone processing of crust and sediments all display such variability that a specific composition (which evolves to HIMU, EM1 or EM2) almost certainly would not be produced twice, and there would be no discrete or recognizable "end-member" reservoirs. On the other hand, and often the strongest criticism of the Standard Model [e.g., *Hawkesworth et al.*, 1984; *Barling and Goldstein*, 1990; *Morgan*, 1999], is that there may be no such things as mantle end-members. Each ocean island array could consist of its own unique isotopic composition, which represents a unique subducted slab from a unique recycling time.

[5] In the present study, we specifically deal with the origin of the Enriched Mantle II (EM2) end-member. Lavas from the Samoan Islands have long been recognized as holding the most extreme signal of EM2 [*Zindler and Hart*, 1986; *Wright and White*, 1987; *Farley et al.*, 1992; *Hauri and Hart*, 1993]. Here we use a new comprehensive

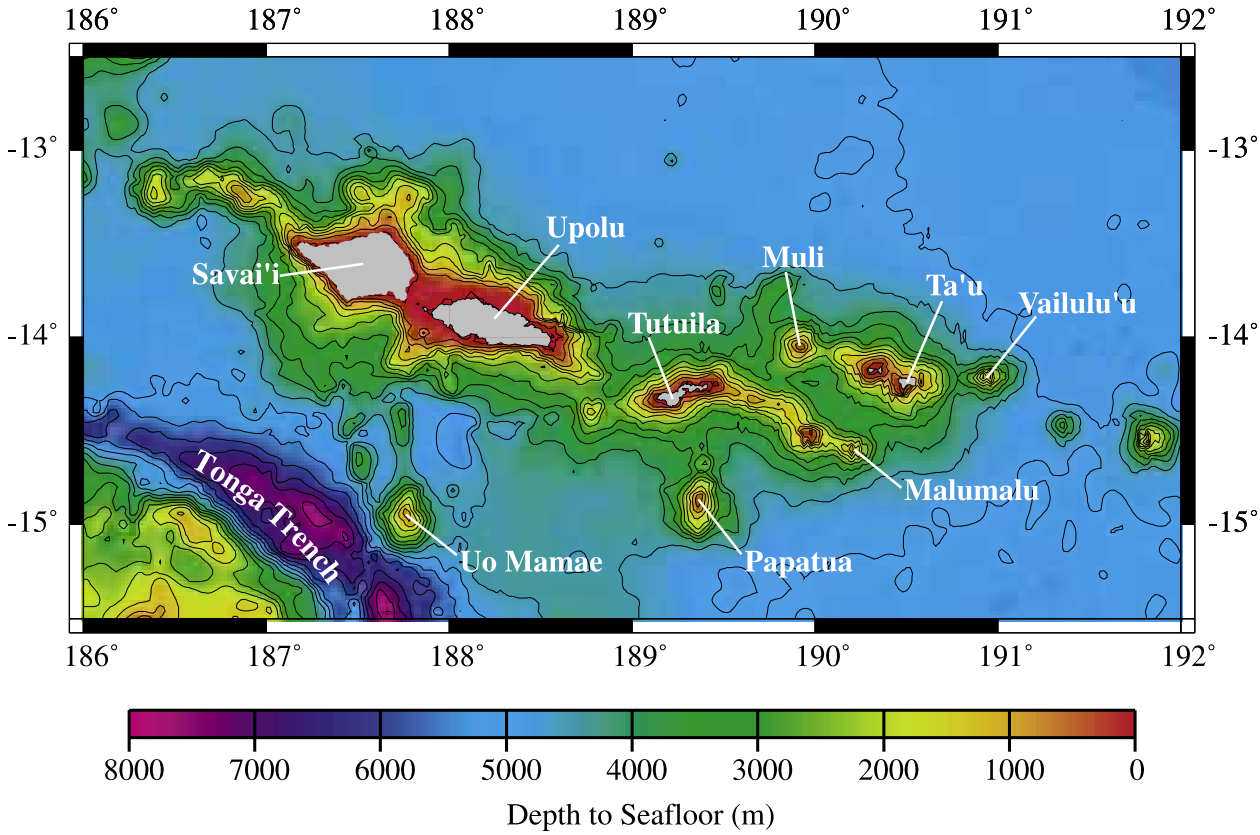

Figure 2. Bathymetric map of the Samoan volcanic chain made from merging inferred bathymetry from *Smith and Sandwell* [1994] with ship track data from both the AVON 2/3 cruise [see *Hart et al.*, 2000] and the GEODAS track line database. Western Samoa is comprised of the two western islands, Savai'i and Upolu; American Samoa is comprised on Tutuila, Ofu, Olosega, and Ta'u. In the southwest corner of the map, where depths are down to 8000 m, is the northern termination of the Tonga Trench. Just off to the west at about 14.5°S is a transform fault bounding the Lau Backarc Basin to the south.

geochemical study to assess possible origins of the EM2 reservoir. This paper outlines why the recycling of sediment/slab cannot be the origin of EM2, and offers an alternative model which will generally result in consistent trace element compositions, and hence isotopic signatures, through time. We assume that mantle end-members do, in fact, exist, and that one process, acting to varying degrees at a variety of times, will produce a fairly homogeneous end-member reservoir, which is available for mixing with other mantle components during upwelling of mantle plumes.

[6] The working model introduced here for the origin of EM2 involves metasomatism (i.e., fluid/melt infiltration) of oceanic lithosphere, followed by subduction zone recycling and long-term storage of this lithosphere. As a process for creating trace element-enriched mantle, metasomatism is not a new idea and has been invoked both for continental lithosphere [*Frey and Green*, 1974; *Brooks et al.*, 1976; *Menzies and Murthy*, 1980; *Menzies*, 1983] and oceanic lithosphere [*Zindler et al.*, 1979; *Kay*, 1979; *Hawkesworth et al.*, 1979, 1984; *Richardson et al.*, 1982; *Roden et al.*, 1984; *Hart et al.*, 1986; *Halliday et al.*, 1992; *Class and Goldstein*, 1997; *Niu et al.*, 1996, 1999; *Niu and O'Hara*, 2003]. The process we envision is much like the SYS model of *Zindler et al.* [1979], and the auto-metasomatic model of *Roden et al.* [1984]. We envision it operating on newly formed lithosphere close to spreading centers, as illustrated by *Niu et al.* [1999] and *Niu and O'Hara* [2003].

[7] We show that a lithosphere impregnated 2.5 Ga with a small-degree upper mantle melt can evolve

to the present-day isotopic composition of EM2. This model provides an EM reservoir with much greater volume than that of oceanic crust and sediment. A more voluminous "package" will have greater resistance to mixing within the convecting mantle and therefore have greater possibility of staying an isolated body for the required 2.5 Ga evolution time. Another benefit of this model is that the lithosphere will be isolated and protected from subduction zone processing (such as elemental fractionations that occur within the subducted oceanic crust and sediments during metamorphism and devolatilization).

2. Geologic Setting

[8] The Samoan islands and seamounts are centered on 14°S latitude and stretch from 169–173°W longitude (Figure 2). They sit ~100 km north of the northern termination of the Tonga Trench, on ~110 Ma oceanic crust of the Pacific Plate which is moving 25.8° WNW at 7 cm/yr [*Sella et al.*, 2002]. The Samoan volcanoes separate into two topographic ridges, both subparallel to the direction of plate motion: the Savai'i - Upolu - Tutuila - Malumalu group define the southwestern (and generally older) lineament, and the Muli - Ofu/Olosega - Ta'u - Vailulu'u group define the northeastern (and younger) lineament. We will designate these the "Malu" and "Vai" Trends, respectively. The recently mapped leading-edge seamount, Vailulu'u, rises from 5000 meter seafloor to a summit depth of 590 m [*Hart et al.*, 2000]. Recent volcanic activity at Vailulu'u has been documented with the following observations: elevated water temperatures and particulate contents within the summit crater, a halo of intense particulate matter surrounding the summit in the depth range of 600–800 meters, high Mn concentrations and $^3He/^4He$ ratios (up to 9 R_A) in the crater water, swarms of seismicity, and dredged rock samples with U-series ages of 5–50 years [*Hart et al.*, 2000]. The age-progression heading west from this present-day hot spot location approximately follows the plate velocity of 7 cm/yr and includes the seamounts Lalla Rookh, Combe, and Alexa, which is 1750 km west of Vailulu'u [*Duncan*, 1985; *Natland and Turner*, 1985; *McDougall*, 1985; *Hart et al.*, 2000; Hart et al., unpublished data, 2003]. Malulu seamount and Rose Atoll to the east of Vailulu'u do not have Samoan isotopic signatures (Hart et al., unpublished data, 2003), and are most likely associated with the Cook-Austral lineament.

[9] As if burning the candle at both ends, post-erosional volcanism has been extensive on the westernmost island of Savai'i (with the most recent eruptive episode taking place from 1905–1911) as well as being documented on the islands of Upolu and Tutuila (but here, all prehistoric, and much less extensive) [*Kear and Wood*, 1959; *Keating*, 1992]. Although the pervasive post-erosional veneer on Savai'i has disrupted the age-progression model (Savai'i should be ~5 Ma based on the plate velocity model) and has lead to debates about the origin of the Samoan volcanoes [e.g., *Natland*, 1980], we believe there is little doubt about the chain originating from hot spot volcanism. The atypical volume of post-erosional volcanism on Savai'i is possibly due to the complicated tectonic setting of the volcanic chain. Since Savai'i is closest to the Tonga Trench, it is reasonable that bending stresses are facilitating additional melt extraction from the upper mantle [e.g., *Hawkins and Natland*, 1975; J. H. Natland, The Samoan Chain: A shallow lithospheric fracture system, manuscript in preparation, 2003].

[10] Tectonic reconstruction of the region [*Brocher and Holmes*, 1985; *Pelletier et al.*, 1998; *Zellmer and Taylor*, 2001] show that the transform-fault bounding the northern Tonga Trench evolved ~6–8 million years ago from the fossil Vitiaz Trench in response to opening of the Lau back-arc basin. Studies of the chemical characteristics of the northern Lau back-arc basin seamounts and seismic profiling beneath the basin collectively suggest leakage of Samoan plume material into the northern Lau Basin through a tear, or window, in the paleo-slab of the Pacific Plate subducted at the Vitiaz Trench. Geochemical evidence includes high $^3He/^4He$ lavas of some Lau Basin seamounts [*Poreda and Craig*, 1992; *Turner and Hawkesworth*, 1998], with trace element and isotopic compositions which are more characteristic of OIBs than MORBs or IABs [*Ewart et al.*, 1998;

Danyushevsky et al., 1995; *Wendt et al.*, 1997]. Seismic studies by *Millen and Hamburger* [1998] and *Chen and Brudzinski* [2001] illustrate a remnant slab of the Vitiaz subduction that has detached from the warped Pacific Plate, thereby providing an unobstructed path for melt/mantle migration from the Samoan plume into the Lau Basin. By speculation, this suggests that the Samoan plume beneath the Pacific Plate is much more widespread than the discrete lineament of volcanoes would indicate. Also, the exact location of the Samoan volcanoes may not necessarily be where the plume upwelling is "strongest", but instead where the plume fortuitously intersects a structural weakness imparted to the lithosphere by tectonic stresses of the local area. The en-echelon nature of the volcanic edifices may provide witness to this structural control (see Natland, manuscript in preparation, 2003, for a full discussion of this idea).

3. Samples and Analytical Details

3.1. Sample Locations and Descriptions

[11] Rock samples utilized in this study have been collected from both land and sea. The seamounts Vailulu'u, Muli, and Malumalu, along with submarine portions of Ta'u, were dredged during the 1999 AVON2/3 cruise of the R/V Melville. Land-based sampling of Savai'i and Upolu, conducted in 2001, was aimed at expanding the coverage of "old shield" (namely, the Fagaloa Volcanic Series [*Kear and Wood*, 1959]), thereby establishing a greater temporal coverage of the Samoan plume. On Upolu, we sampled the southwestern exposure of the Fagaloa Volcanics; this is a topographic high with well-developed river valleys referred to as A'ana by the local inhabitants. Our Upolu samples primarily come from along or near the Matafa'a coastline and Fagalei Bay. Samples from Savai'i were collected from the north-central shore, where exposures of Fagaloa Volcanics were mapped over a 20 km^2 relative topographic high [*Kear and Wood*, 1959]. This area is bound to the east by the village of Vaipouli, contains the Muliolo and Eatelele Streams, and is bound to the west by an escarpment that leads down to the village Paia.

[12] Subaerial sampling of Ta'u, the youngest island of the chain, was conducted in 1999 and was principally concentrated along the coastline. The sampling was temporally diverse, in that all five of the volcanic series mapped by *Stice and McCoy* [1968] are represented. Unlike the older and larger islands of Savai'i and Upolu, Ta'u Island manifests from only one main shield volcano; this simplified structure is reflected in the isotopic homogeneity observed for Ta'u, as will be discussed in following sections.

[13] Phenocryst abundances in Samoan lavas range from 0% to 50% and include the following minerals in decreasing modal abundance: olivine, clinopyroxene, plagioclase, orthopyroxene, and Ti-augite. Phenocrysts are most common in samples from Vailulu'u and least common in samples from Savai'i and Upolu. In thin section, some samples show two populations of olivine in which a coarse-grained population (2–10 mm) shows resorption boundaries and a smaller-grained population (1–2 mm) shows almost no embayed crystal boundaries. However, for most samples, olivine major element compositions (Jackson et al., unpublished data, 2003) show that phenocrystic olivines are in Mg-Fe equilibrium with the coexisting liquids. Some samples (especially T14) have glomerocrysts of olivine (±spinel). Plagioclase, clinopyroxene, and oxides are the most common matrix minerals. Hand-samples can generally be classified as aphanitic basalt, olivine basalt, picrite or (rarely) ankaramite. Alteration, in the form of iron-oxide, is most prevalent in the Savai'i and Upolu samples. Sample 63-11 from Vailulu'u crater shows hydrothermally precipitated quartz rinds along some cracks and grain boundaries.

3.2. Analytical Techniques

[14] Techniques reported here are for samples described above. Additional subaerial samples from Savai'i, Upolu, Tutuila and Ta'u have been collected by K. A. Farley and J. H. Natland over the last two decades and analyzed by K. A. Farley for Sr-Nd-Pb-He isotopic compositions. Additional subaerial samples from Savai'i and Upolu have been collected and analysed for major and trace elements and Sr-Nd-Pb isotopes by M. Regelous.

We include these data in the present manuscript, as they are previously unpublished; any differences in analytical techniques are reported in the corresponding data tables.

[15] Sr, Nd, and Pb isotopic analyses were carried out with conventional ion exchange procedures (references in *Taras and Hart* [1987]), using whole rock powders, prepared in an agate shatterbox, and leached for 1 hour in warm 6.2 N HCl. The TIMS techniques are described by *Hauri and Hart* [1993]. Sr and Nd isotope data carry 2σ precisions of ±35 ppm and ±40 ppm, and are reported relative to 0.71024 (NBS 987) and 0.511847 (La Jolla), respectively. Some samples run for Sr and Nd by NEPTUNE multicollector ICP/MS at W.H.O.I. are of comparable precision to TIMS anaylses. The precision of TIMS Pb data is taken to be 0.05% per mass unit after fractionation-correcting to the NBS 981 values given by *Todt et al.* [1996]. Pb isotopic compositions of some samples were also determined on the P54 multicollector ICP/MS in Lyon, with 2σ precisions of all ratios of ~200 ppm. Additionally, the Upolu and Savai'i sample suite was analyzed on the NEPTUNE multicollector ICP/MS at W.H.O.I.; using a Tl internal standard, the 2σ external reproducibility for these samples was ±100 ppm or better for all ratios [see *Hart et al.*, 2002]. Helium isotopic compositions ($^3He/^4He$ R_A, relative to atmospheric standard) of olivine and/or fresh glass separates (~1–3 mm) were determined at W.H.O.I. by in vacuo crushing, using methods described in *Kurz et al.* [1996]. Analytical errors average ±0.2 Ra at 2σ, for helium concentrations ranging from $\sim10^{-8}$ to 10^{-6} cc/gram. Os isotopic compositions on a select group of olivine-rich samples were determined by sparging of OsO_4 into W.H.O.I.'s Finnigan Element Magnetic Sector ICP-MS, following a flux fusion sample preparation (see *Hassler et al.* [2000] for a detailed Os analytical technique). Fusion blank corrections resulted in 0.06–1.22% corrections to the $^{187}Os/^{188}Os$ ratios. Major elements and some trace elements (Ni, Cr, Sc, V, Ga, Cu, Zn) in unleached whole rock powders were measured by XRF, and all other trace elements by ICP/MS at Washington State University [*Hooper et al.*, 1993]. Submarine glasses have been analyzed for major elements by electron microprobe at Massachusetts Institute of Technology.

3.3. Sample Preservation/Quality

[16] Despite sampling of lavas from older shield and submarine settings, the quality of preservation is generally very good. The Th/U ratios of the sample suite fall entirely within 4.5 ± 1.5 (with the exception of sample S15 at Th/U = 6.7) and show a slight (although rough) positive correlation with Th concentrations. The Ba/Rb ratios have an average of 9.3 ± 1.8 at 1σ (near the canonical value of ~12 for fresh ocean island basalts [*Hofmann and White*, 1983]) and are inversely correlated with Rb concentrations; significant exceptions to this correlation are samples 79-4, S15, and S25, with Ba/Rb ratios of 17.2, 14.0, and 3.7, respectively. We take these two proxies of alteration as indications that elements as or less mobile than Rb and U are very nearly pristine for most samples. However, elevated Rb/Cs ratios (176 ± 70 at 1σ) in the subaerial Upolu and Ta'u samples are most likely explained by chemical weathering and contrast strongly with the roughly canonical values (85–95 [*Hofmann and White*, 1983]) represented by the remaining suite (97 ± 30 at 1σ).

4. Age Relationships and Age Progression

[17] Vailulu'u seamount, the most easterly volcano in the Samoan chain, is currently active and believed to be the present-day hot spot center [*Hart et al.*, 2000]. U-series data constrain two samples from Vailulu'u's summit region to be less than 50 years old; 7 other samples from six dredge locations show excess $^{230}Th/^{238}U$, evidence of ages less than a few hundred thousand years (Sims and Hart, manuscript in preparation, 2004). The oldest K-Ar age from Tau Island is 0.3 Ma [*McDougall*, 1985]. The youngest volcanic series on Tau (Faleasao) is probably younger than 37,000 years, based on ^{14}C ages of coral inclusions in these volcanics (Hart, unpublished data, 2003). Additionally, there was an underwater eruption just west of Tau in 1866 (see description in *Keating* [1992]), evidence that Tau is still in an active shield-building stage.

Table 1. 40/39 Argon Ages From Upolu and Savai'i, Western Samoa[a]

Sample Number	Location	Steps Used/ Total Steps	^{39}Ar Fraction Used	40/39 Total Fusion, my	Weighted Plateau, my
U10	Upolu, A'ana Shield	5/7	3.1–98.8%	0.972 ± 0.020	**0.933 ± 0.011**
U12	Upolu, A'ana Shield	5/6	0–92.8%	2.68 ± 0.03	**2.65 ± 0.02**
S11	Savai'i, Manase Shield	3/6	4.4–64.7%	0.900 ± 0.122	**0.236 ± 0.052**
S23	Savai'i, Manase Shield	5/6	0–91.3%	0.590 ± 0.024	**0.386 ± 0.014**
91SVK-7	Savai'i, Vanu River Shield	–	–	2.05 ± 0.?	–

[a] Step-release heating from 600°–1400°C. 2-sigma errors include measurement uncertainties, and uncertainty in J-value (flux gradient from FCT-3 biotite monitor), but not uncertainty in monitor age. 91SVK-7 is a trachyte cobble from the lower Vanu River, analyzed by K. A. Farley.

As yet, we have no age constraints on Muli seamount, though the samples dredged from there appear "older" than those dredged from Vailulu'u or Tau. Samples from three dredges on Malumalu show ^{230}Th/^{238}U excesses similar to those on Vailulu'u (Sims and Hart, manuscript in preparation, 2004), suggesting that Malumalu is not significantly older than Vailulu'u. K-Ar ages for the Pago and Masefau shields on Tutuila range from 1.0–1.9 Ma [*McDougall*, 1985; *Natland and Turner*, 1985], somewhat younger than the 2.3–2.7 Ma expected from plate motion considerations.

[18] New high-quality ^{40}Ar/^{39}Ar step-release plateau ages are given in Table 1 for the northern shield on Savai'i and the SW shield on Upolu, along with an earlier 40/39 total fusion age for the Vanu River shield on Savai'i. Previous K-Ar ages on the eastern Upolu shield range from 1.54–2.74 Ma [*Natland and Turner*, 1985]; our western shield ages are 0.93 and 2.65 Ma. The older age agrees with the older ages of the eastern shield, though both shields appear younger than the expected plate model age range of 3.9–4.5 Ma. The 0.93 Ma sample (U10) was collected from well within the interior of the eroded SW shield massif, and appears to be reliable evidence for an extended (~2 Ma) period of shield building on Upolu.

[19] There are no published radiometric ages from Savai'i. On the basis of a plate velocity of 7 cm/year, the age expected for shield initiation on Savai'i is about 5.2 Ma; the two ages reported in Table 1 for the northern (Manase) shield, 0.24 and 0.39 Ma, are far younger than this expected plate age. *Kear and Wood* [1959] mapped this northern area as shield largely on the basis of abundant surface streamflow. However, we found no obvious evidence of unconformable erosional morphology in this area, and the geochemical evidence discussed below strongly suggests that this map unit is akin to the post-erosional basalts on Savai'i and Upolu, and unlike the Upolu shield basalts. The young ^{40}Ar/^{39}Ar ages are consistent with a re-assignment of this unit to post-erosional status. In the southern interior of Savai'i, *Kear and Wood* [1959] mapped a small exposure of shield in a gorge on the upper Vanu River. This area is virtually inaccessible, but a trachyte cobble was collected from the lower Vanu River by one of us (KAF) in 1991, and the 40/39 total fusion age of this trachyte is 2.05 Ma (Table 1). While still significantly younger than a plate-model age, this trachyte age is nevertheless very important as it shows that not all of the volcanism on this island can be related to proximity to the Tonga trench, as suggested by *Natland* [1980]; at 2 Ma, the corner of the Tonga trench was almost 400 km west of Savai'i [*Bevis et al.*, 1995]. On the other hand, there can be little doubt that Savai'i has been massively re-surfaced with posterosional volcanism as proposed by *Natland* [1980]. The early history of this island will probably only be accessed by dredging on the deeper flanks, where slope failure provides an exposed record.

[20] All in all, the radiometric ages of shield lavas in Samoa are broadly consistent with a simple age-progressive hot spot track, in that ages generally increase from east to west. However, it is clear that shield ages are overall younger than those predicted by plate motion, most likely because the oldest incipient shield lavas are not sampled at the

surface of present-day volcanoes. While the earliest stages of shield building on Tutuila, Upolu and Savai'i are thus far missing from the sampled record, it would be premature to use this as evidence against a simple hot spot model for Samoa.

5. Magma Generation and Crystal Fractionation

[21] In major element composition, the Samoan basalts and trachy-basalts analyzed for this study are clustered just above the alkali-tholeiite line [*MacDonald and Katsura*, 1964] at 44–49 wt% SiO_2 (Figure 3; Tables 2 and 5). Samples that fall into the tholeiitic field are, for the most part, from Vailulu'u Seamount, and three of these are highly picritic. Post-erosional lavas (on Savai'i, Upolu and Tutuila) overlap with the shield volcanics, but extend to much greater silica-undersaturation (basanites and nephelinites down to 36 wt% SiO_2 [*Hawkins and Natland*, 1975; *Johnson*, 1983; *Hauri and Hart*, 1997]). Mg#'s (molar percent $Mg/[Mg + Fe^{2+}]$) range from 40 in the differentiated Muli samples to 85 in the Vailulu'u picrites. The low MgO/high SiO_2 end of the suite is (vaguely) dominated by samples from Vailulu'u, Malumalu, and Upolu; on the other hand, high MgO/low SiO_2 samples are mainly from Savai'i, Tutuila, and Ta'u. Also plotted on some co-variation plots of Figure 3 are trajectories of near-solidus primary melt compositions at varying pressures of melting in the garnet stability field, using algorithms defined by *Herzberg and Zhang* [1996] through experiments on KLB-1 peridotite. Recent experiments on another fertile peridotite (KR4003 starting material [*Walter*, 1998]) show primary melt compositions with a general shift to higher MgO at a given pressure (by ~5% in the 4–5 kbar pressure range). Most of the Samoan lavas have undergone some amount of crystal fractionation, as indicated by the fact that they have significantly lower Mg#'s than any estimated primary mantle melts.

[22] The relationship between Mg#'s and CaO shown in Figure 4 provides information regarding both magma generation and crystal fractionation. Plotted along with lava compositions is the trajectory of primary mantle melt compositions [*Herzberg and Zhang*, 1996]. To assess the extent of differentiation and the minerals involved, we have used the pMELTS program [*Ghiorso et al.*, 2002] to model anhydrous fractional crystallization (at a best-fit pressure of 3–4 kbar) of some of the more primitive lavas (Ta'u samples T14 and T48, Vailulu'u sample 63-3, and Malumalu sample 78-1). PMELTS trajectories calculated with 1 wt% H_2O, at a given pressure, are nearly identical to anhydrous runs at 1 kbar lower pressure (not shown). All starting compositions have olivine as the second liquidus phase (after spinel), leading to a negative slope for the liquid path on Mg# against CaO (Figure 4). The kink to positive slopes on the liquid lines of descent marks the crystallization of cpx ± olivine ± plagioclase. As CaO content of the starting magma decreases, clinopyroxene (cpx) saturation occurs at lower Mg#'s. A suite of submarine Samoan glasses (Table 3) has also been plotted on Figure 4 and shows that true liquids follow the lines of crystal fractionation predicted by pMELTS.

[23] Suites of lavas from each volcano cluster along fairly distinct Mg#-CaO fractionation trends. By projecting the olivine fractionation trends for the different volcanoes back to the primary mantle melt trajectory, we can interpret that the Samoan lavas were generated in the pressure range of 2.5–6 GPa; the order of increasing pressure of melting would be Vailulu'u < Ta'u/Malumalu < Tutuila/Upolu/Savai'i. The extrapolated primary magmas in this model have an extensive range in MgO, from 11 wt% at lowest pressure to 22 wt% at 6 GPa. To get integrated pressures of melting as high as 6 GPa, melting would have to initiate at depths exceeding 180 km and terminate at depths much deeper than the thickness of the lithosphere (~100 km). Given estimates for potential temperatures of plumes (~1550°C [*Watson and McKenzie*, 1991]) and water-undersaturated solidi [*Hirth and Kohlstedt*, 1996], the depth of *initial* melting is close to 180 km and therefore cannot be the integrated depth of melting. The above approach is strictly valid only if the lavas from each volcano are derived from a constant source composition. We

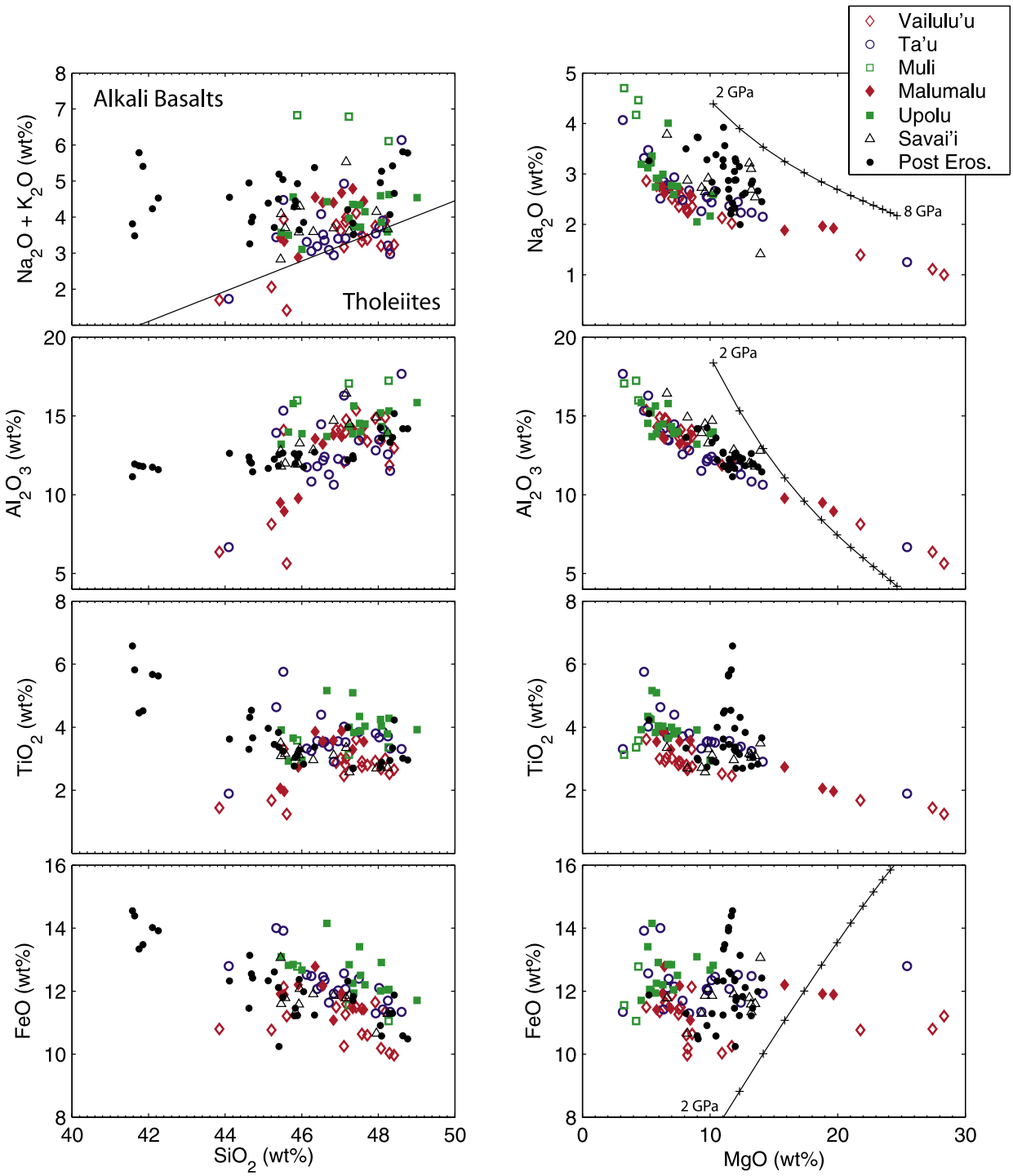

Figure 3. Major element compositions of Samoan basalts. Plots include data from *Hauri and Hart* [1997] for Savai'i lavas. Alkali-tholeiite line is from *MacDonald and Katsura* [1964]. Trajectories of compositions for primary melts from fertile peridotites are plotted on some of the MgO diagrams, using the algorithms of *Herzberg and Zhang* [1996] in the pressure range of 2–8 GPa (tick marks every 0.5 GPa).

Table 2 (Representative Sample). Sample Information and Chemical Data for 70 Total Samples of Samoan Basalts
[The full Table 2 is available in the HTML version of this article at http://www.g-cubed.org]

Volcano	Vailulu'u	Vailulu'u	Vailulu'u	Vailulu'u	Vailulu'u	Vailulu'u	Vailulu'u	Vailulu'u	Vailulu'u
Sample	**63-3**	**63-5**	**63-13**	**64-1**	**68-3**	**68-10**	**68-11**	**68-28**	**68-30**
Latitude (°S)	14.218	14.218	14.218	14.260	14.217	14.217	14.217	14.217	14.217
Longitude (°W)	169.059	169.059	169.059	169.056	169.064	169.064	169.064	169.064	169.064
Water Depth (m)	920	920	920	2630	780	780	780	780	780
Phenocrysts	10% Ol	5% Ol Tr Cpx	Aphyric	3% Ol 2% Cpx	10% Ol	Aphyric	60% Ol	Tr Ol	Aphyric
Major elements (wt%)									
SiO_2	48.29	48.07	47.16	47.71	47.84	48.18	45.61	47.42	48.41
Al_2O_3	11.88	13.42	14.76	13.38	11.86	14.90	5.64	15.37	12.96
TiO_2	2.52	2.67	3.01	2.80	2.55	3.00	1.24	3.62	2.66
FeO*[a]	10.03	10.19	11.59	10.60	10.51	11.34	11.21	11.49	9.97
MnO	0.17	0.17	0.18	0.17	0.17	0.19	0.17	0.18	0.17
CaO	12.78	13.70	12.37	13.48	12.75	12.09	6.23	12.30	14.11
MgO	10.94	8.26	6.57	8.15	10.68	6.06	28.34	5.01	8.21
K_2O	0.96	0.96	1.28	1.07	0.99	1.13	0.41	1.25	0.96
Na_2O	2.13	2.24	2.72	2.31	2.36	2.76	1.00	2.86	2.27
P_2O_5	0.29	0.32	0.37	0.33	0.29	0.36	0.14	0.50	0.30
Mg#[b]	69.58	62.96	54.31	61.72	68.07	52.85	84.13	47.77	63.33
Trace Elements (ppm)									
Ni	285	110	59	104	285	47	1067	21	124
Cr	879	498	110	455	822	66	2771	50	542
V	299	335	339	329	300	351	154	394	314
Ga	16	20	20	19	20	18	6	24	21
Cu	86	59	58	85	82	68	103	26	79
Zn	84	85	95	82	89	94	86	99	82
Cs	0.29	0.13	0.28	0.33	0.30	0.38	0.09	0.38	0.19
Rb	24.7	22.2	33.6	29.6	26.6	24.7	9.3	33.1	22.1
Ba	216	210	279	236	218	239	90	292	209
Th	3.92	3.72	5.15	4.06	4.04	4.67	1.75	4.96	3.56
U	0.85	0.82	1.07	0.87	0.87	0.98	0.54	1.03	0.79
Nb	35.41	34.74	45.14	38.97	36.44	42.41	15.57	48.08	34.11
Ta	2.41	2.32	3.08	2.59	2.50	2.90	1.01	3.25	2.31
La	28.82	28.95	37.44	31.12	29.29	33.97	13.04	41.67	27.34
Ce	58.36	58.29	74.35	63.12	58.67	67.35	26.90	84.11	55.47
Pb	2.41	2.08	2.76	3.04	2.50	2.96	0.66	2.65	2.36
Pr	6.84	7.00	8.74	7.58	6.86	8.07	3.19	10.01	6.83
Nd	27.84	29.05	35.38	31.29	29	32.91	12.96	40.82	28.27
Sr	378	404	470	424	387	434	181	521	392
Zr	168	178	218	189	168	202	80	222	175
Hf	4.46	4.69	5.76	5.13	4.43	5.45	2.03	5.92	4.72
Sm	6.45	6.80	7.83	7.33	6.46	7.62	3.01	9.26	6.73
Eu	2.03	2.13	2.45	2.26	1.99	2.39	0.93	2.81	2.13
Gd	5.75	6.16	7.09	6.72	5.81	6.83	2.58	8.06	6.06
Tb	0.88	0.92	1.08	1.02	0.86	1.06	0.40	1.23	0.93
Dy	4.90	5.17	5.88	5.68	4.83	5.95	2.24	6.64	5.27
Ho	0.87	0.94	1.10	1.01	0.88	1.11	0.41	1.20	0.94
Y	22.08	24.09	27.50	26.43	22.46	27.93	10.47	31.28	24.21
Er	2.14	2.32	2.70	2.53	2.13	2.77	0.99	2.96	2.28
Tm	0.28	0.30	0.35	0.33	0.28	0.36	0.13	0.38	0.30
Yb	1.60	1.75	2.02	1.91	1.63	2.12	0.74	2.24	1.68
Lu	0.24	0.25	0.30	0.27	0.24	0.31	0.11	0.32	0.25
Sc	40.4	42.6	33.4	42.2	40.9	34.0	22.8	32.8	45.1

[a] All Fe reported as FeO.
[b] Mg# = molar ratio of MgO/(MgO + 0.85 * FeO).

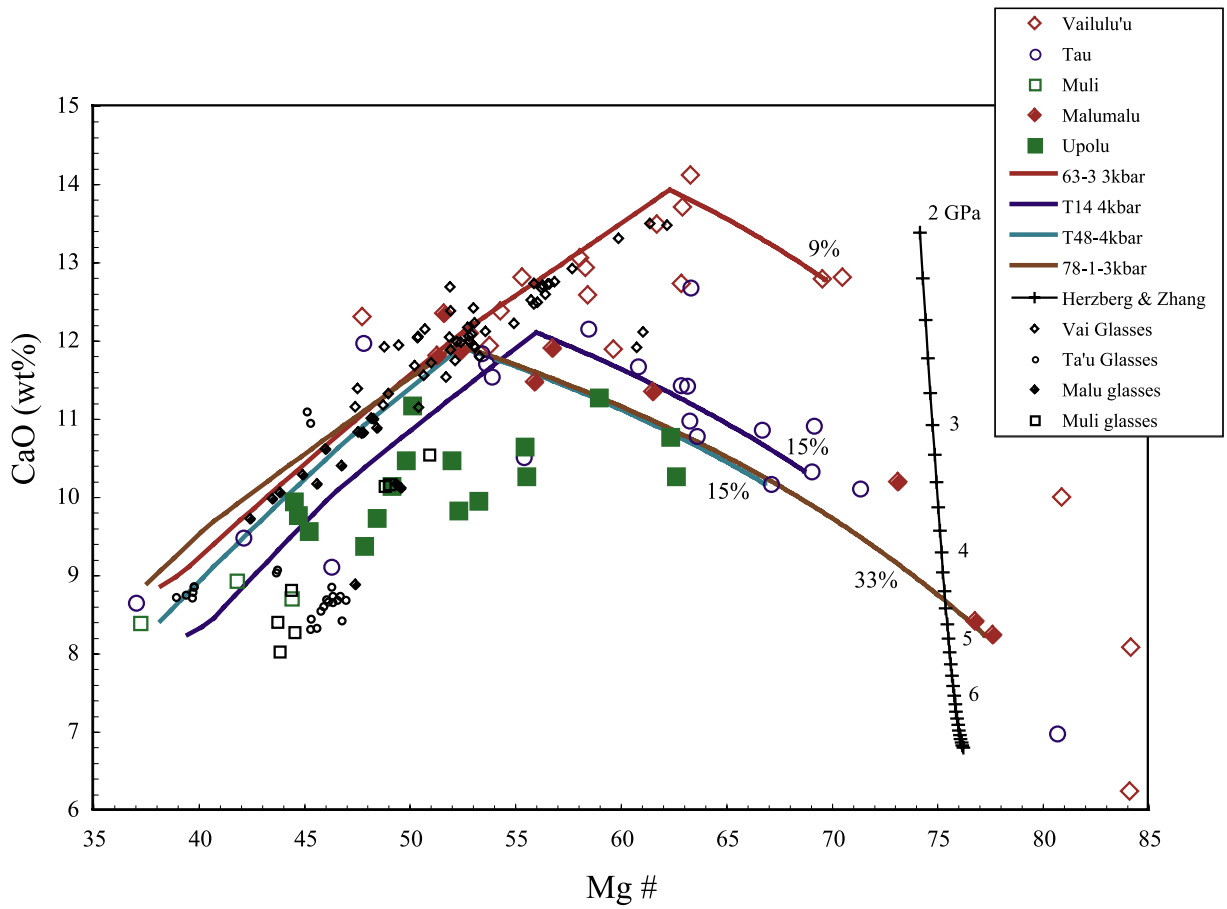

Figure 4. CaO plotted with Mg#'s for Samoan lavas. Mg# is calculated as molar percentage of $Mg/(Mg + Fe^{2+})$ where Fe^{2+} is taken to be 85% of reported FeO. Compositions of primary melts from fertile peridotite are plotted using algorithms from *Herzberg and Zhang* [1996] in the pressure range of 2–8 GPa; tic marks are every 0.2 GPa. Crystal fractionation trends have been calculated using pMELTS at pressures of 3 and 4 kbar for best fits to compositional trends starting with some of the most MgO-rich lavas. Mass of olivine crystallized (expressed as a percent of the total initial mass) before clinopyroxene saturation is noted at the high Mg# end of the liquid lines of descent. Tics along liquid lines mark fractions of initial mass crystallized in steps of 10%, starting with 20%. Primary melts can be interpreted to have integrated depths of melting from 2.5–6 GPa, but CaO variations in the lavas more likely represent CaO contents of a heterogeneous mantle source. Plot includes data from *Hauri and Hart* [1997] for Savai'i lavas.

conclude that this CaO index for pressure of melting is rather rickety, given the isotopic variations between volcanoes that will be discussed further into the paper, and that the order of "increasing pressure of melting" is clouded by the extent to which melts were generated from a depleted (low CaO) material.

[24] The Vailulu'u samples are not only high in CaO (also $Ca/(Ca + Na)$ and CaO/Al_2O_3) at a given MgO value, but they are also low in Na_2O, TiO_2, and FeO. This suggests they have the most promise in being interpreted as the shallowest, highest degree partial melts in the whole sample suite [*Kinzler and Grove*, 1992; *Herzberg and Zhang*, 1996; *Walter*, 1998]. Melting beneath the other volcanoes may be initiated deeper in the mantle, possibly due to (1) differences in source composition (required by isotopic variations), (2) higher potential temperatures and mantle flow rates, or (3) mantle flow paths which affect melt-solid segregation. The Vailulu'u suite is fit fairly

Table 3 (Representative Sample). Major Element Electron Probe Data on Submarine Glasses for 96 Total Samples From Samoa [The full Table 2 is available in the HTML version of this article at http://www.g-cubed.org]

Sample Number	Volcano	SiO_2	TiO_2	Al_2O_3	FeO*[a]	MnO	MgO	CaO	Na_2O	K_2O	P_2O_5	n[b]
63-13	Vailulu'u	47.223	3.428	14.612	12.744	0.187	5.486	11.147	3.045	1.639	0.489	2
68-03	Vailulu'u	47.454	3.079	14.899	11.726	0.152	6.037	12.039	2.820	1.359	0.436	2
68-34	Vailulu'u	46.896	3.167	14.484	12.175	0.171	6.283	12.376	2.697	1.304	0.447	2
68-35	Vailulu'u	47.208	3.230	14.546	12.739	0.177	5.797	11.912	2.683	1.251	0.456	2
68-36	Vailulu'u	46.954	3.237	14.642	12.239	0.144	6.016	12.136	2.873	1.326	0.433	2
68-37	Vailulu'u	47.071	3.285	14.595	12.647	0.177	5.914	11.937	2.662	1.279	0.432	2
68-38	Vailulu'u	48.142	3.128	14.846	11.631	0.162	5.948	11.528	2.924	1.256	0.435	2
68-43	Vailulu'u	47.054	3.297	14.792	12.297	0.173	5.966	12.045	2.572	1.349	0.456	2
68-44	Vailulu'u	47.011	3.217	14.534	12.444	0.171	6.026	12.028	2.776	1.336	0.456	3
70-01	Vailulu'u	48.043	3.001	14.474	11.821	0.194	6.316	11.996	2.674	1.104	0.378	4
70-02	Vailulu'u	47.548	3.229	14.855	12.204	0.170	5.880	11.668	2.705	1.305	0.437	2
70-09	Vailulu'u	48.094	3.206	14.672	12.364	0.191	5.669	11.317	2.827	1.229	0.433	2
71-03	Vailulu'u	46.986	3.187	14.150	10.839	0.129	7.055	12.911	2.834	1.473	0.437	2
71-04	Vailulu'u	47.034	3.137	13.900	11.492	0.148	6.950	12.722	2.731	1.458	0.429	2
71-05	Vailulu'u	47.735	2.955	14.670	11.278	0.176	6.568	12.212	2.609	1.379	0.419	2
71-06	Vailulu'u	47.631	3.161	14.503	11.581	0.176	5.968	12.676	2.392	1.498	0.414	4
71-09	Vailulu'u	46.874	3.119	14.172	11.304	0.166	7.022	12.716	2.721	1.452	0.453	2
71-10	Vailulu'u	47.149	3.119	14.375	11.286	0.156	6.823	12.458	2.737	1.489	0.409	4
71-11	Vailulu'u	47.492	2.984	15.202	11.487	0.151	6.208	11.908	2.785	1.346	0.438	2
71-13	Vailulu'u	47.680	2.956	15.156	11.521	0.159	6.214	11.923	2.646	1.340	0.406	2
71-13D	Vailulu'u	47.799	2.994	15.288	11.351	0.180	6.188	11.792	2.723	1.300	0.385	4
71-14	Vailulu'u	46.956	3.133	14.127	11.395	0.148	6.994	12.668	2.676	1.460	0.444	2
71-16	Vailulu'u	47.679	3.013	15.199	11.551	0.168	6.013	11.736	2.837	1.351	0.451	3
71-22	Vailulu'u	48.190	2.961	15.655	11.406	0.176	5.540	11.138	3.042	1.490	0.403	4
71-23	Vailulu'u	46.975	3.129	14.136	11.314	0.155	6.959	12.697	2.689	1.483	0.462	2
71-24	Vailulu'u	46.963	3.077	14.133	11.199	0.164	6.979	12.717	2.860	1.457	0.451	2
71-25	Vailulu'u	47.021	3.163	14.108	11.105	0.162	6.987	12.746	2.804	1.480	0.425	2
71-26	Vailulu'u	47.099	3.099	14.144	11.369	0.191	6.841	12.510	2.822	1.486	0.441	2
71-27	Vailulu'u	47.094	3.100	14.074	11.273	0.168	6.973	12.581	2.807	1.473	0.457	2
71-28	Vailulu'u	46.886	3.090	14.304	11.446	0.215	6.969	12.483	2.773	1.452	0.382	3
72-02	Vailulu'u	45.953	3.662	15.543	12.494	0.179	5.401	11.380	3.268	1.613	0.508	2
72-04	Vailulu'u	46.292	3.432	14.939	11.785	0.172	6.365	12.222	2.915	1.415	0.463	2
72-07	Vailulu'u	46.014	3.488	15.055	11.808	0.173	6.359	12.410	2.794	1.449	0.449	2
72-10	Vailulu'u	46.842	2.944	13.296	11.599	0.157	8.682	12.103	2.641	1.268	0.468	2
72-12	Vailulu'u	46.324	3.465	15.072	11.824	0.180	6.298	12.159	2.850	1.417	0.412	4
72-13	Vailulu'u	46.549	3.000	13.300	11.869	0.183	8.775	11.905	2.664	1.307	0.448	2
73-01	Vailulu'u	47.342	2.933	15.048	11.551	0.160	6.028	11.977	2.881	1.639	0.442	3
73-03	Vailulu'u	47.213	3.140	15.089	11.877	0.165	5.905	11.709	2.922	1.510	0.470	2
73-04	Vailulu'u	47.495	2.942	15.108	11.582	0.194	5.972	11.872	2.766	1.636	0.431	2
73-07	Vailulu'u	47.364	2.985	15.016	11.470	0.140	6.162	12.073	2.975	1.402	0.412	2
73-12	Vailulu'u	47.585	2.955	15.137	11.211	0.176	5.996	11.976	2.860	1.655	0.449	2
73-13	Vailulu'u	47.603	3.020	15.122	11.447	0.160	6.111	12.052	2.695	1.374	0.417	2
73-15	Vailulu'u	47.268	2.991	15.260	11.335	0.199	5.963	11.967	2.995	1.614	0.409	2
WC1	Vailulu'u	48.855	2.527	12.550	10.614	0.178	8.339	13.467	2.242	0.919	0.309	3
WC2	Vailulu'u	48.765	2.588	12.860	10.628	0.113	8.062	13.491	2.270	0.913	0.310	3
WC3	Vailulu'u	47.956	3.268	14.805	11.958	0.138	5.427	11.164	3.220	1.602	0.463	3
WC4	Vailulu'u	47.921	3.377	14.836	11.645	0.159	5.708	11.546	2.941	1.450	0.416	3
WC6	Vailulu'u	47.966	3.035	14.887	11.251	0.168	6.199	12.108	2.706	1.291	0.388	3
WC7	Vailulu'u	48.467	2.689	13.209	10.765	0.197	7.676	13.297	2.388	0.982	0.329	3
74-2	Ta'u	48.214	3.654	14.988	13.116	0.236	3.984	8.720	4.147	1.953	0.988	2
74-3	Ta'u	45.513	5.399	14.097	14.034	0.216	5.537	10.951	2.784	1.007	0.462	2
74-5	Ta'u	48.400	3.728	15.000	12.699	0.220	3.999	8.854	4.157	1.942	1.002	2
74-10	Ta'u	48.508	3.688	14.903	12.865	0.231	3.987	8.752	4.124	1.946	0.995	2
74-11	Ta'u	48.409	3.715	14.991	12.852	0.235	4.030	8.715	4.151	1.924	0.977	2
74-12	Ta'u	45.473	5.356	14.017	14.165	0.220	5.556	11.096	2.668	0.991	0.459	2
74-13	Ta'u	48.502	3.708	14.870	12.819	0.217	4.024	8.786	4.197	1.916	0.960	2
74-14	Ta'u	48.315	3.737	15.028	12.813	0.210	4.032	8.858	4.123	1.914	0.971	2

[a] All Fe reported as FeO.
[b] n, number of analyses.

well by a crystal fractionation trend at a pressure of 3 kbar, and indicates cpx fractionation has likely occurred for most samples.

[25] For Ta'u and Malumalu, olivine fractionation clearly dominates the spread in lava compositions. A few samples with Mg#'s greater than ~73 have obviously accumulated olivine (they are phenocryst-rich), but most samples lie along olivine fractionation lines or at the intersection of the olivine control line and cpx saturation (Figure 4). Three Ta'u samples have compositions close to those of the Muli samples and have surely undergone cpx fractionation; these samples also have the lowest concentrations of the cpx-compatible elements vanadium and scandium in the whole suite (not shown). If parental magmas for all the Ta'u and Muli samples were of nearly the same composition, liquid lines of descent indicate that these low Mg# lavas have undergone about 15% more olivine fractionation than samples T14 and T48, along with 25% cpx fractionation.

6. Isotopes and Trace Elements

6.1. Global Context

[26] Plotted on the three-dimensional axes of Figure 5 is the mantle tetrahedron of *Hart et al.* [1992], with data from the ocean island chains which quintessentially define the coordinates for each of the mantle components, EM1, EM2, and HIMU. Data arrays for individual island chains, as well as groups of taxonomically similar island chains, quasi-linearly extend from one of the three OIB end-member components toward FOZO, the common mantle; very notable is the serious lack of elongation of arrays along tie-lines between the three OIB components. It is clear that EM2 lavas in general, and Samoan lavas in particular, dominate the range in oceanic $^{87}Sr/^{86}Sr$ values, but are much less variable in $^{143}Nd/^{144}Nd$ than EM1. The variation in $^{206}Pb/^{204}Pb$ found in EM2 basalts is small relative to the composite oceanic suite.

[27] Strontium, neodymium, lead, helium, and osmium isotope ratios for Samoan basalts are given in Tables 4 through 6. Isotope plots (Figures 6–9) show this new data along with data reported in previous studies [*Wright and White*, 1987; *Farley et al.*, 1992; *Hauri and Hart*, 1993]. The wide range in $^{87}Sr/^{86}Sr$ values, 0.7044–0.7089, is correlated with the more narrow range of 0.51293–0.51251 for $^{143}Nd/^{144}Nd$ (Figure 6). Each island or seamount tends to show a unique field of isotopic compositions that, as will be shown, evolve systematically through space and time. Malumalu Seamount contributes the furthest afield EM2 signature and now defines the most radiogenic $^{87}Sr/^{86}Sr$ value (0.7089) of all oceanic lavas. At lower $^{87}Sr/^{86}Sr$ (0.7044), near estimates for Bulk Silicate Earth (BSE), the Samoan array is split into two prongs - the "serpent's tongue". Both prongs, one comprised of lavas from Ta'u Island and the other, at higher $^{143}Nd/^{144}Nd$, comprised of lavas from Upolu and Tutuila, are significantly elevated (at ϵ_{Nd} of +3 and +5, respectively) over the BSE value of 0.512638 [*Hamilton et al.*, 1983]. The other notable EM2 hot spot, the Societies, overlaps the lower prong of the "serpents tongue", and is generally shifted to less-enriched Sr and Nd values. The classic EM1 array (Pitcairn) lies well below the Samoa array.

[28] The sample group on the high $^{143}Nd/^{144}Nd$ prong is also the lowest in $^{206}Pb/^{204}Pb$ and $^{207}Pb/^{204}Pb$ of all the shield lavas (Figure 7). All Samoan lavas lie to the right (high $^{206}Pb/^{204}Pb$ side) of the terrestrial Pb Geochron and are in the mid-range of the elongate, worldwide OIB cluster; they are situated entirely above the Northern Hemisphere Reference Line (NHRL [*Hart*, 1984]) in both $^{207}Pb/^{204}Pb$ and $^{208}Pb/^{204}Pb$ (Figures 7 and 8). The most radiogenic $^{206}Pb/^{204}Pb$ compositions (19.4) are found not in the highest $^{87}Sr/^{86}Sr$ samples, but in samples from Vailulu'u Seamount (of moderate $^{87}Sr/^{86}Sr \sim 0.7055$). On the other hand, the highest $^{207}Pb/^{204}Pb$ (15.65) and $^{208}Pb/^{204}Pb$ (39.8) correspond to the EM2-defining Malumalu lavas, implying that EM2 is an old reservoir of high time-integrated Th/U.

[29] The Society array (not shown in Figure 7) is much steeper, falling below the NHRL at low $^{206}Pb/^{204}Pb$ and crossing above it, to overlap the Malu trend data from Samoa. Interestingly, the highest $^{87}Sr/^{86}Sr$ sample from Tahaa (Societies)

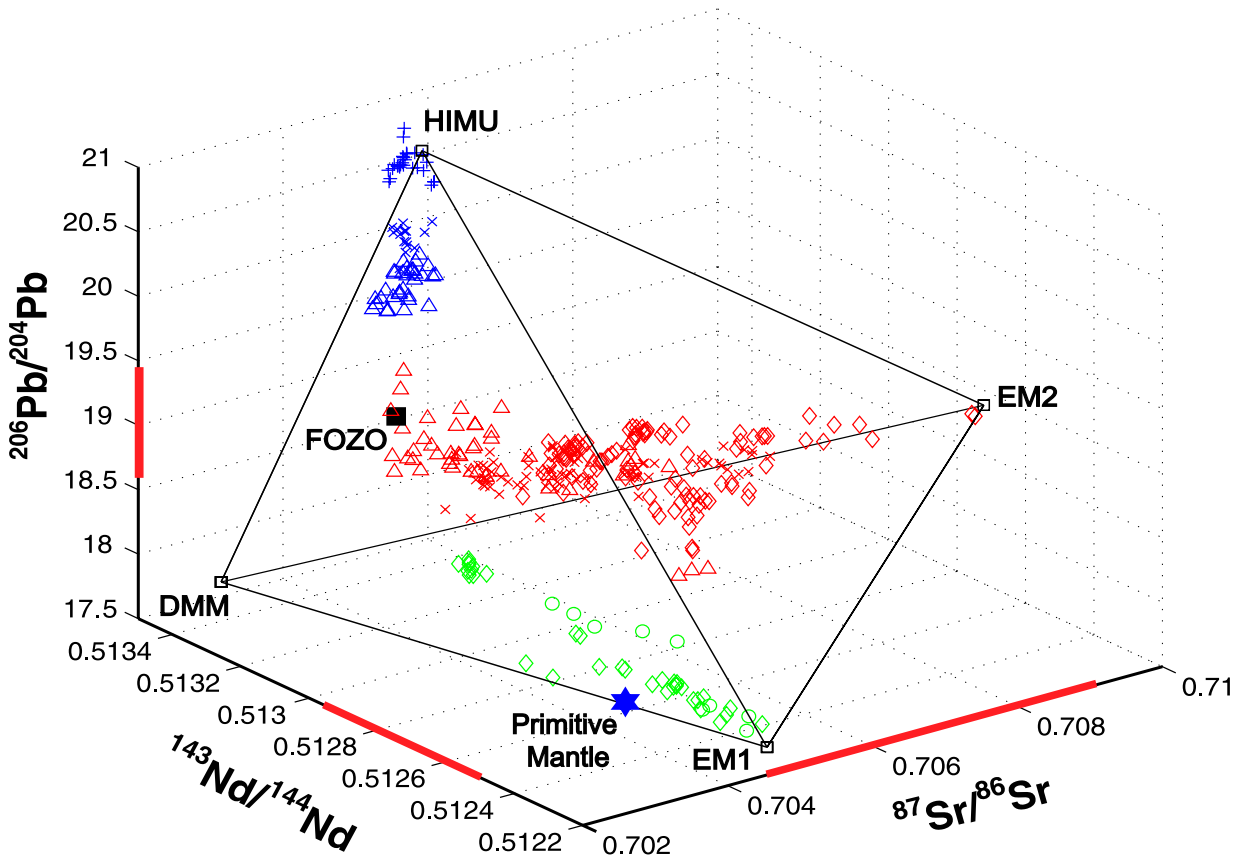

Figure 5. Mantle tetrahedron of *Hart et al.* [1992]. Arrays from end-member defining island chains have been plotted using the GEOROC database and data presented in this manuscript. Island chains plotted for HIMU are in blue and include Tubuaii (crosses), Mangaia (plusses) nd St. Helena (triangles). EM1 islands are in green and include Pitcairn (green diamonds) and Walvis Ridge (green circles). EM2 islands are in red and include Samoa (red diamonds), Societies (red crosses), and the Marquesas (red triangles). Red bars along the axes mark the range of values for the Samoan Islands. EM2 has been extended from its previous coordinate [*Zindler and Hart*, 1986] to values for $^{87}Sr/^{86}Sr$, $^{143}Nd/^{144}Nd$, and $^{206}Pb/^{204}Pb$ at 0.7090, 0.5125, and 19.3, respectively.

lies very close to our extreme $^{87}Sr/^{86}Sr$ sample in $^{207}Pb/^{204}Pb$ - $^{206}Pb/^{204}Pb$, but is far lower than it in $^{208}Pb/^{204}Pb$. Note in Figure 8 that the Society array lies close to the NHRL, and is totally distinct from the Samoa field.

[30] The $^{3}He/^{4}He$ ratios of Samoan lavas range from 8 R_A at high $^{87}Sr/^{86}Sr$ to a maximum of 26 R_A at generally lower $^{87}Sr/^{86}Sr$ (Figure 9). New data support the existence a primitive helium mantle (i.e., PHEM of *Farley et al.* [1992]) but with depleted Sr and Nd isotopic compositions (i.e., FOZO of *Hart et al.* [1992]). With increasing $^{87}Sr/^{86}Sr$, values of $^{3}He/^{4}He$ asymptotically approach ~8 R_A, showing that the helium isotopic composition of EM2 is approximately equivalent to that of MORB and much higher than the atmospheric values of recycled crustal materials (see discussion by *Farley et al.* [1992]). This low $^{3}He/^{4}He$ value of EM2 is either inherent to the EM2 source, or is a product of diffusive equilibrium with the upper mantle over long timescales (see section 9).

[31] The trace element character of the Samoan lavas display typical OIB features [*Hofmann*, 1988; *Weaver*, 1991], with trace element enrichments up to 100 times primitive upper mantle (PUM), the highest normalized concentrations at the highly incompatible elements, and negative anomalies at

Table 4. Isotopic Compositions of Samoan Lavas[a]

Volcano	Sample	$^{86}Sr/^{87}Sr$	$^{143}Nd/^{144}Nd$	$^{206}Pb/^{204}Pb$	$^{207}Pb/^{204}Pb$	$^{208}Pb/^{204}Pb$	$^{3}He/^{4}He$	[He] in cc/gm[b]		$^{187}Os/^{188}Os$	Os (ppb)
Vailulu'u	63-3	0.705453	0.512745	19.350	15.619	39.698	–	–		0.1275	0.261
Vailulu'u	63-5	0.705299	0.512746	19.337	15.604	39.604	–	–		–	–
Vailulu'u	63-13	0.705520	0.512716	19.352	15.624	39.699	–	–		–	–
Vailulu'u	64-1	0.705303	0.512764	19.363	15.606	39.623	–	–		–	–
Vailulu'u	68-3	**0.705396**	–	**19.337**	**15.621**	**39.651**	10.04 (2)	1.16E-07	ol, gl	–	–
Vailulu'u	68-10	0.705373	0.512760	19.325	15.610	39.560	–	–		–	–
Vailulu'u	68-11	0.705594	0.512724	19.357	15.623	39.685	–	–		0.1280	2.039
Vailulu'u	68-28	0.705419	0.512743	19.337	15.598	39.648	–	–		–	–
Vailulu'u	68-30	0.705215	0.512734	19.332	15.615	39.589	–	–		–	–
Vailulu'u	70-1	0.705371	0.512768	19.371	15.608	39.641	–	–		–	–
Vailulu'u	70-2	0.705359	0.512738	19.405	15.618	39.633	–	–		–	–
Vailulu'u	70-9	0.705352	0.512753	19.386	15.619	39.683	8.05	5.78E-08	gl	–	–
Vailulu'u	71-2	0.705943	0.512743	19.332	15.605	39.680	9.48 (2)	1.76E-07	ol, gl	0.1300	1.357
Vailulu'u	71-11	0.705394	0.512743	19.353	15.603	39.630	9.85	5.48E-07	ol	–	–
Vailulu'u	71-22	0.705473	0.512747	19.358	15.602	39.635	9.64	2.99E-08	ol	–	–
Vailulu'u	72-2	0.705395	0.512740	19.365	15.604	39.657	–	–		–	–
Vailulu'u	73-1	0.706720	0.512669	19.215	15.617	39.585	8.1 (3)	2.09E-08	gl	–	–
Vailulu'u	73-2	**0.705424**	0.512742	**19.329**	**15.621**	**39.616**	9.28	1.07E-08	ol	–	–
Vailulu'u	73-3	0.705616	0.512711	19.328	15.602	39.638	–	–		–	–
Vailulu'u	73-12	0.706653	0.512686	19.195	15.600	39.529	–	–		0.1288	0.105
Ta'u	T10	0.704657	0.512789	19.291	15.623	39.497	–	–		–	–
Ta'u	T14	0.704591	0.512806	*18.934*	*15.590*	*39.131*	–	–		–	–
Ta'u	T16	0.704605	**0.512818**	19.290	15.601	39.426	15.13	5.73E-09	ol	0.1294	0.279
Ta'u	T19	0.704582	0.512790	*19.299*	*15.600*	*39.448*	–	–		–	–
Ta'u	T21	0.704751	0.512796	19.313	15.594	39.479	–	–		–	–
Ta'u	T22	0.704701	0.512773	*19.314*	*15.606*	*39.485*	–	–		–	–
Ta'u	T23	0.704706	0.512796	*19.288*	*15.614*	*39.476*	–	–		–	–
Ta'u	T25	**0.704708**	**0.512790**	–	–	–	13.26	1.05E-07	ol	0.1290	0.206
Ta'u	T27	0.704561	**0.512806**	*19.304*	*15.604*	*39.500*	–	–		–	–
Ta'u	T30	0.704528	**0.512822**	*19.305*	*15.594*	*39.382*	–	–		0.1364	0.080
Ta'u	T32	0.704588	0.512797	*19.208*	*15.581*	*39.332*	–	–		–	–
Ta'u	T33	**0.704736**	0.512780	**19.284**	**15.596**	**39.445**	16.62	4.35E-09	ol	–	–
Ta'u	T38	0.704651	0.512785	*19.328*	*15.617*	*39.532*	–	–		–	–
Ta'u	T44	0.705086	0.512755	*19.246*	*15.606*	*39.549*	14.86	9.61E-09	ol	–	–
Ta'u	T45	0.704434	0.512816	*19.337*	*15.595*	*39.425*	–	–		–	–
Ta'u	T46	0.704676	0.512795	*19.231*	*15.584*	*39.369*	–	–		–	–
Ta'u	T47	0.704504	0.512800	*19.253*	*15.595*	*39.366*	–	–		–	–
Ta'u	T48	0.704664	0.512789	*19.249*	*15.595*	*39.397*	–	–		0.1351	0.062
Ta'u	T51	0.704614	0.512794	*19.276*	*15.591*	*39.425*	–	–		–	–
Ta'u	T55	0.704545	**0.512815**	19.178	15.594	39.298	–	–		–	–
Ta'u	74-1	0.704686	**0.512786**	19.29	15.599	39.443	17.97	4.97E-08	ol	0.1291	1.397
Ta'u	74-4	0.704815	0.512784	*19.314*	*15.601*	*39.477*	–	–		–	–
Ta'u	75-10	0.704533	0.512792	*19.266*	*15.597*	*39.39*	–	–		–	–

Table 4. (continued)

Volcano	Sample	$^{86}Sr/^{87}Sr$	$^{143}Nd/^{144}Nd$	$^{206}Pb/^{204}Pb$	$^{207}Pb/^{204}Pb$	$^{208}Pb/^{204}Pb$	$^{3}He/^{4}He$	[He] in cc/gm[b]		$^{187}Os/^{188}Os$	Os (ppb)
Muli	79-4	0.704904	0.512730	*19.279*	*15.617*	*39.517*	–	–		–	–
Muli	79-7	0.704524	0.512812	*19.122*	*15.581*	*39.122*	–	–		–	–
Muli	80-23	0.704914	0.512767	*19.177*	*15.591*	*39.305*	–	–		–	–
Malumalu	76-1	0.707192	0.512637	*19.338*	*15.636*	*39.847*	–	–		–	–
Malumalu	76-8	0.706374	0.512667	*19.294*	*15.633*	*39.710*	–	–		–	–
Malumalu	76-9	0.706745	**0.512669**	19.245	15.596	39.555	15.89	2.12E-08	ol	–	–
Malumalu	76-13	0.706395	**0.512680**	19.237	15.600	39.584	–	–		–	–
Malumalu	77-1	0.706930	**0.512663**	19.251	15.619	39.669	13.45	3.30E-08	ol	–	–
Malumalu	77-9	0.707260	0.512579	*19.331*	*15.635*	*39.853*	10.56	1.92E-08	ol	–	–
Malumalu	78-1	0.708901	0.512521	*19.237*	*15.647*	*39.862*	8.09	9.61E-08	ol	0.1293	0.130
Malumalu	78-3	0.708886	0.512511	19.230	15.641	39.840	8.22	9.15E-08	ol	0.1288	0.427
Malumalu	78-8	0.707614	0.512580	19.276	15.633	39.803	–	–		–	–
Upolu	U10	**0.705365**	**0.512774**	**19.044**	**15.582**	**39.067**	–	–		0.1407	0.013
Upolu	U12	–	–	**18.889**	**15.554**	**38.772**	–	–		–	–
Upolu	U14	–	–	**18.878**	**15.560**	**38.767**	–	–		–	–
Upolu	U16	**0.705171**	**0.512883**	**18.881**	**15.559**	**38.787**	–	–		–	–
Upolu	U19	**0.705278**	**0.512870**	**18.917**	**15.569**	**38.832**	–	–		–	–
Upolu	U21	**0.705011**	–	**18.901**	**15.561**	**38.814**	–	–		–	–
Upolu	U22	–	–	**18.912**	**15.563**	**38.802**	–	–		0.1509	0.022
Upolu	U24	**0.705191**	**0.512854**	**18.955**	**15.569**	**38.875**	–	–		–	–
Savai'i	S11	**0.706195**	**0.512693**	**18.782**	**15.604**	**38.995**	–	–		0.1299	0.107
Savai'i	S12	–	–	**18.799**	**15.603**	**39.002**	–	–		–	–
Savai'i	S15	**0.706039**	**0.512686**	**18.793**	**15.610**	**39.022**	–	–		–	–
Savai'i	S16	**0.706296**	**0.512705**	**18.865**	**15.595**	**39.089**	–	–		–	–
Savai'i	S18	**0.706110**	**0.512730**	**18.884**	**15.596**	**39.118**	–	–		–	–
Savai'i	S23	–	–	**18.795**	**15.599**	**38.985**	–	–		0.1270	0.491
Savai'i	S25	**0.705848**	**0.512706**	**18.797**	**15.600**	**38.982**	–	–		0.1353	0.034

[a] Analyses in plain text are from TIMS, in italics are from MC-ICP-MS in Lyon, and bold are from MC-ICP-MS at WHOI.
[b] Helium analyses on glass (gl) and/or olivine (ol) separates as denoted in adjacent column.

Table 5 (Representative Sample). Sample Information and Chemical Data for 41 Total Samples of Samoan Basalts Collected by M. Regelous[a] [The full Table 5 is available in the HTML version of this article at http://www.g-cubed.org]

Volcano	Upolu	Upolu	Upolu	Upolu	Upolu	Upolu	Upolu	Upolu	Savai'i
Sample	**U 11 F**	**U 13 F**	**U 14 F**	**U 38 F**	**U 39 F**	**U 40 F**	**U 41 F**	**U 43 F**	**S 36 F**
Volcanic Series	Fagaloa	Fagaloa	Fagaloa	Fagaloa	Fagaloa	Fagaloa	Fagaloa	Fagaloa	Fagaloa
Latitude (°S)[b]	13.8537	13.8533	13.9422	13.8453	13.8512	13.8597	13.8648	13.8895	13.2642
Longitude (°W)	171.6886	171.6582	171.5848	171.7093	171.7033	171.6523	171.6436	171.5614	172.3815
Major elements (wt%)									
SiO_2	48.06	45.65	45.78	48.28	47.33	47.53	46.01	46.66	45.93
Al_2O_3	15.20	13.98	15.79	15.32	13.86	14.00	13.87	13.69	11.92
TiO_2	4.24	2.92	3.65	4.28	5.09	3.88	2.96	5.16	3.12
FeO*	12.01	12.82	12.84	12.05	12.25	12.50	12.67	14.15	11.59
MnO	0.16	0.18	0.19	0.17	0.16	0.17	0.18	0.18	0.16
CaO	9.73	10.27	9.82	9.37	10.47	10.26	10.77	9.76	10.05
MgO	5.38	10.24	6.72	5.27	5.80	7.45	10.00	5.46	13.21
K_2O	1.37	0.91	0.56	1.41	1.44	0.97	0.94	1.07	0.48
Na_2O	3.22	2.59	4.00	3.22	2.92	2.75	2.16	3.35	3.10
P_2O_5	0.63	0.44	0.65	0.63	0.68	0.48	0.45	0.50	0.44
Mg#[c]	48.44	62.63	52.31	47.85	49.82	55.54	62.35	44.72	70.51
Trace Elements (ppm)									
Ni	72	249	72	73	79	140	248	35	386
Cr	105	389	75	98	73	220	411	4	603
V	312	272	293	311	341	316	280	389	238
Ga	25	20	23	25	25	22	21	25	19
Cu	71	92	38	69	120	101	98	84	76
Zn	144	123	134	150	154	130	124	160	120
Cs	0.20	0.40	0.54	0.32	0.47	0.14	0.23	0.28	0.40
Rb	32.3	23.8	38.2	33.0	38.2	21.2	23.8	25.0	55.9
Ba	311	259	341	292	305	203	272	213	431
Th	3.79	3.17	5.27	3.77	5.08	2.64	3.27	2.80	3.36
U	1.07	0.76	1.12	1.07	1.26	0.73	0.79	0.82	0.70
Nb	52.18	40.16	52.88	51.82	58.00	35.35	40.33	40.56	42.85
Ta	3.26	2.48	3.07	3.19	3.60	2.23	2.50	2.59	2.65
La	45.10	31.13	49.32	41.43	48.93	27.74	32.16	30.24	31.95
Ce	96.38	66.54	102.63	93.74	105.67	65.00	67.97	72.09	69.29
Pb	2.82	2.40	3.72	2.98	3.48	1.70	2.27	3.15	2.79
Pr	13.21	8.21	12.34	12.49	13.99	9.03	8.43	9.91	8.76
Nd	53.08	31.72	46.48	50.08	55.92	38.14	32.80	42.30	34.84
Sr	683	521	699	664	631	494	543	552	585
Zr	324	179	243	322	335	264	183	301	188
Hf	7.79	4.35	5.71	7.71	8.13	6.46	4.51	7.55	4.71
Sm	11.24	6.62	9.25	10.61	11.76	8.76	6.82	9.98	7.32
Eu	3.60	2.11	2.89	3.36	3.66	2.79	2.18	3.23	2.35
Gd	10.52	6.11	8.19	9.57	10.63	8.18	6.33	9.57	6.67
Tb	1.46	0.87	1.14	1.34	1.46	1.17	0.89	1.37	0.92
Dy	8.11	4.82	6.25	7.37	7.97	6.56	4.95	7.65	4.99
Ho	1.49	0.88	1.13	1.33	1.42	1.21	0.90	1.38	0.87
Y	39.25	21.40	27.44	31.82	34.83	28.89	21.98	33.23	20.89
Er	3.69	2.17	2.75	3.21	3.44	2.94	2.23	3.36	2.06
Tm	0.47	0.29	0.36	0.42	0.44	0.39	0.29	0.44	0.27
Yb	2.69	1.69	2.10	2.42	2.53	2.25	1.71	2.50	1.49
Lu	0.38	0.24	0.30	0.34	0.35	0.32	0.24	0.35	0.21
Sc	22.2	22.7	19.0	21.9	25.3	25.9	24.0	26.0	22.2
$^{86}Sr/^{87}Sr$	0.705361	0.705391	0.705644		0.705180	0.704904	0.705439	0.705179	0.705823
$^{143}Nd/^{144}Nd$	0.512874	0.512783	0.512773			0.512907	0.512777	0.512883	0.512702
$^{206}Pb/^{204}Pb$	18.944	18.914	18.961	18.940	19.143	18.905	18.918	18.848	18.801
$^{207}Pb/^{204}Pb$	15.580	15.582	15.603	15.576	15.606	15.568	15.584	15.564	15.609
$^{208}Pb/^{204}Pb$	38.835	38.996	39.130	38.827	39.273	38.798	39.009	38.783	39.012

[a] See Appendix A for analytical techniques.
[b] Latitude and Longitude are in reference to University of Hawaii map for Western Samoa.
[c] Mg# = molar ratio of MgO/(MgO + 0.85 * FeO).

Table 6. Isotopic Compositions of Samples Previously Collected by KAF[a]

Volcano	Sample	Type	$^{86}Sr/^{87}Sr$	$^{143}Nd/^{144}Nd$	$^{3}He/^{4}He$	$^{206}Pb/^{204}Pb$	$^{207}Pb/^{204}Pb$	$^{208}Pb/^{204}Pb$
Tutuila	91TP-128	upper shield	0.705535	0.512846	–	–	–	–
Tutuila	91TP-134	dike	0.705195	0.512821	24.67	19.065	15.614	39.13
Tutuila	91TP-165	dike	0.705166	0.5128	25.79	–	–	–
Tutuila	91TP-201	dike	0.704971	0.512825	20.49	19.199	15.59	39.171
Tutuila	91TP-133	lower shield	0.70609	0.512709	17.44	–	–	–
Tutuila	91TP-203	lower shield	0.707863	0.512595	14.83	19.106	15.625	39.526
Tutuila	91TP-207	lower shield	0.707143	0.512644	13.97	–	–	–
Tutuila	91TP-144	upper shield	0.705317	0.512858	–	–	–	–
Tutuila	91TP-196	upper shield	0.704476	0.5129	–	18.806	15.543	38.656
Tutuila	91TP-228	upper shield	0.705225	0.512453	–	–	–	–
Tutuila	91TP-252	upper shield	0.706354	0.512657	14.44	–	–	–
Tutuila	91TPK-5	upper shield	0.705192	0.512803	22.59	19.124	15.646	39.224
Upolu	91UF-65B	shield	0.70547	0.512783	11.4	18.974	15.615	39.126
Upolu	91UF-86	shield	0.706389	0.512725	10.25	–	–	–
Upolu	91UF-89B	shield	0.705245	0.512772	16.78	–	–	–
Upolu	91UFK-4	shield	0.705147	0.512851	16.7	–	–	–
Upolu	91UFK-6A	shield	0.704821	0.51285	12.28	18.988	15.627	39.171
Upolu	UPO-10C	shield	0.706447	0.512743	11.27	–	–	–
Upolu	UPO-F-19	shield	0.705133	0.512833	15.8	–	–	–
Upolu	UPO-F-20	shield	0.70522	0.512859	12.92	–	–	–
Upolu	UPO-F9-7	shield	0.70493	0.512912	13.8	–	–	–
Manua	82MT11	shield	0.704569	0.512833	15.23	–	–	–
Manua	82MT17	shield	0.704649	0.512783	13.34	–	–	–
Manua	82MT18	shield	0.704661	0.512781	13.54	–	–	–
Manua	82MT8B	shield	0.704637	0.512776	19.06	19.316	15.593	39.445
Savaii	91SVK-1	PE	0.705589	0.512721	13.7	–	–	–
Savaii	91SVK7	COBBLE	0.7072	0.51277	–	18.872	15.587	39.021

[a] Analytical techniques as described in *Farley et al.* [1992].

Cs, K and Pb (Figure 10). The largest inter-volcano differences are at Pb, Rb, Ba, and Th. *Weaver* [1991] employed the trace element ratios Rb/Nb, Ba/Nb, Ba/Th, and Ba/La to distinguish between the EM1 and EM2 species. He used these trace elements to argue for a recycled sedimentary component as the cause for the EM signature, and ascribed the difference between EM1 and EM2 to a pelagic versus terrigenous sedimentary provenance. Therefore a comparison between the Samoan lavas (extreme EM2) and those from Pitcairn (extreme EM1) should theoretically show the greatest differences in these ratios. However, recent studies on Pitcairn lavas [*Dostal et al.*, 1998; *Eisele et al.*, 2002] show nearly complete overlap with the Samoan lavas for Weaver's classification ratios, unlike the clear distinction between EM1 and EM2 previously reported for lavas with less extreme end-member signatures (Figure 11). This result makes the trace element differences between EM1 and EM2 very difficult to resolve and discourages the description of EM1 and EM2 as having "pelagic" and "terrigenous" components, respectively. Furthermore, the *Plank and Langmuir* [1998] study of the compositions of sediment being subducted at today's convergent margins shows that pelagic and terrigenous sediments are: (1) not notably different in trace element ratios such as Ba/Th, and (2) not typically occurring alone in subducted sedimentary sections, but are instead components of the whole, mixed sedimentary package. Hence generating mantle end-members by recycling of only pelagic or only terrigenous sediment seems physically unlikely.

6.2. Shield Versus Post-Erosional

[32] As initially observed by *Wright and White* [1987], post-erosional (PE) lavas are isotopically distinct from all shield lavas. There is a commonality among the PE lavas from all along the chain (Savai'i, Upolu and Tutuila), in contrast to the

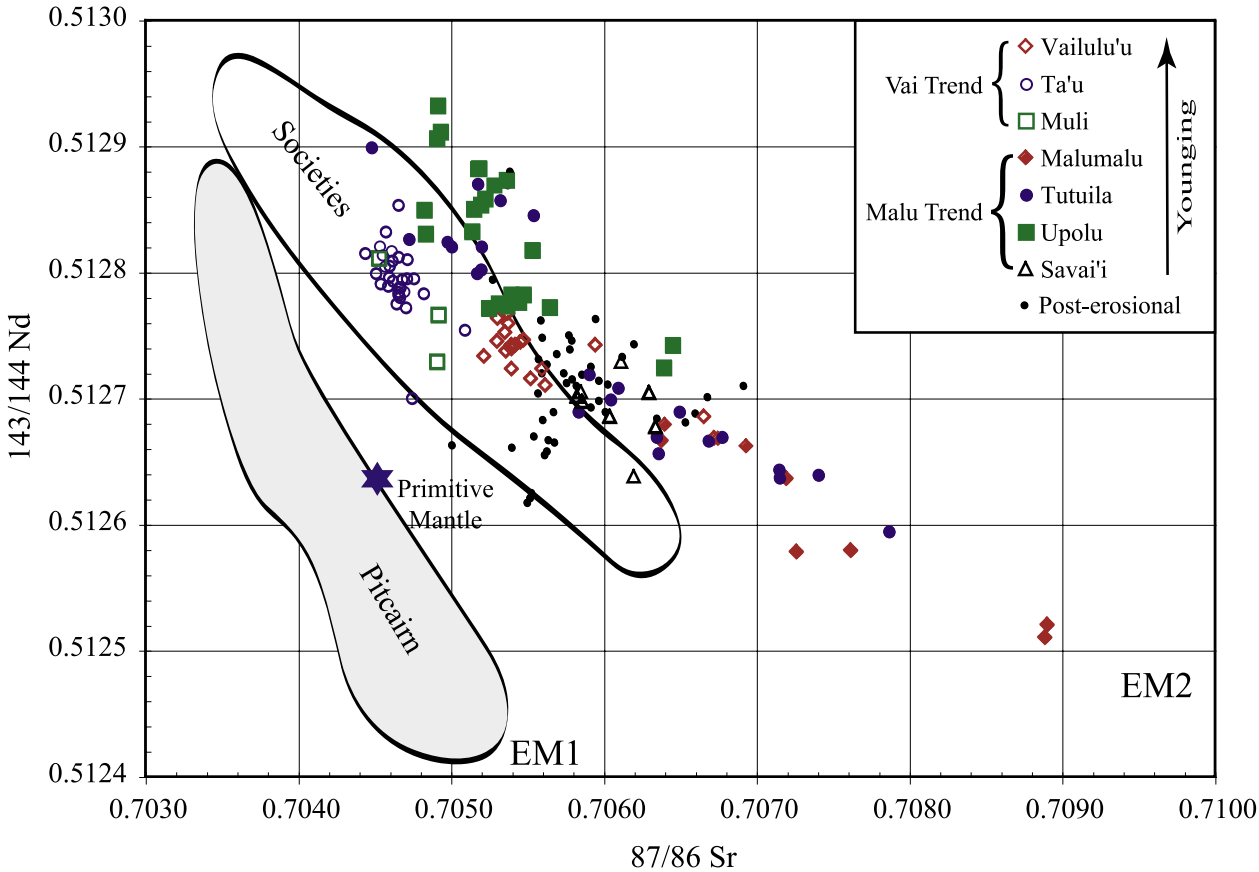

Figure 6. Sr and Nd isotopes for Samoan lavas. This as well as other isotope plots includes data from *Wright and White* [1987], *Farley et al.* [1992], and *Hauri and Hart* [1993]. The legend here applies to all other isotope plots. The Vai Trend and Malu Trend correspond to topographic ridges of the volcanic chain (see Figure 2). Savai'i samples marked with triangles are all from the Fagaloa Volcanic series. Post-erosional lavas include samples from Upolu and Savai'i. Fields for the Societies and Pitcairn were obtained from the GEOROC database. Coordinates for Globally Subducting Sediment (GLOSS) and local Tongan sediment are from *Plank and Langmuir* [1998].

observation that each island displays a unique isotopic birthmark in its shield lavas. The PE lavas show restricted $^{87}Sr/^{86}Sr$ values that plot mid-range in the Samoan field, have the lowest $^{206}Pb/^{204}Pb$ values and some of the lowest $^{208}Pb/^{204}Pb$ values of the whole sample suite (Figures 6 and 8). The PE field on the $^{206}Pb/^{204}Pb$ versus $^{207}Pb/^{204}Pb$ plot (Figure 7) is unusual, as it is elongate in an almost inverse direction to the shield trend [*Wright and White*, 1987].

[33] Overall, the new Savaiian lavas are all of the same chemical nature as the post-erosionals, even though many are samples of the oldest-mapped flow series on the island (Fagaloa Series [*Kear and Wood*, 1959]). These Savai'i lavas, as well as most other PE lavas, are clearly distinguishable from shield lavas by having the highest Nb/U and Ba/(La, Sm, Nb, Th) ratios of the whole sample suite (Figure 12). Given the earlier discussion of the young radiometric ages for this "shield" series, we believe this sequence is in fact post-erosional, and not shield. The alternative explanation, that all of Savai'i is young and not part of an age-progressive Samoan hot spot track, is belied by the 2.05 my age for a trachyte cobble from the Vanu River valley (see above). Either way, we cannot rule out the possibility that PE lavas and shield lavas are geochemically the same on Savai'i, but nowhere else in Samoa.

[34] What accounts for the distinct trace element and isotopic differences between shield and PE lavas? The commonality among Samoan PE lavas

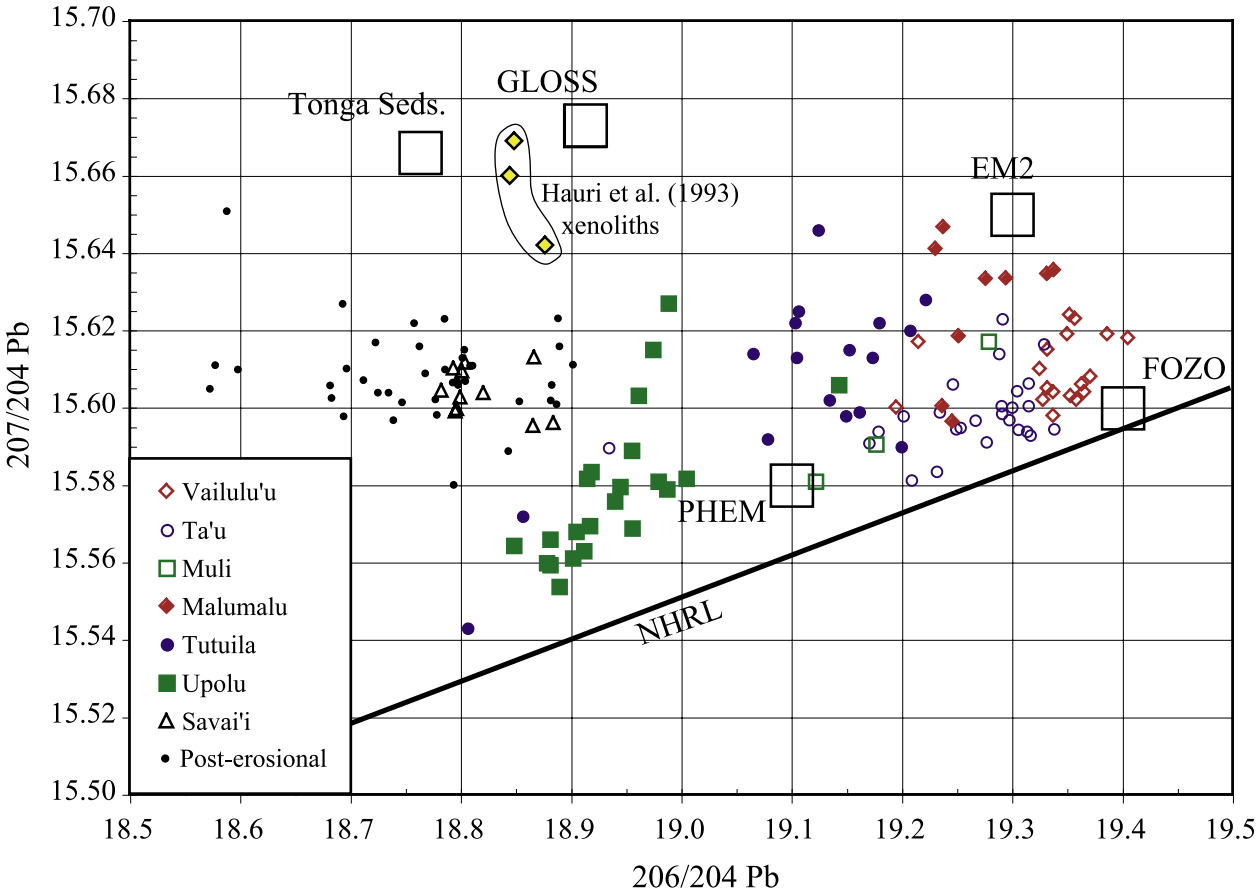

Figure 7. Plot of $^{206}Pb/^{204}Pb$ with $^{207}Pb/^{204}Pb$ of Samoan lavas. The Northern Hemisphere Reference Line (NHRL) lies significantly below the EM2 coordinate. Here, the Vai and Malu topographic lineaments can be distinguished as separate isotopic trends. Note how the post-erosional lavas are askew to the overall array of shield lavas. GLOSS = Globally Subducting Sediment [*Plank and Langmuir*, 1998]; PHEM, Primtive Helium Mantle [*Farley et al.*, 1992]. *Hauri et al.* [1993] xenolith data derives from cpx and glass separates from Savaiian xenoliths. See Figure 6 for other references.

possibly derives from a similar history of being brewed and aged in the crust and lithosphere, unlike shield lavas that may have a shorter residence time in this shallow environment. Local Tongan sediments (from DSDP Site 595/596, about 1000 km southeast of Samoa) have Pb isotopic compositions [*Plank and Langmuir*, 1998] with the general characteristics of PE lavas (Figures 7 and 8). Pb isotopic compositions of marine sediments are highly variable over short distances and other sediments could likely be found nearer to Samoa that provide closer fits to the Samoa post-erosional Pb field (which lies near the lower end of the general marine sediment array [*Abouchami and Goldstein*, 1995; *O'Nions et al.*, 1998; *Plank and Langmuir*, 1998; *Jones et al.*, 2000]). In support of a sediment component in the PE lavas are values for $\delta^{18}O$ of olivine (5.5–5.7‰ [*Eiler et al.*, 1997]) which are elevated over upper mantle values and can be interpreted to reflect the heavy values documented for marine sediments (also see discussion below). In other words, we cannot rule out the late-stage incorporation of modern marine sediments in PE lavas based solely on isotopic compositions. Trace element ratios may provide a stronger constraint on the presence or absence of a modern sediment component; one would expect the PE lavas to inherit the high Pb/Ce, high REE/HFSE, low Sm/Yb, and Ba-enriched ratios characteristic of both local and globally averaged marine sediments (see Figure 17) [*Plank and Langmuir*, 1998]. This is not the case for the

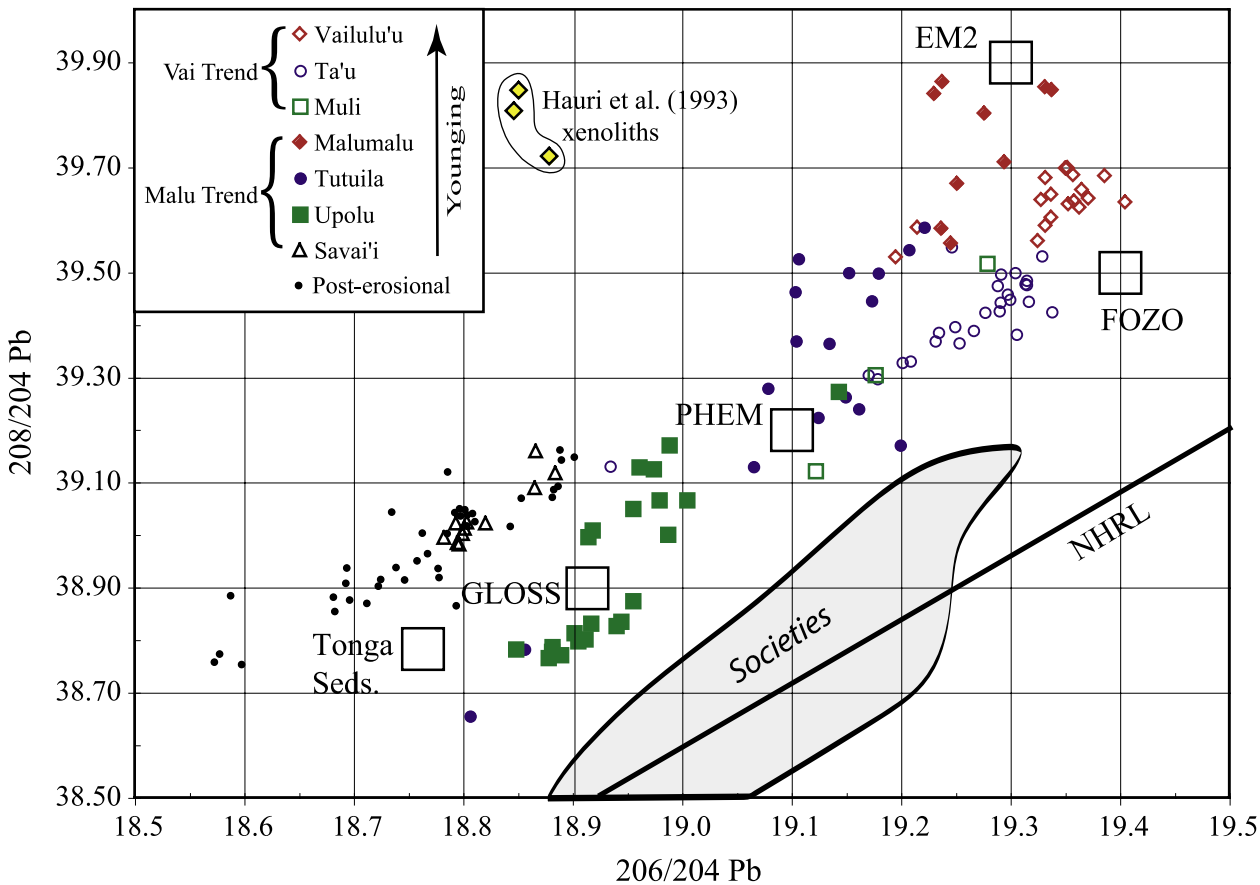

Figure 8. Plot of $^{206}Pb/^{204}Pb$ and $^{208}Pb/^{204}Pb$ of Samoan lavas. Again, the Vai and Malu Trends are separated into two isotopic arrays. Along each trend, the age of volcanoes increases in the direction of lower $^{206}Pb/^{204}Pb$ and $^{208}Pb/^{204}Pb$. See Figure 6 for references.

PEs, which have, of all suspected traits, only notably high Ba (Figures 11 and 12).

6.3. Mixing Arrays

[35] The spread of isotopic compositions in the Samoan lavas can be attributed to either (1) processes that generate an infinite number of chemical (i.e., parent/daughter) heterogeneities within the mantle that, upon long-term storage, evolve into an infinite number of isotopic heterogeneities or (2) processes that produce a small number of unique chemical compositions that, upon long-term storage, result in a limited number of "end-member" isotopic compositions available for mixing. In order for the first option to produce sublinear arrays in 2-D and 3-D isotope space, there must be a single process which acts systematically to varying degrees or at various times. Hence talk of or modeling of the most extreme values (i.e., end-member mantle components) is the same in either case.

[36] The lavas from Malumalu undeniably establish the existence of a reservoir with high $^{87}Sr/^{86}Sr$ (at least 0.7089), low $^{143}Nd/^{144}Nd$ (at most 0.5125), and $^{206}Pb/^{204}Pb$, $^{207}Pb/^{204}Pb$, and $^{208}Pb/^{204}Pb$ values near 19.3, 15.65 and 39.9, respectively. An unaltered sediment reservoir can be immediately ruled out as the cause of the EM2 component in Samoan shield lavas: although Global Subducting Sediment (GLOSS) [*Plank and Langmuir*, 1998] and local Tongan sediment (Site 595/596 [*Plank and Langmuir*, 1998]) each have convincing $^{87}Sr/^{86}Sr$ and $^{207}Pb/^{204}Pb$ compositions (Figures 6 and 7), they are severely inadequate (low) in $^{206}Pb/^{204}Pb$ and $^{208}Pb/^{204}Pb$ to generate the isotopic signatures displayed by the shield

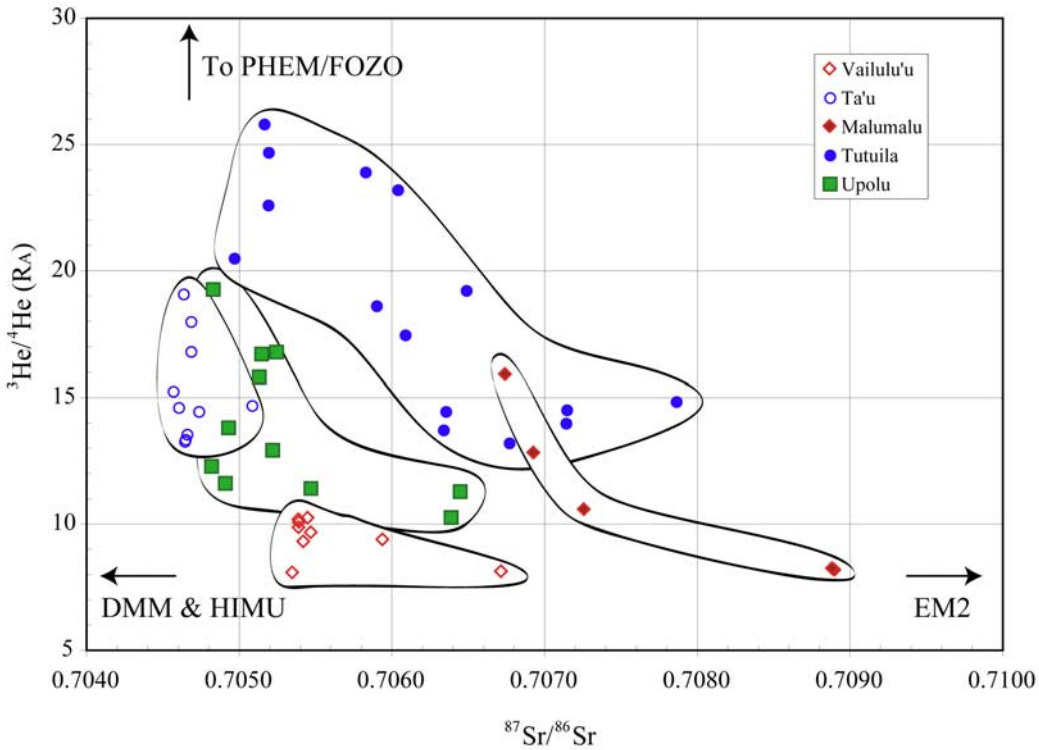

Figure 9. Plot of $^{87}Sr/^{86}Sr$ compositions of Samoan basalts with $^3He/^4He$ (R_A) of olivine phenocrysts and submarine glasses obtained from the same basalts. Some Tutuila samples are from *Farley et al.* [1992]. EM2 is shown here to approach the DMM $^3He/^4He$ value of ~8 R_A at high $^{87}Sr/^{86}Sr$.

lavas (Figure 8). Therefore for recycled sediment to have evolved to the EM2 coordinate in Sr-Nd-Pb isotope space, subduction zone alteration of ancient sedimentary packages needed to be very specific: U/Pb and Th/Pb must increase, while Rb/Sr and Sm/Nd remain very much the same. In the dehydration of subducted oceanic crust, this is shown to be the case for all systems except Rb/Sr: Rb is about 5 times more mobile than Sr [*Ayers*, 1998], so the final dehydrated product has significantly lowered Rb/Sr ratios. Experiments on the dehydration and melting of sediments [*Johnson and Plank*, 1999] give rather inconclusive results for relative trace element partitioning of these parent/daughter ratios, and suggest that partitioning can be extremely variable depending on the minerals present and the degree of dehydration.

[37] Although the Samoan lavas are isotopically extreme, the ''pure'' EM2 signature may be even more extreme. For example, clinopyroxene and glass separates from peridotite xenoliths from Savai'i studied by *Hauri et al.* [1993] yield $^{87}Sr/^{86}Sr$ values up to 0.7128 and have been interpreted to represent metasomatism of oceanic lithosphere by a small degree carbonatitic melt (not diluted by mixing with depleted mantle) from the same source as that which provides melts for Samoan volcanism. However, the Pb isotopes in these rare xenoliths ($^{206}Pb/^{204}Pb$ ~18.86; $^{208}Pb/^{204}Pb$ ~39.76) lie well outside the isotopic array set by the Samoan lavas (Figure 8); this suggests an origin for the enriched component in these xenoliths from a smaller, unique reservoir, unrelated to extant Samoan lavas.

[38] Clearly, though, EM2-rich samples are more rare than samples of a less-enriched nature. On a plot of $^{206}Pb/^{204}Pb$ against $^{87}Sr/^{86}Sr$ (Figure 13), the Samoan samples can be enclosed in a triangle where the high $^{87}Sr/^{86}Sr$ apex is defined by EM2. At lower $^{87}Sr/^{86}Sr$, there are two components, one with higher $^{206}Pb/^{204}Pb$ than EM2 and one with lower $^{206}Pb/^{204}Pb$, but both assuredly depleted according to their high $^{143}Nd/^{144}Nd$ values

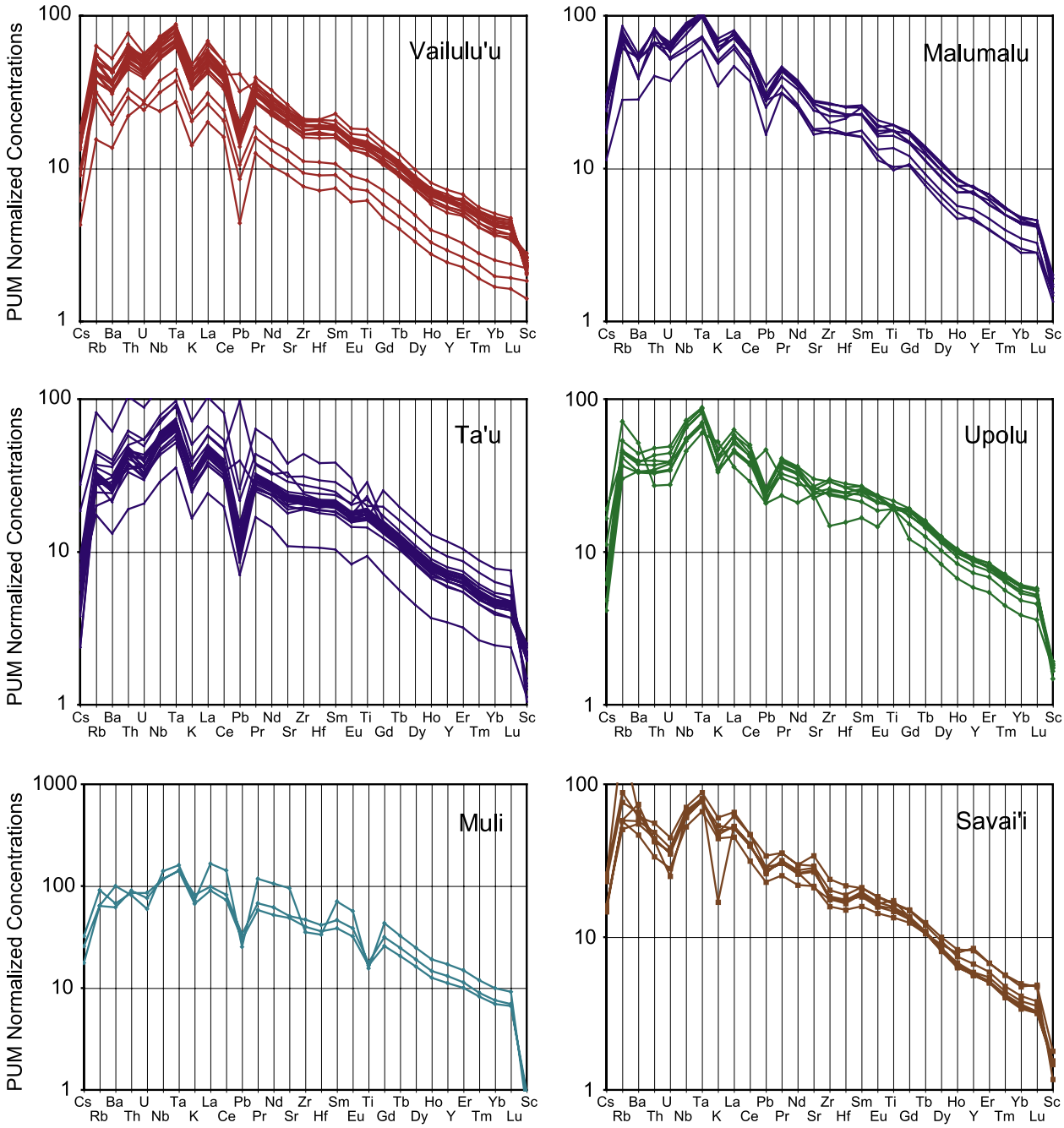

Figure 10. Trace element concentrations of Samoan lavas normalized to primitive upper mantle (PUM) of *McDonough and Sun* [1995]. Note the difference in scale for the Muli lavas. Low concentration patterns are typically picrites (for example, the lowest three samples from Vailulu'u and lowest one from Ta'u). The highest concentration sample from Ta'u is T21, with 50% plagioclase phenocrysts.

(Figure 6). The low $^{206}Pb/^{204}Pb$, low $^{87}Sr/^{86}Sr$ apex (note the Upolu data cluster) has a signature tending toward DMM, but the strict use of the most depleted MORB/DMM isotopic values is not necessarily the only option for describing this component. The sub-Samoan upper mantle has been punctured by multiple mantle plumes in its 110 Myr lifespan, so may no longer be strictly, or homogeneously, pure DMM (see the South Pacific Isotopic and Thermal Anomaly [*Staudigel et al.*, 1991]). Also, we do not absolutely require the low $^{206}Pb/^{204}Pb$ depleted component to reside in the

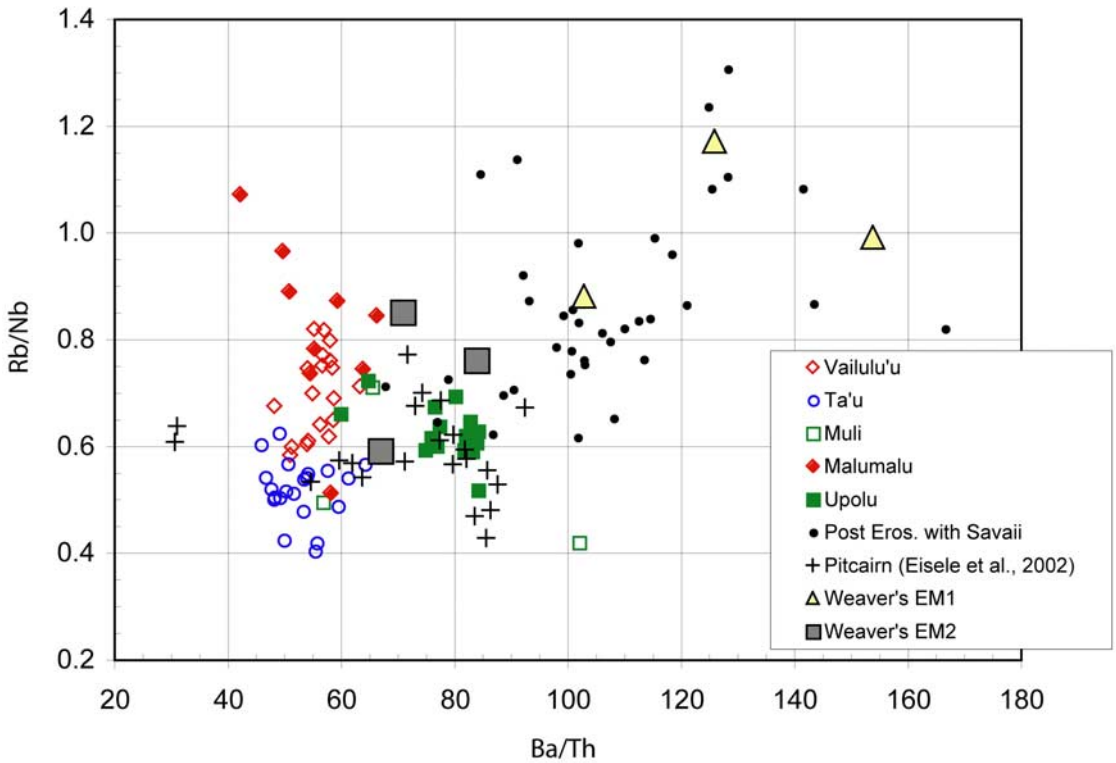

Figure 11. Ba/Th versus Rb/Nb for lavas from Samoa [this study; *Hauri and Hart*, 1997] and Pitcairn [*Eisele et al.*, 2003] showing that *Weaver*'s [1991] distinction between EM1 and EM2 trace element characteristics do not hold up to comparisons of lavas from end-member defining island chains (see Figure 5). Pitcairn and Samoa show complete overlap in Ba/Th and Rb/Nb, whereas *Weaver* [1991] showed separate fields for EM1 and EM2 lavas. *Plank and Langmuir* [1998] report that terrigenous and pelagic sediments have indistinguishable Ba/Th ratios, each with a range of 10–220, with exceptions being rare hydrothermal clays and hemipelagic clays that are heavily enriched in Ba. Therefore the reason for initially identifying EM1 and EM2 as having recycled "pelagic" and "terrigenous" sediment, respectively, proves unfounded with further data collection.

upper mantle (i.e., it could be part of the plume), although it's most easily visualized as being there given current notions of mantle dynamics. Regardless of these disclaimers, the use of anything but a generic DMM isotopic composition is arbitrary, and ultimately only compromises the generality of our observations and conclusions.

[39] The high $^{206}Pb/^{204}Pb$, low $^{87}Sr/^{86}Sr$ component (obvious in the Ta'u and Vailulu'u lavas; Figure 13) is suggestive of mixing with a HIMU mantle component. This component may also be present in the Samoan plume, but there is reason to believe HIMU material has under-plated the Samoan lithosphere in the past. Calculated hot spot tracks show that 20–25 million years ago, the Cook-Austral plume was located beneath the lithosphere on which the Samoan Islands presently sit [*Norton*, 2000]. The Cook-Austral chain shows great variation in isotopic compositions (Figure 14), not all of which would fit the Samoan data in multi-isotope space. However, there is one volcano, Raivavae, which has the isotopic compositions appropriate to be a significant component in the Vai Trend lavas (Figure 14; data from GEOROC database); we are not suggesting that Raivavae itself is contributing to the Samoan lavas, but that isotopically similar material may be underplating the Samoan island chain.

[40] A fourth mixing component must be acknowledged when considering $^{3}He/^{4}He$ values. Figure 9 shows the inverse relationship between $^{87}Sr/^{86}Sr$ and $^{3}He/^{4}He$. The EM2 component can be classified as having a $^{3}He/^{4}He$ signal which asymptotically approaches the average DMM value of $\sim$8 R_A [*Kurz et al.*, 1982] at high $^{87}Sr/^{86}Sr$. HIMU has also been shown to have low $^{3}He/^{4}He$ values

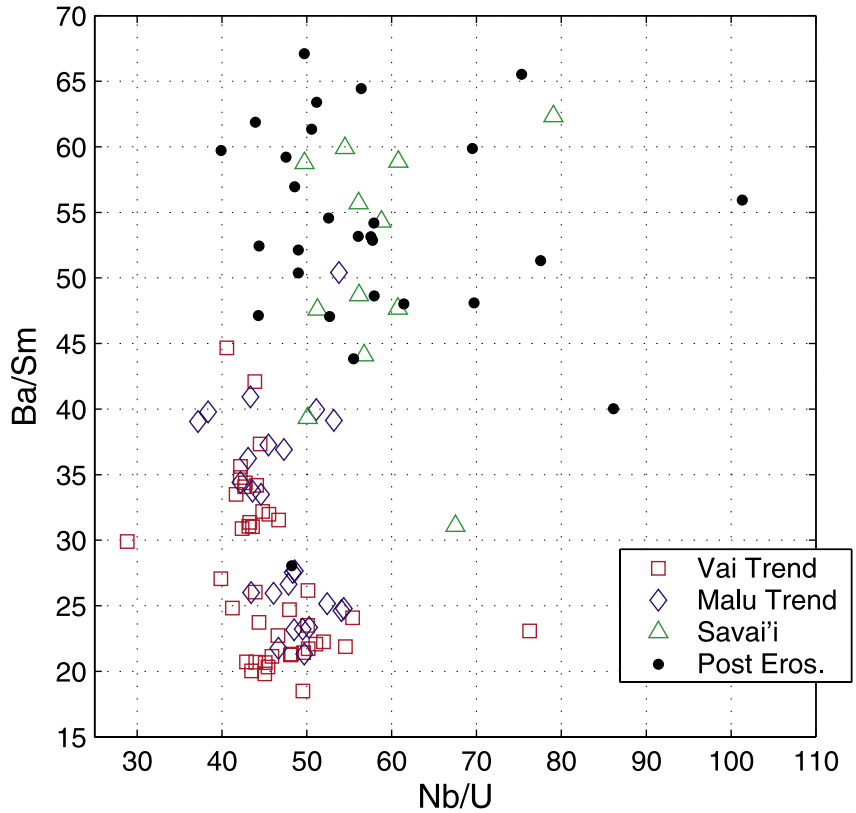

Figure 12. Plot of Nb/U versus Ba/Sm used to highlight the trace element differences between shield and post-erosional lavas in Samoa. The new Savai'i lavas, sampled from the oldest mapped volcanic series on the island (Fagaloa Series [*Kear and Wood*, 1959]), plot in the same field as post-erosional lavas from all along the Samoan chain. This leads to the conclusion that either post-erosional lavas and shield lavas are the same on Savai'i, or post-erosional volcanism has been unusually extensive.

[*Graham et al.*, 1993; *Hanyu and Kanoeka*, 1997; *Hilton et al.*, 2000] and likely explains why Vailulu'u (with the largest HIMU component) is in parallel with Malumalu on Figure 9. Therefore all three end-member components discussed above have low $^{3}He/^{4}He$, thus requiring an additional reservoir to account for high $^{3}He/^{4}He$. High $^{3}He/^{4}He$ values are found in the center of the Samoan Sr-Pb data array, at Ta'u and Tutuila, and generally decrease toward the outer fringes (Figure 13). *Farley et al.* [1992] named this component the primitive helium mantle (PHEM) but new data suggest this reservoir has depleted $^{87}Sr/^{86}Sr$ and $^{143}Nd/^{144}Nd$ (like FOZO of *Hart et al.* [1992]), and not bulk-earth-like values assigned to PHEM.

[41] All four mantle components are in the Samoan plume from a magmatic standpoint. However, what material is coming from the deep mantle is another story. We can make a good case for the depleted component coming from entrainment of the widely documented depleted upper mantle and the radiogenic Pb component (HIMU-ish) coming from entrainment of under-plated lithosphere from the HIMU Cook-Austral chain. This means the deep mantle material within the Samoan plume is dominantly EM2 and PHEM/FOZO. The sequence of mixing these components is difficult to ascertain, as the length scale of compositional heterogeneity and differences in solidus temperatures (i.e., solid versus melt mixing) are unknown.

6.4. Spatial/Temporal Evolution

[42] Samoan shield samples on the $^{206}Pb/^{204}Pb$ - $^{208}Pb/^{204}Pb$ plot form two en echelon trends of positive slope (Figure 8) which are most distinctly

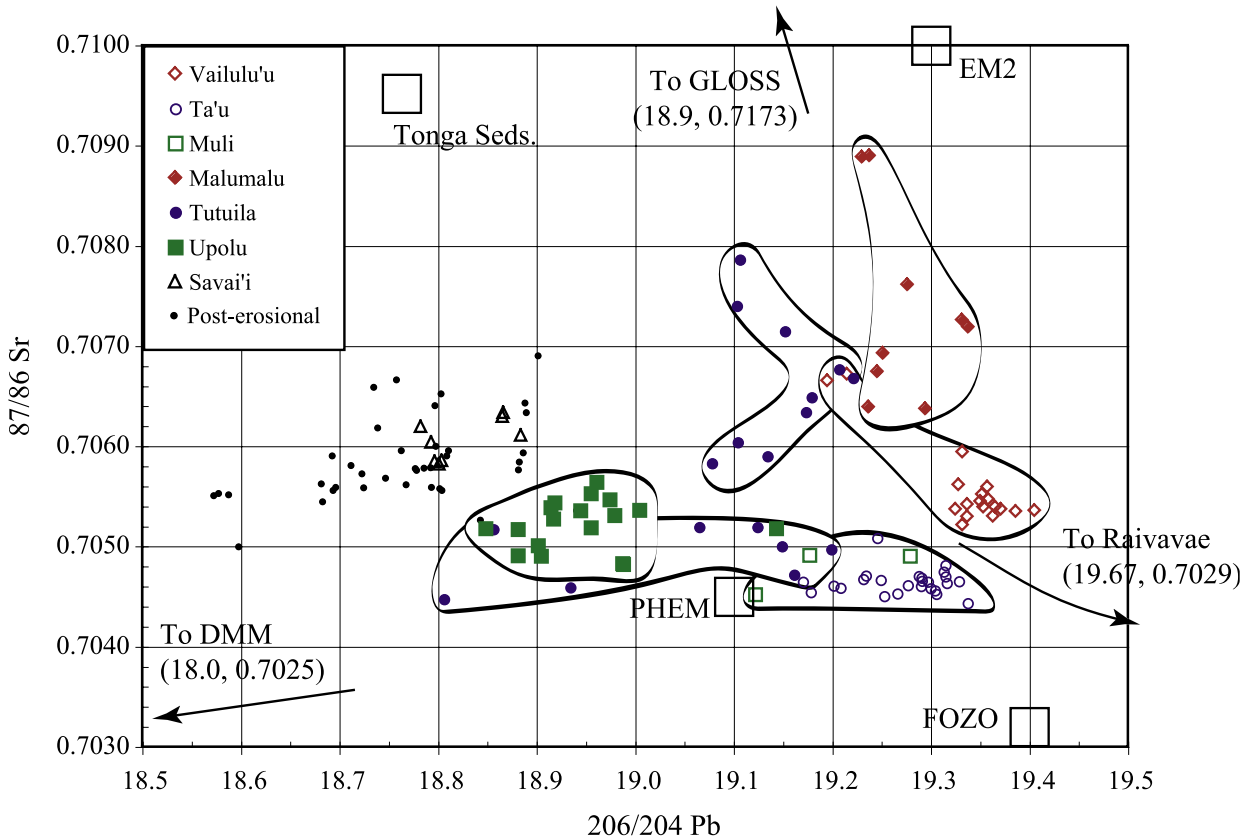

Figure 13. Sr and Pb isotope plot showing two classes of volcanoes – those which are elongate on the $^{206}Pb/^{204}Pb$ axis (Upolu, Tutuila Pago shield, Muli, and Ta'u) and those elongate on the $^{87}Sr/^{86}Sr$ axis. Mixing components are identified as DMM, HIMU, EM2 and the high $^{3}He/^{4}He$ reservoir, PHEM/FOZO. See Figure 6 for references.

separated at high $^{206}Pb/^{204}Pb$, and converge at lower $^{206}Pb/^{204}Pb$. The isotopic trends correspond to the two topographic ridges of the Samoan islands (Figure 2); for a given $^{206}Pb/^{204}Pb$, the southern Malu Trend has higher $^{208}Pb/^{204}Pb$ than the northern Vai Trend. Within each of the two trends, isotopic enrichment increases with decreasing age along the volcanic ridge. This relationship, shown clearly in a plot of distance versus $^{206}Pb/^{204}Pb$ (Figure 15), has remarkable correlation and is striking in its implication of a systematic evolution of plume material or mantle processes. Figure 15 also shows how the Malu and Vai Trends form a continuum though time: even though each ridge independently displays isotopic enrichment with distance/time, the younger Vai Trend is generally higher in $^{206}Pb/^{204}Pb$ than the older Malu Trend (note that Malumalu may overlap in age with Ta'u and Vailulu'u). Of the four mixing components, low $^{206}Pb/^{204}Pb$ values are found only in the DMM reservoir (~18.0; Figure 14). Therefore the increase in $^{206}Pb/^{204}Pb$ with younging of volcanoes is interpreted to be a waning of the DMM component in the Samoan lavas, with a resulting increase in the abundance of EM2 and HIMU components. The separation of the Vai and Malu Trends in Pb-isotopic space indicates a higher HIMU/EM2 ratio in the Vai Trend.

[43] Moving east along each of the two Trends, there are systematic increases in K/Na, Rb/Sr, La/Sm, La/Yb, Ba/Sm, Th/Nb, Th/Zr, Nb/Y, Nd/Sm, Nb/Zr, and U/Nb (Figure 16); in other words, incompatible-element-enrichment increases with Pb isotopic enrichment, distance, and decreasing age. Owing to correlations between isotopes and trace

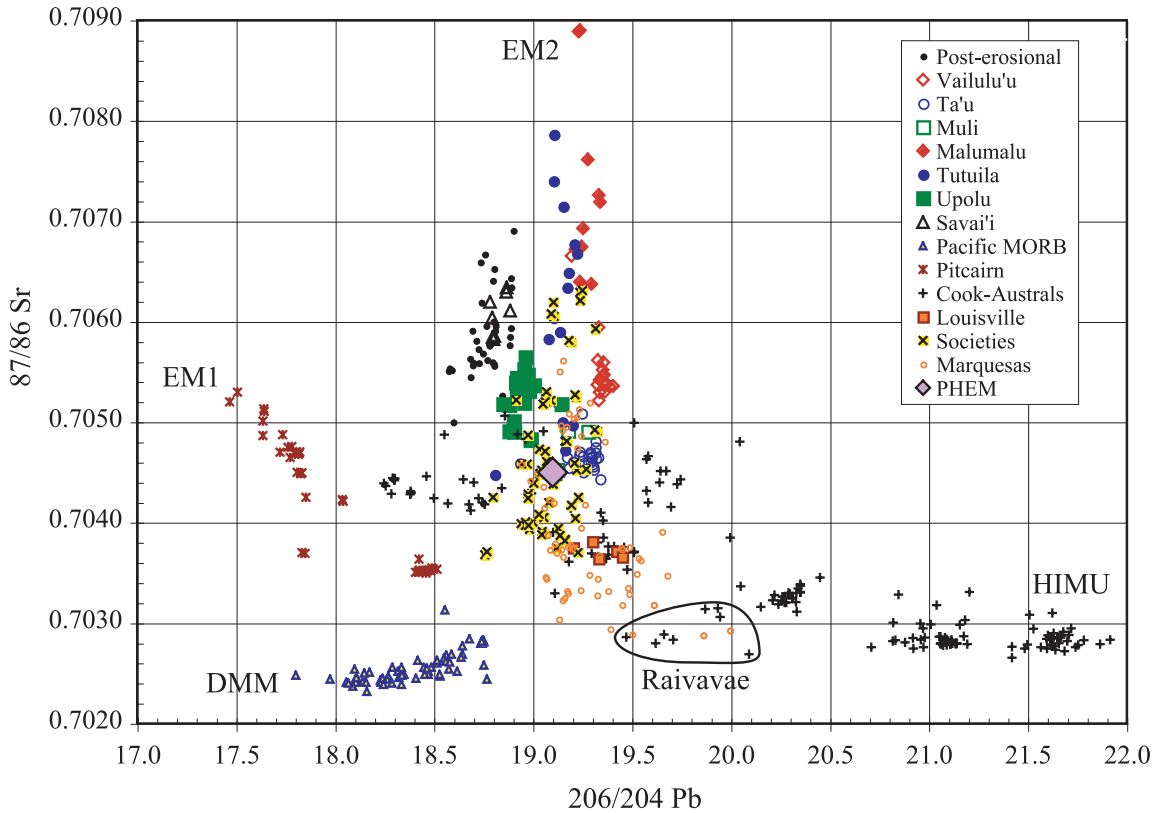

Figure 14. Plot showing Sr and Pb isotopic compositions for ocean islands of the Pacific Ocean. Data has been compiled from this study and the GEOROC database. EM2 dominates the spread in composition for the volcanoes Malumalu and Tutuila. Upolu volcano has a significant DMM component and Vailulu'u and Ta'u have been contaminated by HIMU from the Cook-Austral under-plated Pacific lithosphere.

elements like those seen in Figure 16, variations in trace element ratios are easily attributed to differences in composition between the low $^{206}Pb/^{204}Pb$ source and the high $^{206}Pb/^{204}Pb$ sources. However, we are witness not to the source compositions, but to the products of "source processing". Because the process of melt generation has maintained (or not overly obscured) trace element correlations with isotopic compositions, we can infer some characteristics of the sub-Samoan mantle.

[44] Possible explanations for the systematic chemical evolution of the Samoan plume include the following.

[45] 1. The plume material displays horizontal zonation, implying a length-scale of heterogeneity on the order of volcano spacing, as has been suggested for the Hawaiian Islands (see below). In this case, trace element variations are truly source variations.

[46] 2. The mantle is lithologically homogeneous, for which peridotite components of variable composition occur in the same proportions beneath all Samoa, but exist on a length-scale large enough to allow preservation of disequilibrium between the components. In this case, variable potential temperature of the plume would result in preferential sampling of components based on their respective solidus temperatures. Enriched materials would be sampled at small degrees of melting and trace element enrichment is partly a function of degree of melting.

[47] 3. A vertically stratified plume changes composition and/or physical properties as upwelling

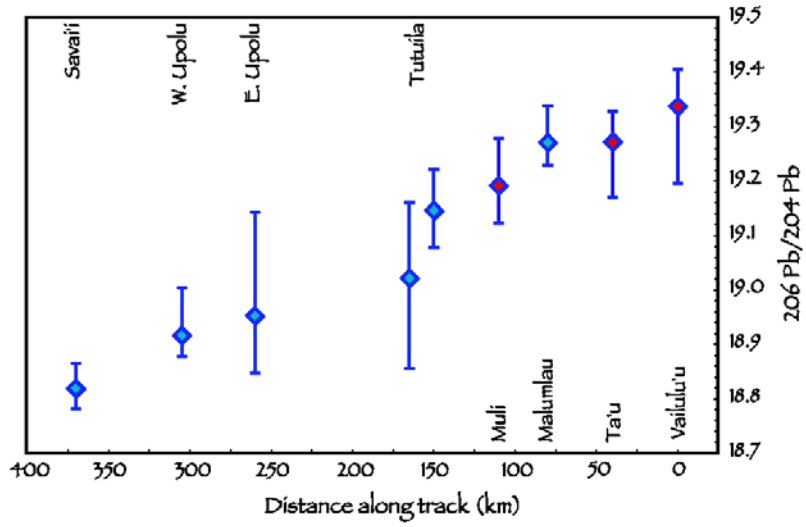

Figure 15. Plot showing a systematic increase in $^{206}Pb/^{204}Pb$ with eastward younging of volcanoes. Distance is measured from the zero-aged leading edge seamount, Vailulu'u. The ''oldest'' volcano (at a distance of 370 km from Vailulu'u) is Savai'i, though no lavas have been shown to be as old as the theoretical 5 Myr age of the island as suggested from age progression models. High $^{206}Pb/^{204}Pb$ values are found in EM2 and HIMU; low $^{206}Pb/^{204}Pb$ values are found in DMM. The increase in $^{206}Pb/^{204}Pb$ with time is therefore a waning of the DMM component in Samoan lavas.

proceeds, affecting the degree of entrainment of ambient upper mantle and lithospheric assimilation.

[48] In the Hawaiian Islands (an EM1 plume), isotopically distinct, topographic en echelons, named the ''Kea'' and ''Loa'' Trends, have also been documented [*Tatsumoto*, 1978; *Staudigel et al.*, 1984; *Abouchami et al.*, 2000]. The Society Islands (another EM2 archipelago) display similar subparallel trends in both geographic and Pb isotopic space (using data compiled in the GEOROC database). However, nothing so temporally systematic as that in Samoa has been previously reported. Chemical zonation of a mantle plume [e.g., *Kurz et al.*, 1995; *Hauri et al.*, 1996; *Lassiter et al.*, 1996; *DePaolo et al.*, 2001] may explain isotopic lineaments within island chains, but fails to address how this chemical heterogeneity may translate into topographic features. On the other hand, creation of topographic lineation as a consequence of either (1) the lithosphere's structural response to loading [e.g., *Hieronymus and Bercovici*, 1999, 2000] or (2) magma rising in ''plumlets'' instead of a continuous stream [*Ihinger*, 1995] ignores the fact of correlative chemical variations. Even so, some common dynamic feature clearly exists, independent of mantle taxonomy, for the way in which plumes forge through the mantle/crust, melt, and arrive at Earth's surface.

7. Calculation of a "Pure" EM2 Lava

[49] The following calculation is aimed at defogging the trace element pattern for lavas of the enriched end-member, through ''un-mixing'' (subtracting) Ta'u lavas (average $^{87}Sr/^{86}Sr = 0.7046$) from the most EM2-rich Malumalu lavas, under the assumption that the highest $^{87}Sr/^{86}Sr$ lavas are, instead of pure EM2 melts, still somewhat contaminated by melts from a depleted/less enriched mantle. As a group, Ta'u lavas are closest to the PHEM mixing component (Figures 13 and 14). By this calculation, trace element differences between un-enriched and enriched mantles are accentuated, and help to clarify the trace element characteristics of the EM2 source.

[50] We extrapolate to the end-member trace element pattern of an EM2 melt in effect by subtracting the averaged trace element composition of Ta'u lavas from the Malumalu lavas until the $^{87}Sr/^{86}Sr$ composition equals 0.7128; this value

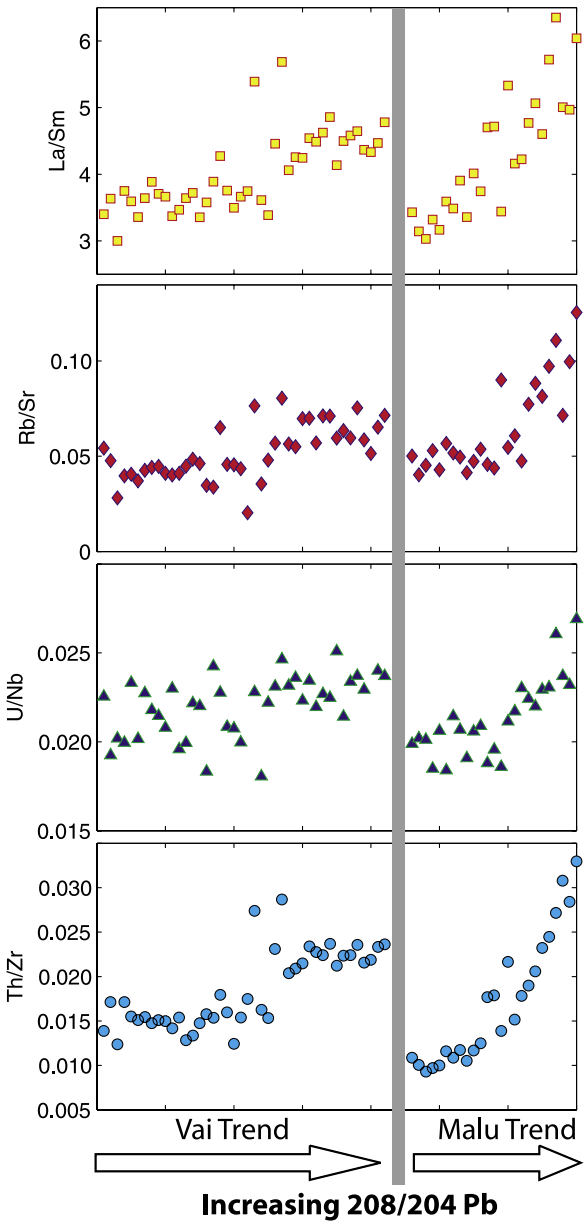

Figure 16. Trace element ratios of Samoan lavas, with the more incompatible element in the numerator, showing correlation with $^{208}Pb/^{204}Pb$ isotopic compositions. The Vai and Malu Trends have been separated into two groups, each sorted by increasing $^{208}Pb/^{204}Pb$, and plotted with trace element ratios.

derives from an analysis of cpx contained in a metasomatized peridotite xenolith from Savai'i [*Hauri et al.*, 1993]. Although these xenoliths are not an extension of the Samoan Pb isotope array (Figures 7 and 8), for lack of a better stopping point, they do place an upper limit on oceanic mantle Sr isotopic ratios.

[51] Mixing between Ta'u and a "pure" EM2 component to make the most enriched Samoan samples (Malumalu samples 78-1 and 78-3) is calculated with the following two equations:

$$\left(^{87}Sr/^{86}Sr\right)_{78-1} = \frac{F[Sr]_{EM2}\left(^{87}Sr/^{86}Sr\right)_{EM2} + (1-F)[Sr]_{Tau}\left(^{87}Sr/^{86}Sr\right)_{Tau}}{F[Sr]_{EM2} + (1-F)[Sr]_{Tau}} \quad (1)$$

$$[Sr]_{78-1} = F[Sr]_{EM2} + (1-F)[Sr]_{Tau} \quad (2)$$

The concentration of Sr ([Sr]) in EM2 and the fraction of the EM2 melt, F, are solved simultaneously so that the right hand of equation (1) equals the $^{87}Sr/^{86}Sr$ composition of the two extreme Malumalu lavas (0.70889). With the value for F, concentrations of all trace elements can be calculated

Table 7. Calculated Trace Element Composition of a "Pure" EM2 Melt[a]

	Average Ta'u	Average Malumalu	EM2 Melt
$^{87}Sr/^{86}Sr$	0.7046	0.70889	0.7128
Cs	0.11	0.41	0.70
Rb	15.17	44.73	73.47
Ba	146.96	281.99	413.29
Th	2.78	6.17	9.46
U	0.62	1.16	1.69
Nb	29.71	43.96	57.83
Ta	2.06	2.92	3.76
K	0.73	1.57	2.39
La	24.16	44.31	63.90
Ce	50.61	82.17	112.85
Pb	2.09	4.35	6.56
Pr	6.27	9.16	11.98
Nd	27.24	34.89	42.33
Sr	367.00	379.09	390.83
Zr	187.15	205.43	223.20
Hf	4.82	5.20	5.57
Sm	6.74	7.15	7.56
Eu	2.15	1.99	1.84
Ti	2.99	2.20	1.42
Gd	6.41	6.28	6.15
Tb	0.95	0.87	0.79
Dy	5.21	4.59	4.00
Ho	0.94	0.80	0.67
Y	24.00	21.89	19.84
Er	2.26	1.91	1.57
Tm	0.29	0.25	0.21
Yb	1.67	1.40	1.13
Lu	0.24	0.21	0.17
Sc	25.76	25.77	25.79

[a] All reported as ppm except K and Ti in wt%. All samples in averages are olivine corrected to Mg# 73.

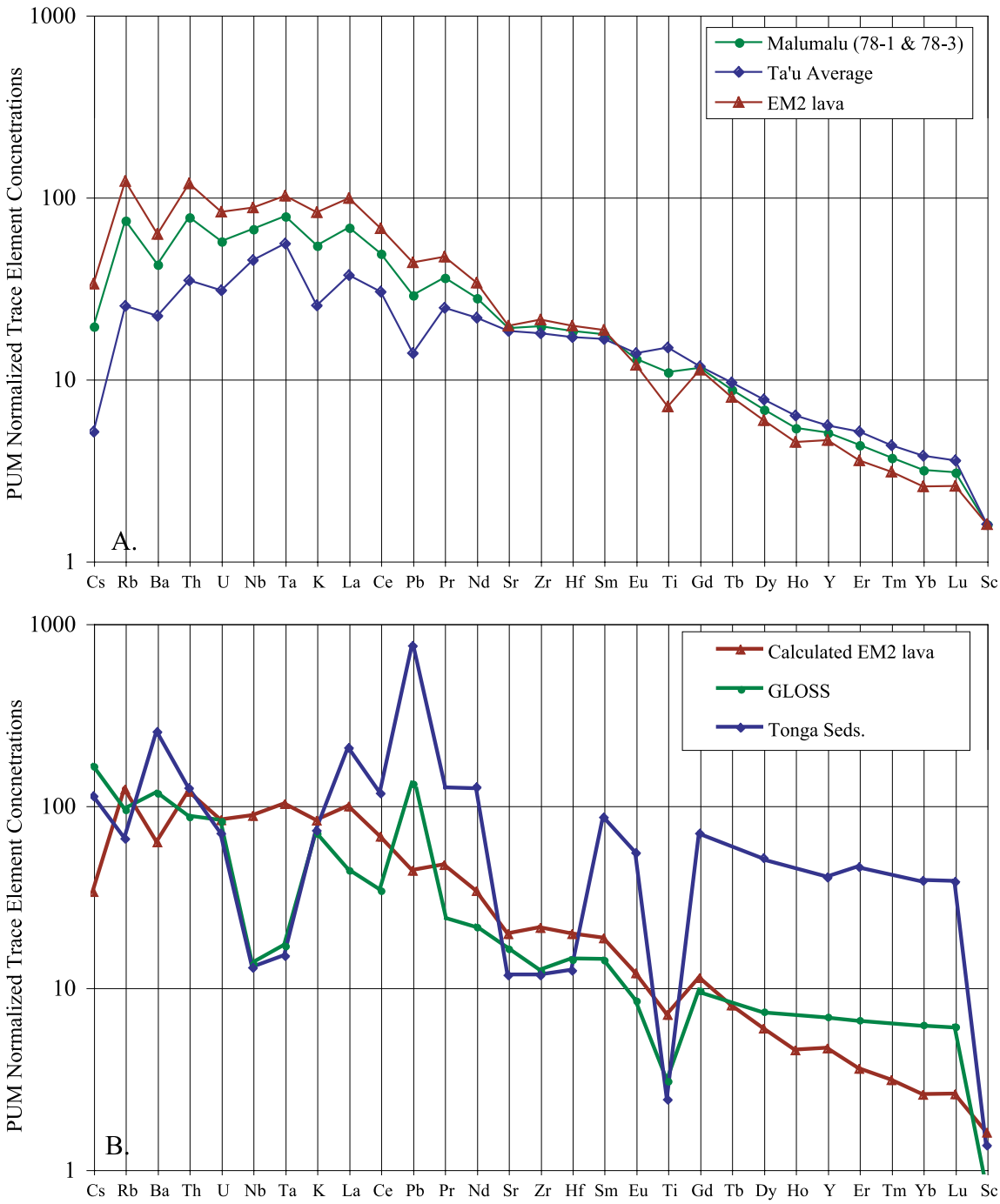

Figure 17. Spidergrams in Figure 17a show the average of Ta'u lavas, the average of the two most enriched Malumalu lavas, and a calculated EM2 lavas based on extrapolation between Ta'u and Malumalu trace element patterns shown here. All lavas have been corrected for olivine fractionation. In Figure 17b, the calculated EM2 lava is compared to trace element patterns for globally subducting sediment (GLOSS) and a local Tongan sediment (both from *Plank and Langmuir* [1998]). Clearly, the trace element patterns between the EM2 lava and sediment are a near-zero match.

for the EM2 melt by using the structure of equation (2) and are reported in Table 7. Lava compositions used in this calculation have been corrected for crystal fractionation by incremental addition of olivine (or subtraction in the case of 78-1, 78-3 and 74-1) until the melt compositions reaches a Mg# of 73 (olivine addition ranges from 10–51%; olivine subtractions are 10%, 7% and 23%, respectively). Note from Figure 4 that Ta'u and Malumalu have very similar crystal fractionation trajectories with minimal cpx loss. All Ta'u samples have been utilized except for T21 which is plagioclase-rich and T44 which is an ankaramite.

[52] The resulting fraction of EM2 "melt" in the Malumalu "mixture" is 51%, and the resulting $^{143}Nd/^{144}Nd$ ratio for the EM2 component equals 0.51235. Figure 17 shows the trace element pattern for the calculated "pure" EM2 melt component; note enrichments at Rb and Th that are almost 120 times PUM, negative anomalies at Cs and Ba, and an almost non-existent Pb anomaly. The REE slope of the calculated EM2 melt is steeper than both Malumalu and Vailulu'u, and the overall trace element pattern from U to the right is remarkably smoother than either the Malumalu or Vailulu'u pattern, save for dips at Sr and Ti. In general, the degree of enrichment in the EM2 melt is greatest for the highly incompatible elements.

[53] The calculated trace element pattern of the "pure" EM2 melt is compared to (1) an estimate of global subducting sediment (GLOSS) [*Plank and Langmuir*, 1998] and (2) a local sediment from DSDP Hole 595/596 analyzed for the GLOSS compilation (Figure 17). Clearly, the sediment trace element patterns are very different from the calculated EM2 component. In particular, the sediment spidergrams are marked by large negative anomalies of the high-field-strength elements (HFSE; Nb, Ta, Zr, and Hf), and large positive Pb and Ba anomalies, whereas the calculated Samoan enriched component has no such features; in fact, the Ba anomaly becomes more negative in the EM2 melt. Also, the heavy rare earth-element slope of the EM2 melt is significantly steeper than the sediment patterns: Sm/Yb for the sediments is 2.1 whereas for the EM2 melt is 7.2. The only argument in favor of sediment addition is the significantly decreased Pb anomaly in the EM2 melt. However, we (1) do not believe this alone lends credence to the sediment theory, and (2) show in our non-sediment model below how Pb in the EM2 source does not have a negative anomaly.

[54] Ultimately, the calculated EM2 spidergram is inconsistent with standard models invoking ancient sediment recycling to explain the enrichment of the EM2 mantle source. As discussed below, it is unlikely that any chemical processing during subduction would so effectively "smooth out" the typically jagged spidergram of oceanic sediment. Alternatively, if the enriched plume material is argued to derive from addition of present-day sediments, the trace element patterns of local sediments should be directly reflected in the EM2 melt and they are not. Therefore late-stage contamination of plume material with local sediment is also an unsatisfactory explanation for the observed chemical characteristics of the enriched Samoan basalts (and this point is strongly supported by the Pb isotope evidence shown in Figures 7 and 8). Production of the EM component by deep mantle fractionations involving high-pressure phases such as Ca or Mg perovskite likewise will lead to jagged, not smooth, spidergrams [*Hirose et al.*, 2004]. Segregation of carbonatitic melts from mantle assemblages has been used to explain elevated trace element concentrations in oceanic lavas [see *Zindler and Hart*, 1986], but this process also causes irregular trace element patterns [e.g., *Klemme et al.*, 1995; *Sweeney et al.*, 1995; *Hoernle et al.*, 2002]. Instead, the remarkably smooth EM2 melt spidergram gives the uncanny impression of having originated from nothing but "unadulterated" melting processes within the upper mantle.

8. Sediment Recycling?

[55] Osmium and oxygen isotopes are thought to be "smoking guns" for sediment/slab recycling [*Eiler et al.*, 1997; *Shirey and Walker*, 1998; *van Keken et al.*, 2002]. Owing to the incompatibility of Re [*Righter and Hauri*, 1998] and compatibility of Os [*Hart and Ravizza*, 1996] in mantle melting, elevated Re/Os ratios in crustal materials should

evolve to radiogenic osmium during long-term storage within the mantle. Altered upper MORB crust and marine sediments are enriched in heavy oxygen ($\delta^{18}O$ of ~15–25‰ [*Savin and Epstein*, 1970; *Lawrence et al.*, 1979; *Staudigel et al.*, 1995; *Alt*, 2003]) by low-temperature fractionation processes at the Earth's surface. This is high above the $\delta^{18}O$ value of 5.2‰ for upper mantle olivine [*Ito et al.*, 1987; *Mattey et al.*, 1994; *Eiler et al.*, 1997]. Therefore the standard theory for the origin of EM2 involving recycling of mafic crust plus terrigenous sediment would suppose Samoan lavas to have both elevated $\delta^{18}O$ and $^{187}Os/^{188}Os$ compositions.

[56] *Eiler et al.* [1997] demonstrated that EM2 basalts from Samoa (Savai'i post-erosional) and the Societies do have the highest $\delta^{18}O$ of all OIB's ($\delta^{18}O$ of olivine up to 6.1‰), explainable by the incorporation of ~5% terrigenous sediment addition to DMM. Using values chosen by *Eiler et al.* [1997] for the concentrations of Sr, Nd, and Pb in DMM and sediments, the sediment contribution to the trace element budget in the EM2 source will be 50%, 68% and 96%, respectively, for these elements. Clearly then, the trace element pattern of EM2 lavas should reflect the trace element patterns of sediment, but they do not (see Figure 17). *Eiler et al.* [1997] also mention the possibility that metasomatism can elevate $\delta^{18}O$ values in magmas, and the present work recommends this idea be further explored.

[57] Osmium isotopic compositions are likewise not so "smoking" of a sediment component. Combining data presented here (Table 4) with those from *Hauri and Hart* [1993], Samoan basalt samples with >80 ppt Os (ranging in $^{87}Sr/^{86}Sr$ from 0.7046 to 0.7089) reveal $^{187}Os/^{188}Os$ ratios of 0.124–0.130 which do not correlate with any other isotope system. Samples with <80 ppt Os (5 out of 21 in total) have elevated $^{187}Os/^{188}Os$ ratios and are interpreted to be contaminated with seawater [see *Shirey and Walker*, 1998]. The small range in $^{187}Os/^{188}Os$ compositions of pristine samples spans values estimated for the primitive upper mantle (0.129 [*Meisel et al.*, 1996]) and DMM (~0.125 [*Standish et al.*, 2002]), and is much lower than the upper limit of 0.16 displayed in HIMU and EM1 lavas [*Hauri and Hart*, 1993; *Reisberg et al.*, 1993; *Eisele et al.*, 2002].

[58] The unradiogenic $^{187}Os/^{188}Os$ values for these Samoan lavas represent either (1) a similarly unradiogenic mantle source, or (2) re-equilibration of more radiogenic Os components with unradiogenic upper/lower mantle through special processes that are not active beneath HIMU or EM1 hot spots. With regard to the former option, and to test the standard model, low Os concentrations in sediments may prevent a sediment component from significantly elevating $^{187}Os/^{188}Os$ ratios in the EM2 source. In a simple case, if DMM with $^{187}Os/^{188}Os = 0.125$ and [Os] = 3000 ppt is mixed with sediment having $^{187}Os/^{188}Os = 1.0$ and [Os] = 30 ppt [*Peucker-Ehrenbrink and Jahn*, 2001], then 35% of sediment is needed to change $^{187}Os/^{188}Os$ from 0.125 to 0.130. Here we are again left with an EM2 source whose trace element budget would be dominated by sediment, but do not observe such trace element patterns in the EM2 lavas nor see the implied correlations with other isotope systems. The second option, suggesting the Os budget derives from re-equilibration, can be ruled out since olivine phenocrysts are in approximate equilibrium with coexisting liquids (Jackson et al., unpublished data, 2003) and have high $^{3}He/^{4}He$ ratios (i.e., are not xenocrystic, but rather truly phenocrystic). We conclude that the mantle sources for Samoan lavas all have inherently unradiogenic $^{187}Os/^{188}Os$ values and are not influenced by a sediment/crustal component.

[59] Although slab/sediment recycling has been a common theory for the origin of EM2 for over two decades (see section 1), there are major flaws in this train of thought. The Standard Model for generating the EM2 reservoir involves the introduction into the deep mantle of (1) oceanic crust which has been depleted of fluid-mobile elements, such as the large-ion-lithophile elements (LILE; e.g., Cs, Rb, K and Pb), by dehydration and (2) a relatively pristine (i.e., elementally unfractionated) continental crust component (i.e., terrigenous sediments). Although not typically considered in the Standard Model, it seems logical that trace elements of subducted sediments (pelagic and/or terrigenous) must be fractionated by the same

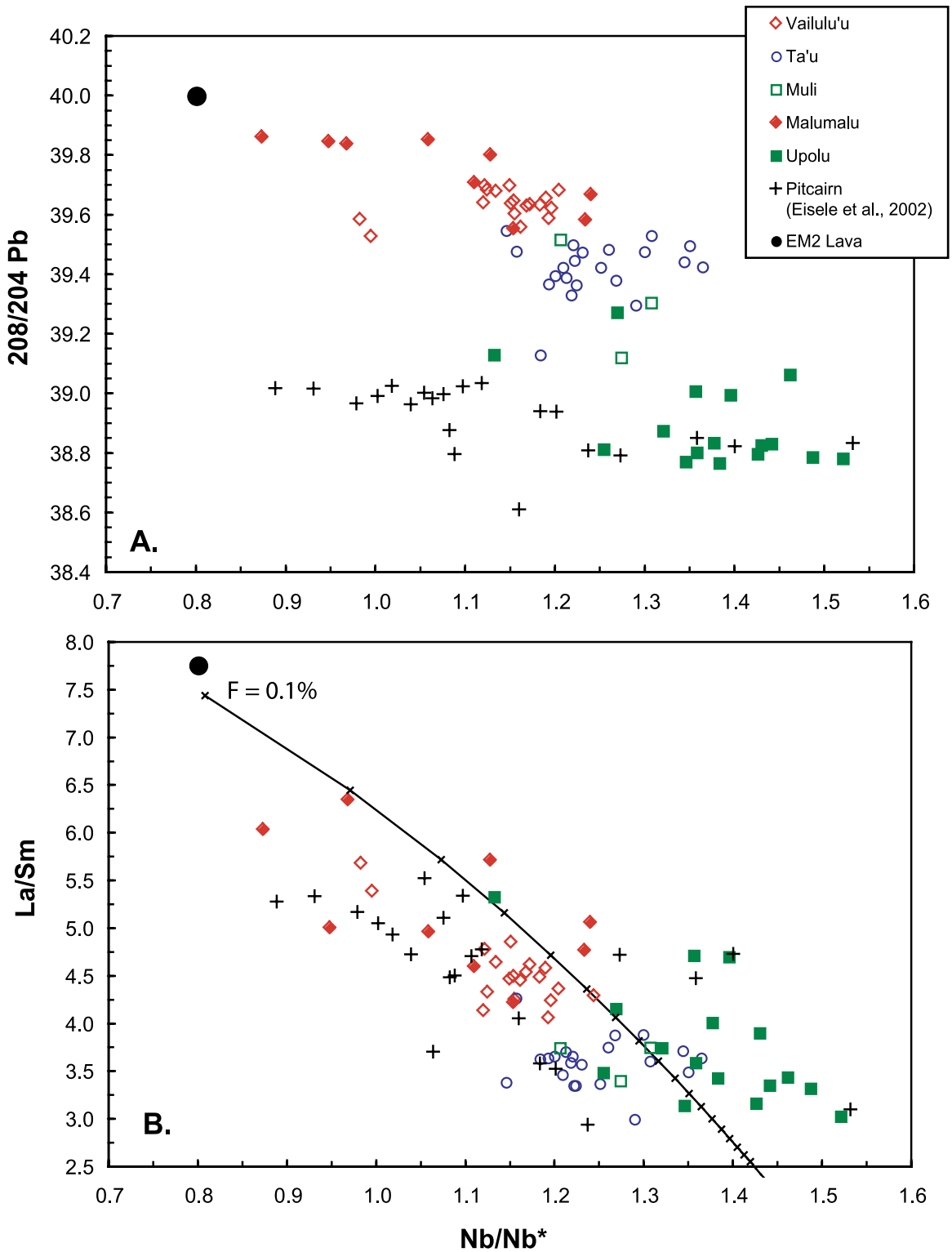
Vailulu'u
Ta'u
Muli
Malumalu
Upolu
Pitcairn
(Eisele et al., 2002)
EM2 Lava
208/204 Pb
A.
F = 0.1%
La/Sm
B.
Nb/Nb*

Figure 18

process by which the subducted ocean crust is fractionated (dehydration) – especially since sediments are closer to the mantle wedge and likely to have greater water contents than the altered ocean crust. Whereas there have been experimental studies showing high trace element mobility during dehydration of subducted ocean crust (especially for the isotopically important elements Rb and Pb; see *Ayers* [1998] and *Stracke et al.* [2003] for overviews), very little similar work has been done on dehydration of subducted sediments [i.e., *Johnson and Plank*, 1999]. Actually, there is growing geochemical evidence that not only a fluid component, but also partial melts of subducted sediments contribute to arc magmas. The high recycling efficiencies (up to 40%) of elements which are not particularly fluid mobile, such as Be, Th and Nd (see discussion by *Johnson and Plank* [1999]), suggest sediment melting is a reality, even though many thermal models predict subsolidus temperatures within the subducted sediment column [e.g., *Peacock*, 1996]. Regardless of the mechanism of trace element fractionations in subducted sediments, it is clear that fractionations will occur and will result in significant loss of incompatible elements, and a decrease in the mass of a possible future EM2 reservoir. Ultimately, it is grossly inconsistent to use modern, surface sediment as an approximation of the trace element and isotopic composition of a "sediment" component in the mantle – once subducted, the sediment will never look the same, especially for parent/daughter ratios like Rb/Sr and Th/Pb.

[60] Additionally, since today's surface, terrigeneous sediments represent what has been extracted by convergent margin volcanism and/or continental crust formation, it is the residue, or complement, to surface sediments which should be our concern for what material is actually recycled deep into the mantle. For example, depletion of the fluid immobile elements Na and Ta in arc volcanics [*Pearce and Peate*, 1995], and hence sediments [*Plank and Langmuir*, 1998], will be matched by Nb-Ta enrichments in the material that is ultimately introduced to the deep mantle. Experiments on partitioning between dehydration fluids and eclogite mineral assemblages (garnet, clinopyroxene and rutile) suggest that depletion of high field-strength elements (including Nb-Ta) in arc volcanics is due to their high compatibility in residual rutile [*Stalder et al.*, 1998] and is therefore not a sediment signature. Enrichment of HFSE in the subducted slab will offset HFSE depletions in the subducted sediment. This is why decreasing Nb anomalies with increasing $^{87}Sr/^{86}Sr$ ratios, as documented for EM1 and EM2 lavas by *Eisele et al.* [2002], are not supporting evidence for sediment recycling.

[61] We believe there is an alternative explanation for correlation between Nb anomalies and isotopic compositions. Figure 18 shows Nb/Nb* (calculated as $Nb_N/\sqrt{(Th_N \times La_N)}$ [*Eisele et al.*, 2002]) plotted with $^{208}Pb/^{204}Pb$ and La/Sm ratios of lavas from Samoa and Pitcairn. We have used $^{208}Pb/^{204}Pb$ as a measure of EM2 abundance instead of $^{87}Sr/^{86}Sr$ only because it provides better correlations. Samoan lavas show inverse relationships between Nb/Nb* and $^{208}Pb/^{204}Pb$ as well as La/Sm. Pitcairn lavas [from *Eisele et al.*, 2003] show a negative correlation between Nb/Nb* and La/Sm, which overlaps with the Samoan lavas, and a more shallow slope than Samoa for Nb/Nb* against $^{208}Pb/^{204}Pb$ (the greatest isotopic variation in the Pitcairn lavas is in $^{143}Nd/^{144}Nd$). Pitcairn and Samoa samples have almost an identical range in both La/Sm and Nb/Nb*, even though the isotopic variability is greater in Samoa. Also plotted in Figure 18 is a trajectory for variable degree of melting of a depleted mantle, showing that small

Figure 18. Nb/Nb* (calculated as $Nb_N/\sqrt{(Th_N \times La_N)}$, as in *Eisele et al.* [2002]) plotted with (a) $^{208}Pb/^{204}Pb$ and (b) La/Sm, of Samoan lavas and Pitcairn lavas [from *Eisele et al.*, 2002]. Pitcairn lavas have little source variation, as seen by a narrow range in $^{208}Pb/^{204}Pb$, but they have a range in Nb/Nb* and La/Sm that is nearly identical to Samoa. This indicates that varying degrees of melting of the same source can provide a wide range of trace element ratios otherwise interpreted to be source variations. The negative correlation in Samoa shows that at small degrees of melting (i.e., high La/Sm and low Nb/Nb*), the enriched component may be preferentially sampled from the mantle. The melting curve is for batch melting of a mantle with the following concentrations in ppm: Th = 0.032, Nb = 0.457, La = 0.32, Sm = 0.326. D values for these elements are respectively 0.00038, 0.0043, 0.0045, 0.04. Tick marks are every 0.1% melting, increasing toward low La/Sm.

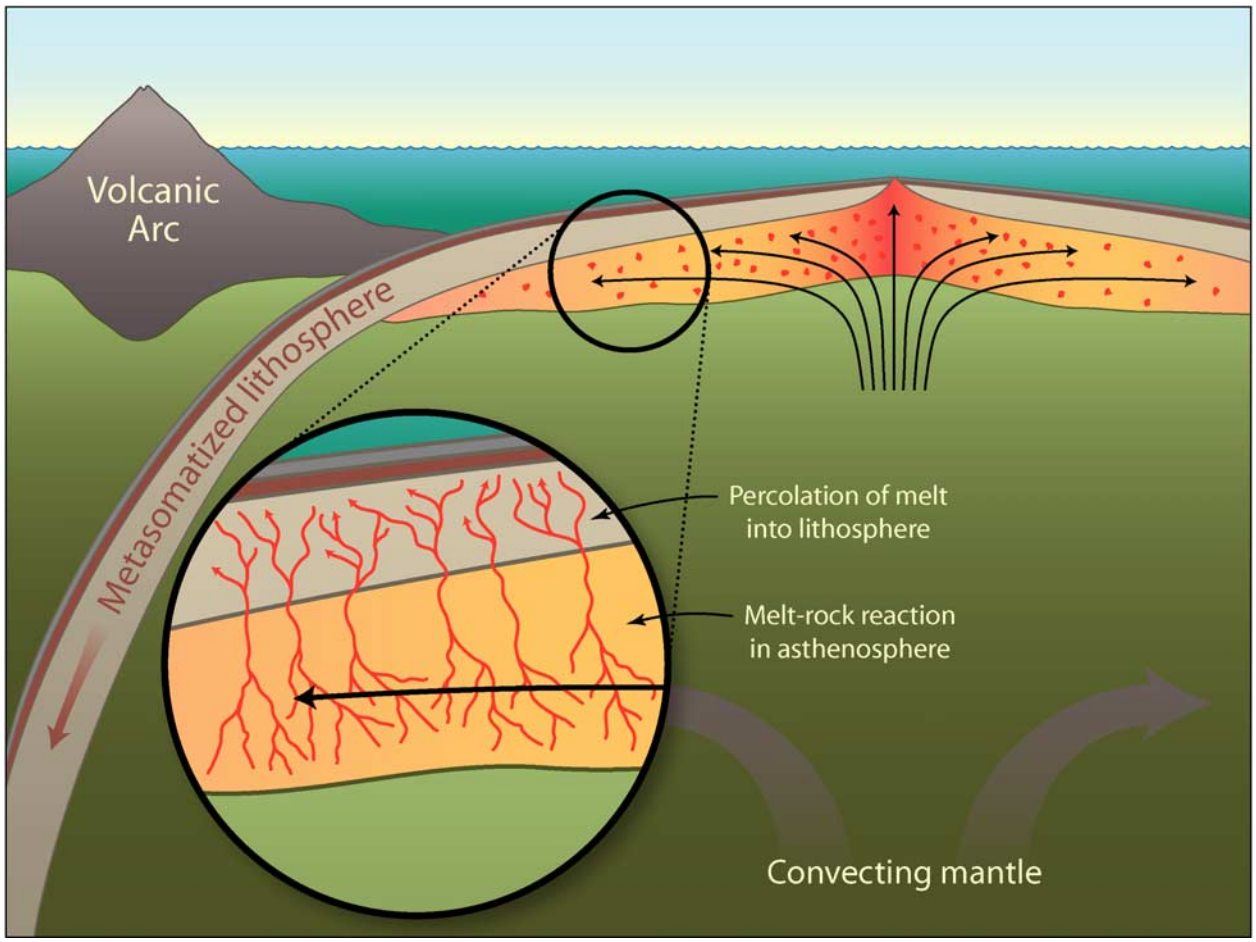

Figure 19. Schematic diagram illustrating a working hypothesis for the origin of the EM2 mantle reservoir. Starting 2.5 Ga, small degree (0.5%) batch melts of the primitive upper mantle migrate through the asthenosphere an impregnate the lithosphere. A mixture of depleted lithosphere with 1.1% of the 0.5% batch melts has the trace element pattern required to evolve to the present-day Sr, Nd, and Hf isotopic compositions of EM2.

changes in F can produce large changes in both La/Sm and Nb/Nb*. Therefore variable Nb/Nb* (previously interpreted as only a source effect) can be produced by recent variations in melt production, and is most likely what causes (1) scatter in the plots of Figure 18 and (2) the same Nb/Nb* variation in Pitcairn as Samoa given less isotopic variation. The correlation of $^{208}Pb/^{204}Pb$ (and $^{87}Sr/^{86}Sr$) with Nb/Nb* can be interpreted as an ancient enrichment of mantle by a small degree (low Nb/Nb*) melt, as suggested by the calculated EM2 melt and modeled below.

9. Metasomatic Origin of EM2

[62] Given the many failures of the "sediment recycling" model for EM2, as enumerated above, we propose here a new model that invokes metasomatic enrichment of ancient oceanic lithosphere, followed by long-term storage in the deep mantle and recent return to the surface as the Samoa plume. Conceptually, this model derives from the autometasomatic process proposed by *Zindler et al.* [1979] and *Roden et al.* [1984]. Numerous authors have appealed to metasomatism of oceanic plates to generate chemical heterogeneities that can be tapped prior to plate subduction [*Hawkesworth et al.*, 1979, 1984; *Halliday et al.*, 1992; *Class and Goldstein*, 1997; *Niu et al.*, 1996]. Recycling of such metasomatized lithosphere, after long-term storage in the mantle, has been advocated by *Richardson et al.* [1982] and *Niu and O'Hara* [2003] as a source for enriched OIB.

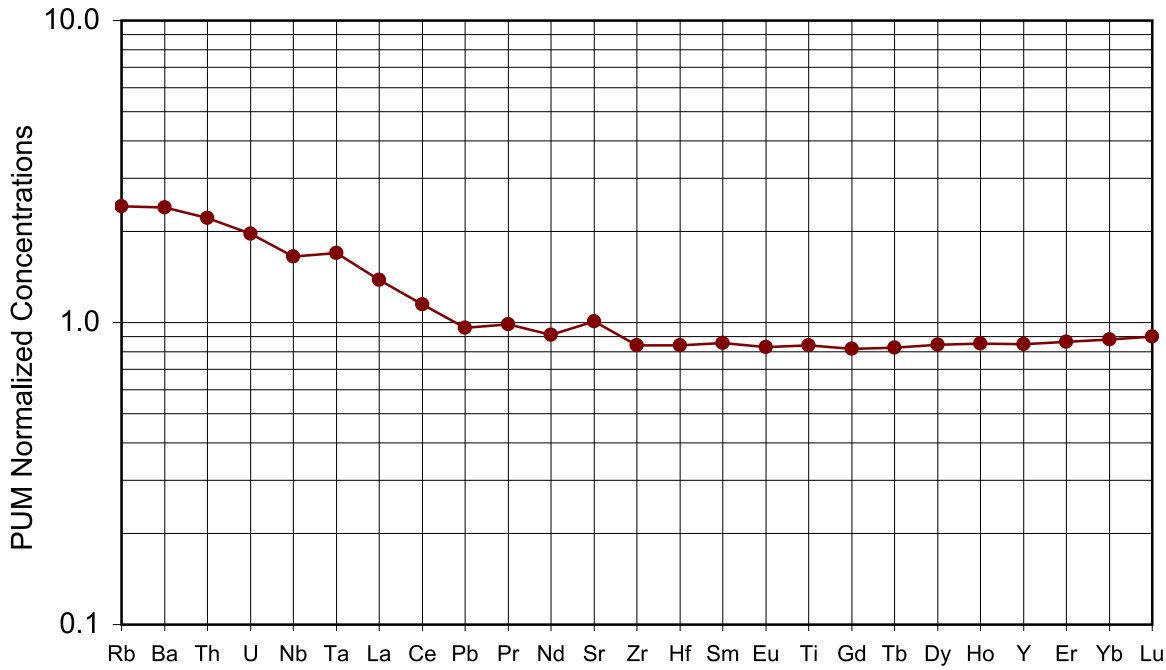

Figure 20. Calculated trace element pattern for the EM2 source. At a theoretical 2.5 Ga, a 0.5% batch melt from a primitive upper mantle source has been calculated with a combination of garnet peridotite D values (weighted 72%) and spinel peridotite D values (weighted 28%) from a compilation by *Kelemen et al.* [2003]. Exceptions to Kelemen's D values are as follows: $D^{Rb} = 0.0001$, and $D^{U} = 0.0016$ for both garnet and spinel field melting; for garnet melting, $D^{Th} = 0.00038$, $D^{Zr} = 0.05$, and $D^{Hf} = 0.08$; for spinel melting, $D^{Th} = 0.0011$. Mixing of 1.1% of this melt into a semi-depleted lithosphere results in the trace element pattern shown.

[63] If we start with the assumption that EM2 is a two-stage differentiate of bulk-earth, the slope on the $^{206}Pb/^{204}Pb$ - $^{207}Pb/^{204}Pb$ plot (Figure 7) yields an age of 2.5 Ga. This is an age older than the commonly quoted average mantle differentiation age of 1.8 Byr [*Hart*, 1984]. At that time, the composition of the mantle would have been more similar to primitive upper mantle than to the depleted mantle observed today (i.e., DMM). Assuming plate tectonics was operating 2.5 billion years ago in much the same way as it is today, this more primitive mantle material would have undergone depletion by melt extraction during upwelling under spreading ridges, then "turned the corner" and solidified to become depleted lithospheric mantle.

[64] In the following calculations, we model the case in which small degree, deep melts not extracted at the ridge crest percolate up through the asthenosphere and impregnate the overlying lithosphere that had just undergone melt extraction on the ridge crest. This is essentially a metasomatic process. This metasomatized lithosphere then is recycled and stored in the mantle to become today's EM2 reservoir (Figure 19). The melt fraction, amount of melt impregnation, and ratio of garnet to spinel peridotite melting are calculated so as to match parent/daughter ratios of EM2 for the Rb-Sr, Sm-Nd, U-Pb, Th-Pb and Lu-Hf systems, based on evolution from bulk earth 2.5 billion years ago. Bulk partition coefficients used for melting a primitive mantle source [*McDonough and Sun*, 1995] are based on a compilation of D's from *Kelemen et al.* [2003] for melting of garnet and spinel peridotite, with the few exceptions listed in Figure 20. Bulk partition coefficients are weighted 72% garnet peridotite to 28% spinel peridotite. The best match to parent/daughter ratios is with a 1.1% impregnation of a depleted lithosphere by a 0.5% batch melt of a primitive mantle. The lithosphere represents a mantle depleted by 2% melt extraction, as calculated using the method of *Workman and Hart* [2003] and as reported in

Table 8. Source Composition of EM2

	Primitive Mantle,[a] ppm	2% Melt Depleted Mantle, ppm	Bulk D Values	EM2 Source, ppm	PUM Normalized
Rb	0.6	0.140	0.00001	1.456	2.427
Ba	6.6	1.587	0.00008	15.857	2.403
Th	0.0795	0.020	0.00058	0.177	2.224
U	0.0203	0.006	0.0016	0.040	1.968
Nb	0.658	0.289	0.0040	1.087	1.653
Ta	0.037	0.019	0.0042	0.063	1.698
La	0.648	0.287	0.0067	0.895	1.381
Ce	1.675	0.823	0.0117	1.923	1.148
Pb	0.15	0.027	0.0092	0.144	0.959
Pr	0.254	0.146	0.0214	0.251	0.987
Nd	1.25	0.772	0.0317	1.140	0.912
Sr	19.9	10.803	0.0185	20.044	1.007
Zr	10.5	6.686	0.0472	8.835	0.841
Hf	0.283	0.195	0.0644	0.238	0.841
Sm	0.406	0.290	0.0692	0.347	0.855
Eu	0.154	0.114	0.1088	0.128	0.829
Ti	1072.1	829.471	0.1428	900.5	0.840
Gd	0.544	0.417	0.1800	0.445	0.818
Tb	0.099	0.079	0.2730	0.082	0.826
Dy	0.674	0.554	0.3504	0.569	0.845
Ho	0.149	0.125	0.4649	0.127	0.853
Y	4.3	3.651	1.0829	3.655	0.850
Er	0.438	0.374	0.5708	0.378	0.864
Yb	0.441	0.387	1.0784	0.387	0.878
Lu	0.0675	0.061	1.3710	0.061	0.900

[a] Primtive Upper Mantle (PUM) from *McDonough and Sun* [1995].

Table 8. Figure 20 shows the resulting trace element pattern of the EM2 source (also see Table 8). Rb/Sr has been fit to within <1%, Sm/Nd and Lu/Hf have been fit to within 3%, and Th/U has been fit to within 4%. The "unfortunate fits" are for U/Pb and Th/Pb, which are 53% and 58% too high respectively in the calculated EM2 source. This is clearly more a Pb problem than anything else. If the compatibility of Pb is lower by about a factor of two, as suggested by experimental partitioning data [*Hauri et al.*, 1994; *Salters et al.*, 2002], the U/Pb and Th/Pb ratios may be more precisely modeled. Because the mass fraction of melt added to the FOZO lithosphere (1.1%) is twice the degree of melting (0.5%) required to generate that impregnating melt, the mass of the mantle which melts must be twice as large as the mass of the metasomatized lithosphere.

[65] Does this source lead to the observed $^3He/^4He$ values of 8 R_A for EM2? Given the general trace element enrichment in the impregnating melt, and making the standard assumption of extreme incompatibility of He, it is likely that the calculated EM2 source would have high He/U ratios and hence evolve to $^3He/^4He$ values higher than 8 R_A. There are two possible solutions. One concerns the relative compatibility of He and U; if at high pressure and low degree of melting He is more compatible than U (this has not been proven nor disproven), then the impregnating melt will have low He/U and potentially evolve to DMM-like $^3He/^4He$ values (by coincidence). The second option is that the EM2 "package" has had a residence time in the upper mantle long enough (~1–2 Ga) to result in diffusive equilibrium of He (see model by *Moreira and Kurz* [2001] for example); this option has obvious implications for the primary home of recycled lithosphere.

[66] Although the above model leaves several questions unanswered, such as the scale length of the heterogeneities created by the metasomatism, and the resulting lithologies (mafic veins or enriched peridotite), it is successful in producing the observed isotopic and trace element characteristics of the Samoan mantle source. It does not require ad hoc chemical manipulations in the subduction zone, as does the standard crust/sediment-recycling model. In fact, as the enrichment zone is limited to the lower parts of the lithosphere, it will be nearly invulnerable to subduction zone processing. It calls on a process for which there is abundant evidence, particularly in the subcontinental lithosphere [*Frey and Green*, 1974; *Menzies and Murthy*, 1980; *Menzies*, 1983; *Menzies and Hawkesworth*, 1987]. And insofar as small-degree melts are ubiquitous in the upper oceanic asthenosphere, the process is virtually guaranteed. We note also that the small-scale convection usually invoked for this part of the mantle (i.e., Richter rolls) provides an efficient means of upward advection of standing melt fractions, as well as the consequent decompression that will augment the melt fractions and facilitate melt/solid segregation.

10. Conclusions

[67] A large suite of recently collected basalts from the Samoa hot spot chain have been analyzed for

Sr, Nd, Pb, Os and He isotopes, and major and trace elements. Localities include the subaerial islands of Savai'i, Upolu and Ta'u, and the submarine seamounts Muli, Malumalu and Vailulu'u.

[68] 1. Samoan basalts are isotopically (Sr-Nd-Pb) the most extreme EM2 lavas in the oceanic database ($^{87}Sr/^{86}Sr$ up to 0.7089). The Samoan isotopic arrays can be explained by mixing among four mantle components: DMM, EM2, HIMU and PHEM/FOZO. The deep plume material is most likely composed of EM2 and PHEM/FOZO, whereas the HIMU and DMM components are entrained into the plume in the upper mantle.

[69] 2. Systematic temporal and spatial variations in lava chemistry occur while going from west (older) to east (younger) along the chain: e.g., $^{206}Pb/^{204}Pb$, La/Sm, Rb/Sr, Th/Zr. This indicates a waning of the DMM component and waxing of the EM2 and HIMU components in Samoan volcanoes over the last few million years.

[70] 3. The standard recycling model (ocean crust plus terrigenous sediment) fails as an explanation for producing Samoan EM2, as witnessed by the smooth spidergrams for EM2 lavas with negative Ba anomalies, low $^{187}Os/^{188}Os$ ratios, high $^{3}He/^{4}He$ (>8 Ra) and mismatched Pb isotopic compositions.

[71] 4. The EM2 mantle source can be successfully modeled with the ancient (2.5 Ga) formation of metasomatised oceanic lithosphere, followed by storage in the deep mantle and return to the surface in the Samoan plume.

Appendix A

[72] Samples analyzed by M. Regelous were crushed in a steel jaw crusher to 3–5 mm sized chips, washed in deionised water, dried and hand-picked in order to avoid chips which were visibly altered, or which contained vesicles. A portion of these chips was set aside for isotope analysis, the rest was powdered in an agate swing mill. Major element analyses were carried out by X-ray fluoresence at the Universität Mainz, Germany, using a Phillips PW 1404 instrument. Trace element concentrations were determined by ICPMS using a Fisons Plasmaquad II instrument at the University of Queensland, Australia. Full details of the procedure are given in *Niu and Batiza* [1997]. The external precision on the concentrations of most of the trace elements measured is <3%. The long-term average values for the BHVO-1 rock standard are reported in Table 5. Pb isotope measurements were carried out at the Max Planck Institut für Chemie, Mainz, following the procedure outlined by *Abouchami et al.* [2000]. Between 50 and 100 mg of rock chips were washed in deionised water in an ultrasonic bath, then ultrasonicated in 6M HCl for 15 minutes, before being leached in hot 6M HCl for 1 hour. The HCl leachate was pipetted off, and the residue was rinsed, soaked in deionised water for 15 minutes, rinsed again and dried. This leaching procedure appears to remove much of the non-magmatic Pb that is contained in less-resistant components (surface contamination or alteration products), as discussed by *Abouchami et al.* [2000] and *Eisele et al.* [2003]. The leached residues were dissolved in HF-HNO3, treated repeatedly with HNO_3 and HCl until completely in solution, and Pb separated on anion exchange resin using HBr-HNO_3 mixtures [*Abouchami et al.*, 2000]. All reagents used were double-distilled, and total precedural blanks for the Pb chemistry were below 50 pg. The eluent from the Pb columns was twice evaporated to dryness with 15M HNO_3, and redissolved in 3M HNO_3. Sr and Nd were separated from this fraction at the University of Bristol, U.K., using methods adapted from *Pin et al.* [1994]. The sample in 3M HNO_3 was loaded onto columns containing 0.15 ml of TRU spec resin, positioned so as to drip directly into a second column containing 0.1 ml of Sr spec resin. After rinsing with 3M HNO_3, the columns were separated, and Sr was eluted from the Sr spec column in H_2O. The light- and middle-rare earth elements were recovered from the TRU spec resin by rinsing with 2.5M HCl. Nd was separated from this fraction using conventional HDEHP columns and 0.3M HCl. Pb isotope analyses were carried out using a triple spike technique to correct for instrumental mass fractionation. About 5% of the purified Pb fraction was transferred to a second beaker and spiked with a ^{204}Pb-^{206}Pb-^{207}Pb triple spike. The spiked and unspiked fractions were loaded onto

separate Re filaments with silica gel-H_3PO_4. Isotope compositions were measured using a Finnigan MAT-261 multicollector mass spectrometer (M.P.I. Mainz) in static mode, and the data for spiked and unspiked fractions were combined off-line to obtain the fractionation-corrected Pb isotope composition of the sample [*Galer*, 1999]. During this study, the NBS981 Pb standard gave $^{206}Pb/^{204}Pb$, $^{207}Pb/^{204}Pb$ and $^{208}Pb/^{204}Pb$ ratios of 16.9403 ± 0.0022, 15.4974 ± 0.0020 and 36.7246 ± 0.0058 respectively (2s, n = 19). Sr and Nd isotope measurements were carried out on a Finnigan Triton multicollector mass spectrometer (University of Bristol) in static mode, and within-run exponential fractionation corrections applied using $^{86}Sr/^{88}Sr = 0.1194$ and $^{146}Nd/^{144}Nd = 0.7219$. The NBS987 Sr and J&M Nd standards gave $^{87}Sr/^{86}Sr$ and $^{143}Nd/^{144}Nd$ ratios of 0.710247 ± 0.000008 (2 sigma, n = 15) and 0.511113 ± 0.000004 (n = 12) respectively, during the period of the sample measurements.

Acknowledgments

[73] Without Alberto Saal, we likely would have done none of this. He once printed an earthquake map that identified activity in a place that shouldn't have any. This led to the 1999 AVON 3 cruise, and discovery of active volcanism at Vailulu'u volcano. It also led to the dredging of tons of basalts that are the backbone of this paper. We thank Alberto for all of this, especially his help on the AVON 3 cruise and his help during fieldwork on Ta'u Island. Anthony Koppers was enormously helpful with data and sample processing during and following the AVON 3 cruise. We are also grateful to the captain and crew of the R/V Melville, along with the student volunteers, for catching and processing these tons of rocks. We thank Francis Albarède for access to the Lyon ICP/MS, and to Ken Sims and Sylvain Pichatt for their 24/7 efforts there in running many Pb isotope analyses. We thank Steve Galer and Wafa Abouchami for many tutorials in implementing the Mainz Pb chemistry at WHOI. The output of high-precision Pb data from the WHOI NEPTUNE is due largely to Lary Ball's skill and tenacity; our many thanks. Megan Coetzee's work on the Western Samoan seamounts, during a summer internship at WHOI, provided enthusiastic counterpoint to our work on the eastern volcanoes. We acknowledge NSF support, through grant OCE-9819038 (SRH and HS), and EAR-0125917 (SRH). Very constructive reviews were provided by Yaoling Niu and Rick Carlson. Finally, our gratitude to Jim Natland, for his generosity in sharing Samoan rocks, data and ideas, and for being an enduringly collegial provocateur. M. Regelous thanks A. Greig, Y. Niu, J. I. Wendt, W. Abouchami, S. Galer, C. Coath and C. Counsell for help and advice with the analytical measurements, and Warren Jopling of Safua Hotel for sharing his geological knowledge of Savai'i.

References

Abouchami, W., and S. L. Goldstein (1995), A lead isotopic study of Circum-Antarctic manganese nodules, *Geochim. Cosmochim. Acta*, *59*, 1809–1820.

Abouchami, W., S. J. G. Galer, and A. W. Hofmann (2000), High precision lead isotope systematics of lavas from the Hawaiian Scientific Drilling Project, *Chem. Geol.*, *169*, 187–209.

Alt, J. C. (2003), Stable isotopic composition of upper oceanic crust formed at a fast spreading ridge, ODP Site 801, *Geochem. Geophys. Geosyst.*, *4*(5), 8908, doi:10.1029/2002GC000400.

Armstrong, R. L. (1968), A model for the evolution of strontium and lead isotopes in a dynamic Earth, *Rev. Geophys.*, *6*, 175–199.

Ayers, J. (1998), Trace element modeling of aqueous fluid - peridotite interaction in the mantle wedge of subduction zones, *Contrib. Mineral. Petrol.*, *132*, 390–404.

Barling, J., and S. L. Goldstein (1990), Extreme isotopic variations in Heard Island lavas and the nature of mantle reservoirs, *Nature*, *348*, 59–62.

Bevis, M., et al. (1995), Geodetic observations of very rapid convergence and back-arc extension at the Tonga arc, *Nature*, *374*, 249–251.

Brocher, T. M., and R. Holmes (1985), Tectonic and Geochemical Framework of the Northern Melanesian Borderland: An Overview of the KK820316 Leg 2 Objectives and Results, in *Investigations of the Northern Melanesian Borderland*, *Earth Sci. Ser.*, vol. 3, edited by T. M. Brocher, vol. 3, pp. 1–12, Circum-Pacific Counc. for Energy and Miner. Resour., Houston, Tex.

Brooks, C., D. E. James, and S. R. Hart (1976), Ancient lithosphere: Its role in young continental volcanism, *Science*, *193*, 1086–1094.

Chase, C. G. (1981), Ocean island Pb: Two-stage histories and mantle evolution, *Earth Planet. Sci. Lett.*, *52*, 277–284.

Chen, W., and M. R. Brudzinski (2001), Evidence for a large-scale remnant of subducted lithosphere beneath Fiji, *Science*, *292*, 2475–2479.

Class, C., and S. L. Goldstein (1997), Plume-lithosphere interactions in the ocean basins: Constraints from the source mineralogy, *Earth Planet. Sci. Lett.*, *150*, 245–260.

Cohen, R. S., and R. K. O'Nions (1982), Identification of recycled continental material in the mantle from Sr, Nd and Pb isotope investigations, *Earth Planet. Sci. Lett.*, *61*, 73–84.

Danyushevsky, L. V., A. V. Sobolev, and T. J. Falloon (1995), Northern Tongan high-Ca boninite petrogenesis: The role of Samoan plume and subduction zone-transform fault transition, *J. Geodyn.*, *20*, 219–241.

DePaolo, D. J., and M. Manga (2003), Deep origins of hotspots: The mantle plume model, *Science*, *300*, 920–921.

DePaolo, D. J., J. G. Bryce, A. Dodson, D. L. Shuster, and B. M. Kennedy (2001), Isotopic evolution of Mauna Loa and

the chemical structure if the Hawaiian plume, *Geochem. Geophys. Geosyst.*, *2*, Paper number 2000GC000139.

Dostal, J., B. L. Cousins, and C. Dupuy (1998), The incompatible element characteristics of an ancient subducted sedimentary component in ocean island basalts from French Polynesia, *J. Petrol.*, *39*, 937–952.

Duncan, R. A. (1985), Radiometric ages from volcanic rocks along the New Hebrides-Samoa lineament, in *Investigations of the Northern Melanesian Borderland*, *Earth Sci. Ser.*, vol. 3, edited by T. M. Brocher, pp. 67–76, Circum-Pacific Counc. for Energy and Miner. Resour., Houston, Tex.

Eiler, J. M., K. A. Farley, J. W. Valley, E. H. Hauri, H. Craig, S. R. Hart, and E. M. Stolper (1997), Oxygen isotope variations in ocean island basalt phenocrysts, *Geochim. Cosmochim. Acta*, *61*, 2281–2293.

Eisele, J., M. Sharma, S. J. G. Galer, J. Blichert-Toft, C. W. Devey, and A. W. Hofmann (2002), The role of sediment recycling in EM-1 inferred from Os, Pb, Hf, Nd, Sr isotope and trace element systematics of the Pitcairn hotspot, *Earth Planet. Sci. Lett.*, *196*, 197–212.

Eisele, J., W. Abouchami, S. J. G. Galer, and A. W. Hofmann (2003), The 320 kyr Pb isotope evolution of Mauna Kea lavas recorded in the HSDP-2 drill core, *Geochem. Geophys. Geosyst.*, *4*(5), 8710, doi:10.1029/2002GC000339.

Ewart, A., K. D. Collerson, M. Regelous, J. I. Wendt, and Y. Niu (1998), Geochemical evolution within the Tonga-Kermedec-Lau Arc-Back-arc systems: The role of varying mantle wedge composition in space and time, *J. Petrol.*, *39*, 331–368.

Farley, K. A., J. H. Natland, and H. Craig (1992), Binary mixing of enriched and undegassed (primitive?) mantle components (He, Sr, Nd, Pb) in Samoan lavas, *Earth Planet. Sci. Lett.*, *111*, 183–199.

Frey, F. A., and D. H. Green (1974), The mineralogy, geochemistry, and origin of lherzolite inclusions in Victorian basanites, *Geochim. Cosmochim. Acta*, *38*, 1023–1059.

Galer, S. J. G. (1999), Optimal double and triple spiking for high precision lead isotopic measurement, *Chem. Geol.*, *157*, 255–274.

Ghiorso, M. S., M. M. Hirschmann, P. W. Reiners, and V. C. Kress III (2002), The pMELTS: A revision of MELTS for improved calculation of phase relations and major element partitioning related to partial melting of the mantle to 3 GPa, *Geochem. Geophys. Geosyst.*, *3*(5), 1030, doi:10.1029/2001GC000217.

Graham, D. W., S. E. Humphris, W. J. Jenkins, and M. D. Kurz (1993), Helium isotope geochemistry of some volcanic rocks from Saint Helena, *Earth Planet. Sci. Lett.*, *110*, 121–131.

Halliday, A. N., G. R. Davies, D.-C. Lee, S. Tommasini, C. R. Paslick, J. G. Fitton, and D. E. James (1992), Lead isotope evidence for young trace element enrichment in the oceanic upper mantle, *Nature*, *359*, 623–627.

Hamilton, P. J., R. K. O'Nions, D. Bridgewater, and A. Nutman (1983), Sm-Nd studies of Archean metasediments and metavolcanics from West Greenland and their implications for the Earth's early history, *Earth Planet. Sci. Lett.*, *38*, 26–43.

Hanyu, T., and I. Kanoeka (1997), The uniform and low $^{3}He/^{4}He$ ratios of HIMU basalts as evidence for their origin as recycled materials, *Nature*, *390*, 273–276.

Hart, S. R. (1984), A large-scale isotope anomaly in the Southern Hemisphere mantle, *Nature*, *309*, 753–757.

Hart, S. R. (1988), Heterogeneous mantle domains: Signatures, genesis and mixing chronologies, *Earth Planet. Sci. Lett.*, *90*, 273–296.

Hart, S. R., and G. E. Ravizza (1996), Os Partitioning Between Phases in Lherzolite and Basalt, in *Earth Processes: Reading the Isotopic Code*, *Geophys. Monogr. Ser.*, vol. 95, edited by R. Basu and S. R. Hart, pp. 123–134, AGU, Washington, D. C.

Hart, S. R., and H. Staudigel (1989), Isotopic characterization and identification of recycled components, 15–28, in *Crust/Mantle Recycling at Convergence Zones*, edited by S. R. Hart and L. Gulen, *NATO ASI Series*, *Ser. C*, vol. 258, Kluwer Acad., Norwell, Mass.

Hart, S. R., D. C. Gerlach, and W. M. White (1986), A possible new Sr-Nd-Pb mantle array and consequences for mantle mixing, *Geochim. Cosmochim. Acta*, *50*, 1551–1557.

Hart, S. R., E. H. Hauri, L. A. Oschmann, and J. A. Whitehead (1992), Mantle plumes and entrainment: Isotopic evidence, *Science*, *256*, 517–520.

Hart, S. R., et al. (2000), Vailulu'u undersea volcano: The New Samoa, *Geochem. Geophys. Geosyst.*, *1*, Paper number 2000GC000108.

Hart, S. R., R. K. Workman, M. Coetzee, J. Blusztajn, L. Ball, and K. T. M. Johnson (2002), The Pb isotope pedigree of western samoan volcanics: New insights from high-precision analysis by NEPTUNE ICP/MS, *Eos Trans. AGU*, *83*(47), Fall Meet. Suppl., Abstract U11A-0004.

Hassler, D. R., B. Peucker-Ehrenbrink, and G. E. Ravizza (2000), Rapid determination of Os isotopic composition by sparging OsO_4 into a magnetic-sector ICP-MS, *Chem. Geol.*, *166*, 1–14.

Hauri, E. H., and S. R. Hart (1993), Re-Os isotope systematics of HIMU and EMII oceanic island basalts from the south Pacific Ocean, *Earth Planet. Sci. Lett.*, *114*, 353–371.

Hauri, E. H., and S. R. Hart (1997), Rhenium abundances and systematics in oceanic basalts, *Chem. Geol.*, *139*, 185–205.

Hauri, E. H., N. Shimizu, J. J. Dieu, and S. R. Hart (1993), Evidence for hotspot-related carbonatite metasomatism in the oceanic upper mantle, *Nature*, *365*, 221–227.

Hauri, E. H., T. P. Wagner, and T. L. Grove (1994), Experimental and natural partitioning of Th, U, Pb and other trace element between garnet, clinopyroxene and basaltic melts, *Chem. Geol.*, *117*, 149–166.

Hauri, E. H., J. C. Lassiter, and D. J. DePaolo (1996), Osmium isotope systematics of drilled lavas from Mauna Loa, Hawaii, *J. Geophys. Res.*, *101*, 1793–1806.

Hawkesworth, C. J., M. J. Norry, J. C. Roddick, and R. Vollmer (1979), $^{143}Nd/^{144}Nd$ and $^{87}Sr/^{86}Sr$ ratios from the Azores and their significance in LIL-element enriched mantle, *Nature*, *280*, 28.

Hawkesworth, C. J., N. W. Rogers, P. C. W. van Calsteren, and M. A. Menzies (1984), Mantle enrichment processes, *Nature*, *311*, 331–335.

Hawkins, J. W., and J. H. Natland (1975), Nephelinites and Basanites of the Samoan linear volcanic chain: Their possible tectonic significance, *Earth Planet. Sci. Lett.*, *24*, 427–439.

Herzberg, C., and J. Zhang (1996), Melting experiments on anhydrous peridotite KLB-1: Compositions of magmas in the upper mantle and transition zone, *J. Geophys. Res.*, *101*, 8271–8295.

Hieronymus, C. F., and D. Bercovici (1999), Discrete alternating hotspot islands formed by interaction of magma transport and lithospheric flexure, *Nature*, *397*, 604–607.

Hieronymus, C. F., and D. Bercovici (2000), Non-hotspot formation of volcanic chains: Control of tectonic and flexural stresses on magma transport, *Earth Planet. Sci. Lett.*, *181*, 539–554.

Hilton, D. R., C. G. Macpherson, and T. R. Elliott (2000), Helium isotope ratios in mafic phenocrysts and geothermal fluids from La Palma, the Canary Islands (Spain): Implications for HIMU mantle sources, *Geochim. Cosmochim. Acta*, *64*, 2119–2132.

Hirose, K., N. Shimizu, W. van Westrenen, and Y. Fei (2004), Trace element partitioning in Earth's lower mantle, *Phys. Earth Planet. Int.*, in press.

Hirth, G., and D. L. Kohlstedt (1996), Water in the oceanic upper mantle: Implications for rheology, melt extraction and the evolution of the lithosphere, *Earth Planet. Sci. Lett.*, *144*, 93–108.

Hoernle, K., G. Tilton, M. J. LeBas, S. Duggen, and D. Garbe-Schönberg (2002), Geochemistry of oceanic carbonatites compared with continental carbonatites: Mantle recycling of oceanic crustal carbonate, *Contrib. Mineral Petrol.*, *142*, 520–542.

Hofmann, A. W. (1988), Chemical differentiation of the Earth: The relationship between mantle, continental crust and oceanic crust, *Earth Planet. Sci. Lett.*, *90*, 297–314.

Hofmann, A. W. (1997), Mantle geochemistry: The message from oceanic volcanism, *Nature*, *385*, 219–229.

Hofmann, A. E., and W. M. White (1982), Mantle plumes from ancient oceanic crust, *Earth Planet. Sci. Lett.*, *57*, 421–436.

Hofmann, A. W., and W. M. White (1983), Ba, Rb and Cs in the Earth's Mantle, *Z. Naturforsch*, *38*(a), 256–266.

Hooper, P. R., D. M. Johnson, and R. M. Conrey (1993), *Major and Trace Element Analyses of Rocks and Minerals by Automated X-Ray Spectrometry*, Washington State Univ., Pullman.

Ihinger, P. D. (1995), Mantle flow beneath the Pacific Plate: Evidence from seamount segments in the Hawaiian-Emperor Chain, *Am. J. Sci.*, *295*, 1035–1057.

Ito, E., W. M. White, and C. Gopel (1987), The O, Sr, Nd, and Pb isotope geochemistry of MORB, *Chem. Geol.*, *62*, 157–176.

Johnson, K. T. M. (1983), *The Petrology and Tectonic Evolution of Seamounts and Banks of the Northern Melanesian Borderland, southwest Pacific*, Thesis, Univ. of Hawaii, Manoa, Honolulu.

Johnson, M. C., and T. Plank (1999), Dehydration and melting experiments constrain the fate of subducted sediments, *Geochem. Geophys. Geosyst.*, *1*, Paper number 1999GC000014.

Jones, C. E., A. N. Halliday, D. K. Rea, and R. M. Owen (2000), Eolian inputs of lead in the North Pacific, *Geochim. Cosmochim. Acta*, *64*, 1405–1416.

Kay, R. W. (1979), Zone refining at the base of lithospheric plates: A model for a steady-state asthenosphere, in *Processes at Mid-Ocean Ridges*, edited by J. Francheteau, *Tectonophysics*, *55*, 1–6.

Kear, D., and B. L. Wood (1959), The geology and hydrology of Western Samoa, *New Zealand Geol. Surv. Bull.*, *63*, 1–90.

Keating, B. H. (1992), The geology of the Samoan Islands, in *Geology and Offshore Mineral Resources of the Central Pacific Basin*, *Earth Sci. Ser.*, vol. 14, edited by B. H. Keating and B. R. Bolton, pp. 127–178, Circum-Pacific Counc. for Energy and Miner. Resour., Houston, Tex.

Kelemen, P. B., G. M. Yogodzinski, and D. W. Scholl (2003), Along-strike variation in the Aleutian island arc: Genesis of high Mg# andesite and implications for continental crust, in *Inside the Subduction Factory*, *Geophys. Monogr. Ser.*, vol. 139, edited by J. Eiler, pp. 223–276, AGU, Washington, D. C.

Kinzler, R. J., and T. L. Grove (1992), Primary magmas of mid-ocean ridge basalts: 1. Experiments and methods, *J. Geophys. Res.*, *97*, 6885–6906.

Klemme, S., S. R. van der Laan, S. F. Foley, and D. Günther (1995), Experimentally determined trace and minor element partitioning between clinopyroxene and carbonatite melt under upper mantle conditions, *Earth, Planet. Sci. Lett.*, *133*, 439–448.

Koppers, A. A. P., J. P. Morgan, J. W. Morgan, and H. Staudigel (2001), Testing the fixed hotspot hypothesis using $^{40}Ar/^{39}Ar$ age progressions along seamount trails, *Earth Planet. Sci. Lett.*, *185*, 237–252.

Kurz, M. D., W. J. Jenkins, J. G. Shilling, and S. R. Hart (1982), Helium isotopic variations in the mantle beneath the central North Atlantic Ocean, *Earth Planet. Sci. Lett.*, *58*, 1–14.

Kurz, M. D., T. C. Kenna, D. P. Kammer, J. M. Rhodes, and M. O. Garcia (1995), Isotopic evolution of Mauna Loa volcano: A view from the submarine southwest rift, in *Mauna Loa Revealed: Structure, Composition, History and Hazards*, *Geophys. Monogr. Ser.*, vol. 92, edited by J. M. Rhodes and J. P. Lockwood, pp. 289–306, AGU, Washington, D. C.

Kurz, M. D., T. C. Kenna, J. C. Lassiter, and D. J. Depaolo (1996), Helium isotopic evolution of Mauna Kea: First results from the 1-km drill core, *J. Geophys. Res.*, *101*, 11,781–11,791.

Lassiter, J. C., D. J. DePaolo, and M. Tatsumoto (1996), Isotopic evidence of Mauna Kea volcano: Results from the initial phase of the Hawaiian Scientific Drilling Project, *J. Geophys. Res.*, *101*, 1769–1780.

Lawrence, J. R., J. Drever, T. F. Anderson, and H. K. Brueckner (1979), Importance of alteration of volcanic material in the sediments of Deep Sea Drilling Site 323, $^{18}O/^{16}O$ and $^{87}Sr/^{86}Sr$, *Geochim. Cosmochim. Acta*, *43*, 537–588.

MacDonald, G. A., and T. Katsura (1964), Chemical composition of the Hawaiian lavas, *J. Petrol.*, *5*, 83–133.

Mattey, D., D. Lowry, and C. Macpherson (1994), Oxygen isotope composition of mantle peridotite, *Earth Planet. Sci. Lett.*, *128*, 231–241.

McDonough, W. F., and S.-S. Sun (1995), The composition of the Earth, *Chem. Geol.*, *120*, 223–253.

McDougall, I. (1985), Age and evolution of the volcanoes of Tutuila, American Samoa, *Pacific Sci.*, *39*, 311–320.

Meisel, T., R. J. Walker, and J. W. Morgan (1996), The osmium isotopic composition of the Earth's primitive upper mantle, *Nature*, *383*, 517–520.

Menzies, M. (1983), Mantle ultramafic xenoliths in alkaline magmas: Evidence for mantle heterogeneity modified by magmatic activity, in *Continental Basalts and Mantle Xenoliths*, edited by C. J. Hawkesworth and M. J. Norry, pp. 92–110, Shiva, Nantwich, Cheshire.

Menzies, M. A., , and C. J. Hawkesworth (Ed.) (1987), *Mantle Metasomatism*, Academic, San Diego, Calif.

Menzies, M., and V. R. Murthy (1980), Nd and Sr isotope geochemistry of hydrous mantle nodules and their host alkali basalts: Implications for local heterogeneities in metasomatically veined mantle, *Earth Planet. Sci. Lett.*, *46*, 323–334.

Millen, D. W., and M. W. Hamburger (1998), Seismological evidence for tearing of the Pacific plate at the northern termination of the Tonga subduction zone, *Geology*, *26*, 659–662.

Molnar, P., and J. Stock (1987), Relative motions of hotspots in the Pacific, Atlantic and Indian Oceans since late Cretaceous time, *Nature*, *327*, 587–591.

Montelli, R., G. Nolet, F. A. Dahlen, G. Masters, E. R. Engdahl, and S.-H. Hung (2004), Finite-Frequency Tomography Reveals a Variety of Plumes in the Mantle, *Science*, *303*, 338–343.

Morgan, J. P. (1999), Isotope topology of individual hotspot basalt arrays: Mixing curves or melt extraction trajectories?, *Geochem. Geophys. Geosyst.*, *1*, Paper number 1999GC000004.

Moreira, M., and M. D. Kurz (2001), Subducted oceanic lithosphere and the origin of the 'high μ' basalt helium isotopic signature, *Earth Planet. Sci. Lett.*, *189*, 49–57.

Natland, J. H. (1980), The progression of volcanism in the Samoan linear volcanic chain, *Am. J. Sci.*, *280-A*, 709–735.

Natland, J. H., and D. L. Turner (1985), Age progression and petrological development of Samoan shield volcanoes: Evidence from K-Ar ages, lava compositions, and mineral studies, *Investigations of the Northern Melanesian Borderland*, *Earth Sci. Ser.*, vol. 3, edited by T. M. Brocher, pp. 139–171, Circum-Pacific Counc. for Energy and Miner. Resour., Houston, Tex.

Niu, Y., and R. Batiza (1997), Trace element evidence from seamounts for recycled oceanic crust in the Eastern Pacific mantle, *Earth Planet. Sci. Lett.*, *148*, 471–483.

Niu, Y., and M. J. O'Hara (2003), Origin of ocean island basalts: A new perspective from petrology, geochemistry, and mineral physics considerations, *J. Geophys. Res.*, *108*(B4), 2209, doi:10.1029/2002JB002048.

Niu, Y., G. Waggoner, J. M. Sinton, and J. J. Mahoney (1996), Mantle source heterogeneity and melting processes beneath seafloor spreading centers: The East Pacific Rise 18°–19°S, *J. Geophys. Res.*, *101*, 27,711–27,733.

Niu, Y. K., D. Collerson, R. Batiza, J. I. Wendt, and M. Regelous (1999), The origin of E-type MORB at ridges far from mantle plumes: The East Pacific Rise at 11°20′, *J. Geophys. Res.*, *104*, 7067–7087.

Norton, I. O. (2000), Global hotspot reference frames and plate motion, in *The History and Dynamics of Global Plate Motions*, *Geophys. Monogr. Ser.*, vol. 121, edited by M. A. Richards, R. G. Gordon, and R. D. van de Hilst, pp. 339–357, AGU, Washington, D. C.

Peacock, S. M. (1996), Thermal and petrologic structure of subduction zones, in *Subduction Top to Bottom*, *Geophys. Monogr. Ser.*, vol. 96, edited by G. E. Bebout et al., pp. 119–133, AGU, Washington, D. C.

Pearce, J. A., and D. W. Peate (1995), Tectonic implications of the composition of volcanic arc magmas, *Ann. Rev. Earth Planet. Sci.*, *23*, 251–285.

Pelletier, B., S. Calmant, and R. Pillet (1998), Current tectonics of the Tonga-Hebrides region, *Earth Planet. Sci. Lett.*, *164*, 263–276.

Peucker-Ehrenbrink, B., and B.-M. Jahn (2001), Rhenium-osmium isotope systematics and platinum group element concentrations: Loess and the upper continental crust, *Geochem. Geophys. Geosyst.*, *2*, Paper number 2001GC000172.

Pin, C., D. Briot, C. Bassin, and F. Poitrasson (1994), Concomitant separation of strontium and samarium-neodymium for isotopic analysis in silicate samples, based on specific extraction chromatography, *Anal. Chim. Acta*, *298*, 209–217.

Plank, T., and C. H. Langmuir (1998), The chemical compositions of subducting sediments and its consequences for the crust and mantle, *Chem. Geol.*, *145*, 325–394.

Poreda, R. J., and H. Craig (1992), He and Sr isotopes in the Lau Basin mantle: Depleted and primitive mantle components, *Earth Planet. Sci. Lett.*, *113*, 487–493.

Reisberg, L., A. Zindler, F. Marcantonio, W. White, D. Wyman, and B. Weaver (1993), Os isotope systematics in ocean island basalts, *Earth Planet. Sci. Lett.*, *120*, 149–167.

Richardson, S. H., A. J. Erlank, A. R. Duncan, and D. L. Reid (1982), Correlated Nd, Sr and Pb isotope variation in Walvis Ridge basalts and implications for their mantle source, *Earth Planet. Sci. Lett.*, *59*, 327–342.

Righter, K., and E. H. Hauri (1998), Compatibility of rhenium in garnet during mantle melting and magma genesis, *Science*, *280*, 1737–1741.

Roden, M. F., S. R. Hart, F. A. Frey, and W. G. Melson (1984), Sr, Nd and Pb isotopic and REE geochemistry of St. Paul's Rocks: The metamorphic and metasomatic development of an alkali basalt mantle source, *Contrib. Mineral. Petrol.*, *85*, 376–390.

Russell, S. A., T. Lay, and E. J. Garnero (1998), Seismic evidence for small-scale dynamics in the lowermost mantle at the root of the Hawaiian hotspot, *Nature*, *396*, 255–258.

Salters, V. J. M., E. J. Longhi, and M. Bizimis (2002), Near mantle solidus trace element partitioning at pressures up to 3.4 GPa, *Geochem. Geophys. Geosyst.*, *3*(7), 1038, doi:10.1029/2001GC000148.

Savin, S. M., and S. Epstein (1970), The oxygen and hydrogen isotope geochemistry of ocean sediments and shales, *Geochim. Cosmochim. Acta*, *34*, 43–63.

Sella, G. F., T. H. Dixon, and A. Mao (2002), REVEL: A model for Recent plate velocities from space geodesy, *J. Geophys. Res.*, *107*(B4), 2081, doi:10.1029/2000JB000033.

Shen, Y., S. C. Solomon, I. T. Bjarnason, and C. J. Wolfe (1998), Seismic evidence for a lower-mantle origin of the Iceland plume, *Nature*, *395*, 62–65.

Shirey, S. B., and R. J. Walker (1998), The Re-Os isotope system in cosmochemistry and high-temperature geochemistry, *Ann. Rev. Earth Planet. Sci.*, *26*, 423–500.

Smith, W. H. F., and D. T. Sandwell (1994), Sea Floor Topography Predicted From Satellite Altimetry and Ship Depth Measurements, MGG-09, World Data Cent. A, Mar. Geol. and Geophys., Boulder, Colo.

Stalder, R., S. F. Foley, G. P. Brey, and I. Horn (1998), Mineral-aqueous fluid partitioning of trace elements at 900–1200°C and 3.0–5.7 GPa: New experimental data for garnet, clinopyroxene, and rutile, and implications for mantle metasomatism, *Geochem. Cosmochem. Acta*, *62*, 1781–1801.

Standish, J. J., S. R. Hart, J. Blusztajn, H. J. B. Dick, and K. L. Lee (2002), Abyssal peridotite osmium isotopic compositions from cr-spinel, *Geochem. Geophys. Geosyst.*, *3*(1), 1004, doi:10.1029/2001GC000161.

Staudigel, H., A. Zindler, S. R. Hart, T. Leslie, C.-Y. Chen, and D. Clague (1984), The isotope systematics of a juvenile intraplate volcano: Pb, Nd, and Sr isotope ratios from Loihi Seamount, Hawaii, *Earth Planet. Sci. Lett.*, *69*, 13–29.

Staudigel, H., K.-H. Park, M. Pringle, J. L. Rubenstone, W. H. F. Smith, and A. Zindler (1991), The longevity of the south Pacific isotopic and thermal anomaly, *Earth Planet. Sci. Lett.*, *102*, 24–44.

Staudigel, H., G. R. Davies, S. R. Hart, K. M. Marchant, and B. M. Smith (1995), Large scale isotopic Sr, Nd, and O isotopic anatomy of altered oceanic crust: DSDP/ODP sites 417/418, *Earth Planet. Sci. Lett.*, *130*, 169–185.

Steinberger, B., and R. J. O'Connell (1998), Advection of plumes in the mantle flow: Implications for hotspot motion, mantle viscosity and plume distribution, *Geophys. J. Int.*, *132*, 412–434.

Stice, G. C., and F. W. McCoy Jr. (1968), The Geology of the Manu'a Islands, Samoa, *Pacific Sci.*, *22*, 427–457.

Stracke, A., M. Bizimis, and V. J. M. Salters (2003), Recycling oceanic crust: Quantitative constraints, *Geochem. Geophys. Geosyst.*, *4*(3), 8003, doi:10.1029/2001GC000223.

Sweeney, R. J., V. Prozesky, and W. Przybylowicz (1995), Selected trace and minor element partitioning between peridotite minerals and carbonatite melts at 18–46 kb pressure, *Geochim. Cosmochim. Acta*, *59*, 3671–3683.

Taras, B. D., and S. R. Hart (1987), Geochemical evolution of the New England seamount chain: Isotopic and trace-element constraints, *Chem. Geol.*, *64*, 35–54.

Tatsumoto, M. (1978), Isotopic composition of lead in oceanic basalts and its implication to mantle evolution, *Earth Planet. Sci. Lett.*, *38*, 63–87.

Todt, W., R. A. Cliff, A. Hanser, and A. W. Hofmann (1996), Evaluation of a ^{202}Pb-^{205}Pb double spike for high-precision lead isotope analysis, in *Earth Processes: Reading the Isotopic Code*, *Geophys. Monogr. Ser.*, *95*, edited by A. Basu and S. R. Hart, pp. 429–437, AGU, Washington, D.C.

Turner, S., and C. Hawkesworth (1998), Using geochemistry to map flow beneath the Lau Basin, *Geology*, *26*, 1019–1022.

van Keken, P. E., E. H. Hauri, and C. J. Ballentine (2002), Mantle mixing: The Generation, preservation, and destruction of chemical heterogeneity, *Annu. Rev. Earth Plant. Sci.*, *30*, 493–525.

Walter, M. J. (1998), Melting of garnet peridotite and the origin of komatiite and depleted lithosphere, *J. Petrol.*, *39*, 29–60.

Wang, S., and R. Wang (2001), Current plate velocities relative to hotspots: Implications for hotspot motion, mantle viscosity and the global reference frame, *Earth Planet. Sci. Lett.*, *189*, 133–140.

Watson, S., and D. McKenzie (1991), Melt generation by plumes: A study of Hawaiian volcanism, *J. Petrol.*, *32*, 501–537.

Weaver, B. L. (1991), The origin of ocean island basalt end-member compositions: Trace element and isotopic constraints, *Earth Planet. Sci. Lett.*, *104*, 381–397.

Wendt, J. I., M. Regelous, K. D. Collerson, and A. Ewart (1997), Evidence for a contribution from two mantle plumes to island-arc lavas from northern Tonga, *Geology*, *25*, 611–614.

White, W. M. (1985), Source of oceanic basalts: Radiogenic isotopic evidence, *Geology*, *13*, 115–118.

Workman, R. K., and S. R. Hart (2003), Trace element composition of the depleted upper mantle, *Eos Trans. AGU*, *84*(46), Fall Meet. Suppl., Abstract V52D-02.

Wright, E., and W. M. White (1987), The origin of Samoa: New evidence from Sr, Nd, and Pb isotopes, *Earth Planet. Sci. Lett.*, *81*, 151–162.

Zellmer, K. E., and B. Taylor (2001), A three-plate kinematic model for Lau Basin opening, *Geochem. Geophys. Geosyst.*, *2*, Paper number 2000GC000106.

Zhao, D. (2001), Seismic structure and origin of hotspots and mantle plumes, *Earth Planet. Sci. Lett.*, *192*, 251–265.

Zindler, A., and S. R. Hart (1986), Chemical Geodynamics, *Ann. Rev. Earth Planet. Sci.*, *14*, 493–571.

Zindler, A., S. R. Hart, F. A. Frey, and S. Jakobsson (1979), Nd and Sr isotope ratios and REE abundances in Reykjanes peninsula basalts: Evidence for mantle heterogeneity beneath Iceland, *Earth Planet. Sci. Lett.*, *45*, 249–262.